2020-01-24

Towards the optimization of lipid and antioxidant production in microalgae: A metabolic study

Ujan, Safina Naz

UNIVERSITY OF CALGARY

Towards the optimization of lipid and antioxidant production in microalgae: A metabolic study

by

Safina Naz Ujan

A THESIS

SUBMITTED TO THE FACULTY OF GRADUATE STUDIES

IN PARTIAL FULFILLMENT OF THE REQUIREMENTS FOR THE

DEGREE OF MASTER OF SCIENCE

GRADUATE PROGRAM IN CHEMICAL ENGINEERING

CALGARY, ALBERTA

JANUARY, 2020

Abstract

This research explores the design of cultivation strategies for a microalgal system, which will enable production of selected products based on economic value and market size. The microalgae are cultivated under heterotrophic conditions, which involves a nutrient feed of organic carbon substrate, to prevent light dependency. Glucose yields high cell density and lipid content for biofuel production from *Auxenochlorella protothecoides* under nitrogen-deplete conditions but leads to chloroplast bleaching. Hence, waste streams from the biodiesel industry, in the form of glycerol, are incorporated in the batch level system in order to modulate the pigment content. The glycerol rich conditions enabled production of significantly high levels of lutein and beta-carotene at about 52.43 $mg.L^{-1}$ and 6.2 $mg.L^{-1}$ respectively. High biomass growth of 11.53 $g.L^{-1}$ was reported for C:N ratio of 10:1 in glucose rich conditions. Since distinct nutrients promote accumulation of specific products, a mathematical model is used to simulate and predict micro-algal response to varying cultivation conditions in the batch level operation. For a reliable model, the biochemical reactions within the micro-algae are reconstructed and calibrated to predict the performance results for varying nutrient conditions. The mathematical model enables scale-up and control of process conditions within the bioreactor system. A sustainable and feasible solution for a micro-algal production system strengthens the bio-economy and renewable energy sector.

Preface

This thesis is original, unpublished, independent work by the author, S. Ujan.

Acknowledgements

بِسْمِ ٱللَّهِ ٱلرَّحْمَٰنِ ٱلرَّحِيمِ

First and foremost, I am thankful to Allah for blessing me with opportunities and challenges that have expanded my knowledge and understanding of the world.

Secondly, I would like to convey my deepest appreciation and gratitude to my research project supervisor, Dr. Hector De La Hoz Siegler for his constant guidance and support for the entirety of my research project. Dr. Hector promoted a great deal of independent learning by pushing me to resolve faults in research and the greater thought process.

I would like to thank National Sciences and Engineering Research Council (NSERC) for providing financial support. I am appreciative of Schulich School of Engineering and Alberta Graduate Excellence Scholarship for recognizing my academic achievement with scholarships.

I am gratified to be part of a remarkably supportive and resourceful research group 'IamBio' that created a positive environment for achieving high caliber research work. Particularly, I feel obliged to mention Maria Camila Caceres Falla and Cigdem Demirkaya for providing emotional support through stressful times.

I am appreciative for the persistence demonstrated by summer student Thinh Tuan Tong at the preliminary stages of the research project.

Lastly and most importantly, I would like to thank my parents and siblings for cheering me on through the difficult days. You hold a special place in my heart for your unwavering belief in my abilities.

Dedication

I would like to dedicate this thesis to my loving parents for believing in my potential especially when the world seemed leaps and bounds ahead. Thank you for celebrating my achievements no matter how small they seemed!

Table of Contents

List of Tables

List of Figures and Illustrations

List of Symbols

Symbol	Definition
c_i	Initial concentration (mmol.gDW^{-1})
c_{ext}	Concentration of intracellular nutrients (mmol.gDW^{-1})
e_i	Error value
k_{cat}	Turnover rate of an enzyme (1.s^{-1})
k_m	Michaelis-Menten constant (mmol.L^{-1})
m_t	Mass of a tube (g)
m_{t+p}	Mass of tube and pellet (g)
m_b	Mass of biomass (g)
r_{max}	Maximal rate of a reaction (mmol.sec^{-1})
r	Rate of a reaction (mmol.sec^{-1})
[S]	Concentration of a metabolite in Michaelis-Menten equation (mmol.gDW^{-1})
$v_{biomass}$	Rate of biomass growth (gDW.s^{-1})
$v_{glucose}$	Rate of glucose consumption (mmol.s^{-1})
v_{ATP}	Rate of ATP consumption or generation (mmol.s^{-1})
V_{input_i}	Rate of consumption (mmol.s^{-1})
V_{output_j}	Rate of generation (mmol.s^{-1})
V_{max}	Specific activity of the enzyme (mmol.sec^{-1}.mgE^{-1})
w_i^K	Weight associated with a given value
$x(t)$	Concentration as a function of time (mmol.gDW^{-1}.s^{-1})

x_{act}	Activated substrate
x_{inh}	Inhibited substrate
$\in$	Element
$\forall$	Predicate logic, which holds for all instances

List of Abbreviations

Abb.	Definition
ATP	Adenosine triphosphate
ADP	Adenosine diphosphate
NAD^+	Nicotinamide adenine dinucleotide
NADH	Nicotinamide adenine dinucleotide hydrogen
NADPH	Nicotinamide adenine dinucleotide phosphate hydrogen
NADPx	Nicotinamide adenine dinucleotide phosphate
GLC	D-glucose
GLY	Glycerol
H_2O	Water
GCN	Glycine
G6P	D-Glucose-6-Phosphate
F6P	D-Fructose-6-Phosphate
F16BP	D-Fructose 1,6-biphosphate
GCNP	Glycerone phosphate
G3P	D-glyceraldehyde 3-phosphate
OP	Orthophosphate
3BPG	1,3-Biphosphoglycerate
H^+	Hydrogen ion
SG30	sn-Glycerol 3-phosphate

OA	Oxaloacetate
PEP	Phosphoenolpyruvate
GL6P	Glucono-1,5-lactone 6-phosphate
6PG	6-phospho-D-gluconate
R5P	D-Ribulose 5-phosphate
X5P	D-Xylulose 5-phosphate
CT	Citrate
CoA	Coenzyme A
IC	Isocitrate
AKG	alpha-Ketoglutarate
MCoA	Malonyl-CoA
SM	(S)-Malate
R15B	D-Ribulose 1,5-biphosphate
3PG	3-phospho-D-glycerate
PY	Pyruvate
SAMP	S-Aminomethyldihydrolipoylprotein
METF	5,10-Methylenetetrehydrofolate
NH_3	Ammonia
GTM	Glutamate
LGM	L-Glutamine
DX5P	1-Deoxy-D-xylulose 5-phosphate
DPH	Diphosphate
PPDP	Prephytoene diphosphate

15cP	15-cis-phytoene
LYC	Lycopene
LTN	Lutein
BCRT	Beta-Carotene
ZXN	Zeaxanthin
MADP	Dimethylallyl diphosphate
IPP	isopentenyl diphosphate
BCRT	(E)-4-hydroxy-3-methylbut-2-en-1-yl diphosphate
GDP	Geranyl diphosphate
FDP	Farnesyl diphosphate
CO_2	Carbon dioxide
ACoA	Acetyl-Coenzyme A
GGDP	Geranylgeranyl diphosphate
ABTS	2,2'-azino-bis(3-ethylbenzothiazoline-6-sulfonic acid
OPA	O-Phthalaldehyde
C/N	Carbon to Nitrogen

Chapter 1: Introduction

An integrated biorefinery framework is a promising approach for microalgal biofuels to reduce dependency on fossil fuel sources, which result in greenhouse gas emissions and contribute to global warming. A biorefinery is like a traditional oil refinery since it involves conversion of crude biomass to obtain biofuels, energy, and high-value co-products. Microalgae are a viable source of biofuels showing potential in producing co-products such as antioxidants, bioactive compounds and pigments [1]. As proof of concept, this project focuses on the simultaneous production of both fuels and antioxidants. Antioxidants such as lutein and zeaxanthin, specific for preventing and treating ophthalmic diseases, are high-value co-products found in significant quantities in the chloroplast membrane of the micro-algal strain *Auxenochlorella protothecoides* [2].

1.1 Problem definition

One of the main challenges of micro-algal process systems is the low economic value of biodiesel as a product. As a result, the biorefinery must regulate product composition based on market demand to ensure high process economy and sustainability. The primary product (lipids) and the secondary co-products (antioxidants) require distinct nutrient conditions for accumulation [3]. In this research, microalgae consume organic substrates in the form of glucose or glycerol instead of using their photosynthetic functionality in order to prevent light dependency [4]. Glucose causes lipid accumulation but also chloroplast bleaching, which limits antioxidant yields. On the other hand, glycerol modulates and enhances antioxidant production [5].

Microalgae are extensively versatile in their metabolic pathways, which offers exciting applications for antioxidant rich microalgal cultures in the pharmaceutical and food industry [1].

Antioxidants among other bioactive compounds suppress the effect of free radicals within the human body by inhibiting cellular damage or obstructing the chain reaction that results in oxidation [2]. Current research is limited by non-specific knowledge on the antioxidant profile and bioactivity of individual microalgal strains [1]. Hence, the heterotrophic cultivation of *A. protothecoides*, known for high lipid and antioxidant content, is explored to produce high biomass yield as well as increased lipid and carotenoid productivity by optimizing the macronutrient concentrations.

Nitrogen is a primary source for cell division and growth in microalgae. However, nitrogen-rich cultures contribute to high biomass with limited lipid accumulation as most of the energy is utilized for cell division [13]. In this research, nitrogen-limited conditions are explored to enrich the intracellular organelles with more energy rich components such as lipids and carbohydrates as opposed to biomass growth. Experimental variation of the carbon to nitrogen ratio in batch cultivation shows high biomass growth for increasing nitrogen under nitrogen-limited conditions. When glucose and glycerol proportions were altered, the lipid content significantly decreased with lower glucose in the culture media. Glucose forms intermediate metabolites that circumvent the metabolic route through the chloroplast resulting in chloroplast bleaching [3]. Since, chloroplasts are rendered inactive by glucose assimilation and nitrogen-limiting conditions hinder chloroplast production, the chloroplasts disintegrate for lipid accretion in the microalgal cell. Whereas, the presence of high glycerol content in culture media maintains metabolic activity through the chloroplast and in spite of nitrogen limiting conditions, glycerol metabolism modulates antioxidant production in microalgae [4].

Another challenge in the sustainable operation of an integrated biorefinery is the ability to regulate microalgal behaviour and adjust product yields to suit economic trends. This requires a

mathematical model to simulate micro algal performance with variation in external process conditions of the bioreactor. Moreover, to enable the design, scale-up, optimization, and control of the proposed process we require a mathematical model that predicts micro-algal response to different metabolic stressors. Researchers have developed unstructured kinetic models using empirical datasets; however, they lack a biological basis, which limits their reliability. Hence, metabolic reconstruction of biosynthesis pathways in the microalgae can facilitate the regulation of product yields to enhance process economy. The biochemical processes within the microalgae are a network of complex enzymatic reactions with several hundred unknown parameters [6]. Current information on microalgae contain non-specific kinetic parameters, which require calibration using experimental data through a dynamic model.

The mathematical model uses the Michaelis-Menten equation to evaluate the flux of enzyme catalyzed reactions [9]. The reactions account for the metabolic assimilation of glucose and glycerol within the intracellular organelles among other nutrients, while the robust pathways are lumped together to reduce the number of parameters that require optimization [5]. The kinetic parameters and stoichiometry of the biochemical reactions for the synthesis of biomass, macromolecules, nucleic acid, intermediate metabolites and energy are assembled from current literature. The mathematical model forms a non-linear set of ordinary differential equations (ODE) which are evaluated using an ODE solver and subsequently an optimization algorithm for evaluating optimal solutions for kinetic parameters based on experimental datasets. The optimization problem approximates the enzyme content for a given cell through a linear objective under specified constraints. A series of linear objectives, such as high substrate assimilation, high biomass yield, increased ATP usage or fitting experimental data, are investigated and enforced on the programming system, which allows the solver to determine an optimum solution.

This research will enable the development of an optimal cultivation strategy to maximize the economic value of algal biomass by regulating the production of biodiesel and high value co-products according to market demands. Since algal production systems are renewable, the proposed biorefinery process will result in a sustainable supply of both fuels and chemicals, replacing unsustainable and polluting fossil-based traditional refineries.

1.2 Research objectives

While the principal question in this research is, whether a sustainable and economical biorefinery is feasible through the development of optimal strategies based on metabolic modelling approach. The research objectives specific to this study attempt to fill in the research gaps highlighted in the literature review.

- Study the effect of bi-substrate cultivation using glucose and glycerol on product composition.
- Reconstruct the metabolic pathways and calibrate kinetic parameters of genome-specific enzymes.
- Design a dynamic metabolic model in order to simulate the microalgal behaviour for changing process conditions.

1.3 Research Scope

This research project works on enhancing the biofuel and antioxidant production of the microalgal strain *Auxenochlorella protothecoides.* The literature review contains a meta-critical analysis of current strategies in research on microalgal cultivation systems. The review helps derive the optimal cultivation conditions for lipid accumulation and antioxidant production. Additionally, a review on modelling schemes, mathematical models and boundary conditions informs the framework of the metabolic model. Furthermore, the genome-specific metabolic

pathways are reassembled for *A. protothecoides* from current literature in order to model essential biochemical functions towards cellular growth and maintenance. The chapter on materials and methods elucidates the experimental methods employed towards the batch level cultivation system and the subsequent analysis of the biomass yield, antioxidant and lipid content. Chapter 4, 5 and 6 provide an overview description of the data collected and results obtained from the research. Chapter 4 discusses observations and production yields of the experimental results at different proportions of carbon source and nitrogen content. Chapter 5 includes the reconstruction and assembly of the metabolic pathways. Subsequently, the dynamic modelling framework and its experimental validation is examined in Chapter 6. Ultimately, the key findings and recommendations from the research project are put forward in Chapter 7.

Chapter 2: Literature Review

In this chapter, a meta-critical review was performed of the existing microalgal biotechnology, modelling methodologies and metabolic pathways from current literature in order to inform the decisions made towards the research project. Significant findings were highlighted and tabulated to report the substantial results from other research studies. Current technologies on microalgal cultivation show increased productivity and yield with the integration of carbon source in the cultivation medium. The attractive characteristics of the microalgal strain towards biosynthesis of high value products and biofuel production demonstrate its efficacy for a biorefinery system. The metabolic pathways elucidate the distribution of nutrients in the biosynthesis and cellular maintenance cycles, which explains the changes in product composition between antioxidants and lipids. Since, antioxidants and lipids share precursors then production yields are dependent on the variation in carbon and nitrogen content. This distinct microalgal characteristic can be employed to tailor the product composition to market trends for enhanced economic sustainability.

2.1 Microalgal biotechnology

Microalgae are single-celled microscopic organisms typically found in marine and freshwater systems all over the world [6]. They are a highly biodiverse group consisting of an estimated 200,000 to 800,000 species, which vary in size from a few micrometers to hundreds of micrometers [7]. Microalgae are eukaryotic microphytes, which are partly responsible for the world's primary productivity as they convert solar energy, using carbon-dioxide in the process, to produce organic compounds and oxygen [8]. They have demonstrated higher proficiency at conversion of sunlight while taking up harmful pollutants from the environment, not requiring

arable land and consuming lower resources in comparison to terrestrial plants [9]. An assortment of bioproducts, including carbohydrates, lipids, proteins, and other biochemical constituents such as vitamins, polysaccharides and antioxidants can be sourced from microalgal biomass [10]. Microalgae are tolerant towards a wide range of abiotic stress factors such as temperatures, salinities, pH values, light intensities, and nutrient depletion [11]. Their adaptability renders them suitable for large-scale production of animal feed, dietary supplements, renewable fuels, industrial chemicals, and pharmaceuticals [12].

Microalgae have an extensive range of industrial applications with a significant number of literature reported on biofuel production and wastewater treatment [13]. Microalgae reportedly contain 20-50 % oil content of their dry weight and the oil yield has been substantially enhanced through modulation of the growth techniques [14]–[16]. Microalgae can be used to generate biofuel in the form of bio-oil through hydrothermal liquefaction, biogas from anaerobic digestion of residual biomass, biodiesel from transesterification of extracted oil and bio-hydrogen from fermentation of algal biomass as reported by Abhishek et al. [17]. Other researchers such as Benemann et al. [18] argue substantive development is called for algal cultivation techniques to ameliorate the high capital cost of biodiesel production. Genetic engineering has enabled development of algal strains that do not require costly downstream processes for product recovery, which facilitates a competitive price for the biofuel [12]. On the other hand, valuable co-products from the residual biomass are routinely identified for employment in animal, poultry and fish feed. Additional applications of microalgal systems consist of recovery of valuable chemicals or molecular compounds for manufacturing biodegradable, non-toxic green plastics, green detergents and cleaning products [19]. The biotechnological applications of several microalgal strains in various industries are listed in Table 2.1.

Table 2.1: Biotechnological applications of microalgal strains in various industries.

Microalgal strain	**Biotechnology/Uses**	**Commercial application/Uses**	**Ref**
Arthrospira (Spirulina)	Health promoting supplement for mitigation of hyperlipidemia and hypertension	Pharmaceutical industry	[20]
Chlorella	Food additive and food coloring	Food industry	[21]
D. salina	B-carotene content	Food industry	[22]
Isochrysis	Food additive and food coloring	Animal feed industry	[23]
Cyanobacteria	Biofertilizer and biocontrollers	Agricultural industry	[24]
Scenedesmus	Biogas (methane and hydrogen) production	Energy industry	[25]
C. vulgaris	Reduction of sewage effluent and nitrogenous waste	Wastewater treatment	[26]
Limnothrix planctonica	Detoxification of heavy metals	Wastewater treatment	[27]
C. reinhardtii	Plasticized microalgae for development of bioplastics	Bioplastics industry	[19]

2.1.1 Microalgal production systems

2.1.1.1 Cultivation technology

Industry has explored different technologies for microalgal growth in large-scale cultivation systems. The microalgal species or even specific strain involved in the process influences the design of the cultivation technology based on growth characteristics such as temperature, light and salinity. For instance, the growth of hypersaline microalgae in open pond systems lowers maintenance requirements as it inhibits growth of extraneous algae, protozoa and bacteria [28]. Alternatively, high salinity would not be suitable for heterotrophic cultivation because frequent sterilization at high-temperatures would have corrosive effects on the equipment [29].

Figure 2.1: Microalgal cultivation systems a) circular open pond [30] **b) cascade raceway pond** [31] **c) horizontal tubular reactor** [30] **d) flat-plate reactor** [32] **e) vertical photo bioreactors** [33] **f) plastic bag cultivation systems** [34].

Open pond cultivation systems, as seen in Figure 2.1 a-b, offer convenience in overall cost construction and operation. In addition to natural ponds or lakes, three primary man-made designs are inclined systems, circular and raceway ponds. Inclined systems require pumping and gravity induced flow, circular ponds involve mixing by rotating arm and raceway ponds involve circulation of culture by paddle wheels through an interminable loop [35]. Circular systems are a popular choice for large-scale cultivation of *Chlorella* in Japan, Korea and Indonesia [6]. Similarly, raceway ponds are widely used for growth of *Dunaliella bardawil* in Japan and Israel, but a trade-off has to be maintained between shallow depths to prevent light limitation and sufficient liquid levels to preclude excessive evaporation [36]. However, the variability of the operating conditions largely effects the biomass yields and as a result the productivity of the system.

Conversely, closed systems provide efficient uptake of carbon dioxide and other flue gases, lower chances of contamination and increased control of operating conditions [34]. Closed cultivation systems are not limited to but include plastic bags or tanks, photo-bioreactors, hybrid

and fermentation systems. Hatcheries employ disposable plastic bags for microalgal cultivation as live feed for fostering aquaculture animals [6]. Photobioreactors, as seen in Figure 1(c-f), are bioreactors often designed in tubular, flat-plate or stirred tank design for enhanced productivity without light limitation. Even so, Vo et al. [34] disputes inadequate mixing and illumination efficiency can lead to emergence of dead zones where cells lack access to sufficient light intensity.

A majority of microalgal species are phototrophic but phototrophic growth does not yield high cell density for commercial use [37]. Heterotrophic cultivation has several benefits over the phototrophic mode which includes higher biomass productivity, easier scaling up process and the ability to manipulate biomass and production yields by varying the organic substrate to stimulate certain metabolic pathways [38]. Moreover, heterotrophic cultivation accumulates lipids as the metabolism of organic carbon is faster than cell division which pushes excess carbon conversion into lipids [39].

Heterotrophic cultivation of microalgae is an aerobic process which involves metabolism of organic carbon sources (for e.g. glucose, acetate, lactate, glutamate or glycerol) to generate energy through the oxidative phosphorylation pathway and oxygen consumption [40]. Microalgal strains such as *Amphora, Ankistrodesmus, Chlamydomonas, Chlorella, Chlorococcum, Dunaliella* and *Euglena* have the potential to grow in heterotrophic conditions [40]–[43]. Certain species of microalgae have the capacity to grow under mixotrophic conditions, which includes sequential or simultaneous cultivation through phototrophic and heterotrophic growth mechanisms [44]. Swapna et al. [45] reported high cell density and increased pigment and lipid content in cells for microalgal species such as *Chlorella protothecoides, Chlamydomonas reinhardtii, Haematococcus pluvialis, Dunaliella salina* and *Crypthecodinium cohnii* in mixotrophic growth conditions.

Henceforth, multiphase cultivation strategies combine open and closed technology systems to maximize production yields by altering cultivation conditions to suit changes in the environment and microalgal bioproducts. In this framework, the production of biomass is increased in one stage and desired products accumulated in the subsequent stages [6]. Richmond [46] reported an integrated system which included a flat panel reactor connected to a tubular reactor for growth of *Haematococus pluvialis*. In the first phase, the microalgal cells were allowed to reach high biomass yields in the flat panel reactor. Subsequently, the culture was shifted to the tubular reactor to promote carotenogenesis for high bio-product yield.

2.1.1.2 Microalgal strain

In this research, the microalgal strain of interest is *Auxenochlorella protothecoides,* which is an oleaginous eukaryote with photosynthetic functionality [47]. The cellular space is occupied with multiple mitochondria, a singular concave shaped chloroplast, firm cell wall and the exterior lacks flagella [48]. The faculty to perform the Calvin-Benson cycle was developed through the endosymbiosis of a cyanobacterium by a heterotrophic protist organism [49].

This single-celled organism can assimilate and metabolize sugars, also known as organic carbon substrates, to produce useful means of energy for heterotrophic growth [50]. In heterotrophic cultivation conditions, *A. protothecoides* undergoes degeneration of plastids towards the inhibition and subsequent exclusion of photosynthetic functionality [49]. Nevertheless, this is a reversible process and recovery of the plastids can be induced through the presence of higher nitrogen content, glycerol or mixotrophic conditions. In contrast to obligate autotrophs, the cell undergoes substantial structural changes in heterotrophic conditions. Therefore, the microalgal strain is a very attractive option for biodiesel production, since the disintegration of chloroplasts results in accumulation of lipids in the form of triacylglycerols (TAGs) [48]. While glucose hinders

the economic viability of the production process, the incorporation of other waste streams as organic substrates can significantly lower the economic and environmental cost of the heterotrophic cultivation system. Lignocellulosic biomass, derived from agricultural waste and further disintegrated through enzymatic hydrolysis or fungal treatment, can be used to enhance the economic viability of the process system [51], [52]. The cultivation of *A. protothecoides* using alternative sources of carbon is shown in Table 2.2.

Table 2.2: Production of *A. protothecoides* on different waste streams and the derived production yields for the specific cultivation system.

Microalgal Strain	Carbon source	Cultivation system	Production yield	Ref.
***Auxenochlorella protothecoides* 249**	Acetate	Mixotrophic	29.45 ± 0.84% lipid content	[53]
***Auxenochlorella protothecoides* 249**	Acetate	Heterotrophic	52.38 ± 25.77% lipid content	[53]
***Auxenochlorella protothecoides* FACHB-3**	WAS (Waste activated sludge) hydrolysate containing a mixture of VFA	Heterotrophic	21.5 ± 1.44% lipid content	[54]
***Auxenochlorella protothecoides* UTEX 25**	Acetic acid, propionic acid and butyric acid	Heterotrophic	48.7 ± 2.2 % lipid content (0.317 ± 0.01 g/L)	[55]
Auxenochlorella protothecoides	Enzyme hydrolysed forest biomass	-	66.00 ± 0.33 % lipid content (8.40 ± 0.12g/L)	[56]

The biofuel potential of *A. protothecoides* has been explored by various studies such as [48], [50]. As a result, the microalgal derived biodiesel has been found to be suitable and compatible with the US biodiesel standards (ASTM 6751) [57]. A variety of bioactive compounds and pigments identified in *A. protothecoides,* as seen in Table 2.3, have generated commercial interest with a shift in consumer preferences towards reducing animal-derived products and processing stages. *Chlorella* is considered a food grade strain with a GRAS (Generally Recognized As Safe) designation in several countries [58]. *A. protothecoides* is a great resource for chlorophyll

and other pigments such as carotenoids, which can protect lipid oxidation in emulsive formulations based on microalgae [21]. Additional work on *Chlorella* includes applications as moisturizing and thickening agents in the cosmetic industry [59]. Furthermore, researchers have investigated the recovery of protein rich fractions from fresh or commercially available biomass for enhanced nutritional content [60], [61].

Table 2.3 A variety of bioactive compounds and pigments recovered from *A. protothecoides* for commercial applications.

Cultivation conditions	Max. biomass concentration (gL^{-1})	Desired product	Maximum production yield ($mgL^{-1}day^{-1}$)	Commercial application	Ref.
Mixotrophic	22.4	Lutein	18.14	Colouration of foods, drugs and cosmetics	[62]
Heterotrophic	17.2	β-Carotene	2.02	Dietary supplement	[62]
Mixotrophic	22.4	Chlorophyll a	158.9	Precursor of vitamin A	[62]
Batch	10.68	Omega-3 fatty acids	-	Prevents cardiovascular diseases	[63]
-	-	Linolenic acid	-	Anti-inflammatory	[23]
Batch	10.68	Protein	-	Animal feed	[63]

2.1.1.3 Growth limitations

Patel [64] reported high cell density of an order of 100 gL^{-1} and high production yields under heterotrophic conditions in microalgal cultures [14]. Nonetheless, heterotrophic cultivation face several challenges in terms of examining the optimal carbon source, nitrogen content, oxygen supply and feeding strategies for a continuous system [1]. In heterotrophic conditions, microalgae can shift to metabolizing organic carbon for energy and cell division instead of depending on light source for photosynthesis [65]. Typically, glucose, glycerol and acetate are primary sources of organic carbon to derive energy for cellular growth [66]. Glucose as the carbon source yields high lipid accumulation in microalgae but contributes to a loss of pigmentation and disruption in

transcription of photosynthetic proteins [67]. Furthermore, glucose is an expensive carbon source, which lowers the economic value of biodiesel production. For instance, techno economic assessments have reported that 80% of the costs for biodiesel production are derived from glucose [68].

Although higher growth rate was found in microalgal cultures using glucose as the sole carbon source, the addition of glycerol was found to effectively modulate both overall substrate to biomass yield and antioxidant profile [69]. The biomass and antioxidant productivity are enhanced by the use of glycerol, a typical waste product in the biodiesel industry, which further enhances the economic viability of the microalgal production process. Likewise, rice straw, corn powder, cassava, sugarcane, sweet sorghum, waste molasses, soy whey are other types of inexpensive carbon sources, which are used for heterotrophic cultures [64].

Nitrogen is a primary source for cell division and growth in microalgae. However, nitrogen-rich culture media contribute to high biomass with limited lipid accumulation as most of the energy is utilized for cell division [70]. Hence, nitrogen starvation and nitrogen-limited conditions are explored to enrich the intracellular organelles with more energy rich components such as lipids and carbohydrates as opposed to nitrogen rich components. Furthermore, nitrogen depletion causes cells to gradually convert nitrogen containing cell components to lipids which results in high accumulation of lipids in biomass [71]. At the same time, antioxidants and other bioactive compounds are concentrated in nitrogen-rich compartments such as the chloroplast. Therefore, nitrogen depletion inversely results in the loss of the chloroplasts due to lipid accumulation [15], [71]. Hence, optimal nitrogen content in the feed is required to maintain sufficient yields of both lipid and antioxidant concentrations within the resulting biomass.

Oxygen is required to maintain dark respiration in the microalgal culture which promotes the biosynthesis of intracellular metabolites relevant to cell growth [66]. While oxygen can become a limiting factor in heterotrophic growth, it has an inhibitory effect on photosynthesis rates in mixotrophic conditions [72]. Hence, aeration of the heterotrophic cultures is an important parameter that influences growth rates. A suitable agitation technique should be applied that provides sufficient oxygen for cell growth, prevents cell settling and enhances mass transfer rates without sheering the microalgal biomass [40], [73].

2.1.2 Microalgal potential in integrated biorefinery

Growing research in microalgal growth under heterotrophic conditions through conventional bioreactors is attracting increasing commercial interest. Feeding strategies for cultivation in bioreactors include batch, fed-batch and continuous modes. Fed-batch cultivation allows microalgae to achieve high biomass concentration in a short timeframe as growth is no longer inhibited by the constant presence of high substrate concentrations [29]. According to Bosma et al. [74], osmotic or toxic effects due to high carbon content in the culture media can be prevented through fed-batch cultures. The intermittent flow of carbon source through fed-batch cultures allows microalgae to reach high cell densities as shown in Table 2.4. Research studies have investigated the optimization of a singular target product under different operating modes. Consequently, a significant increase in biomass and product yields was observed for fed-batch cultures as opposed to batch cultures.

Table 2.4: Comparison and contrast of microalgal growth and products yields with distinct feeding strategies.

Microalgal strain	Culture operating mode	Max. biomass concentration (gL^{-1})	Desired product	Maximum production yield ($mgL^{-1}day^{-1}$)	Ref.
Auxenochlorella protothecoides	Batch	3.30	Lipids	343	[75]
	Fed-batch	15.50	Lipids	3790	[75]
	Fed-batch, N-limited	140	Lipids	10320	[76]
	Fed-batch, N-sufficient	46.9	Lutein	22	[36]
Chlorella sorokiniana	Batch	1.5	Lipids	0.5	[77]
	Batch	1.1	Biomass	0.37	[77]

The optimal feeding strategy for continuous cultivation (for e.g. batch, semi-cyclic or continuous) should be investigated through growth kinetics, substrate consumption and product accumulation specific to the microalgal strain [78]. For sustainability and economic feasibility of a microalgal biorefinery that enables production of a primary and secondary product, two or more production stages (semi-cyclic bioreactor) should be implemented to enhance product yields [73]. González-Figueredo et al. [79] promotes the implementation of mathematical models to identify optimal growth conditions for microalgal production systems. He argues empirical models are unsuitable for simulating the highly intricate and complex characteristics of the biochemical pathways within a microorganism [80].

2.2 Metabolic model

Advances in the industrial applications of biotechnology has promoted the rise of databases, which compound a wide array of data sources on the mechanisms for the biological activity of cellular systems [81]. Computational methods are required to handle the gargantuan task of assembling and organizing the multi-dimensional data sets required for a system analysis

of an organism. In recent years, metabolic models are increasingly employed to administer the control and performance of microorganisms in large-scale commercial applications.

2.2.1 Metabolic modelling framework

Metabolic modelling frameworks include isotope labeling-based, kinetic-based, and constraint-based strategies [82]. Constraint based modelling, also addressed as stoichiometric modelling, involves less parameters for the reactions, which makes it suitable for large-scale genome-level development [83]. Additional constraints such as lower and upper boundary conditions of fluxes, metabolite concentrations and reaction pathways enhance the accuracy of model predictions [84]. Despite the convenience of model construction in a constraint-based approach, the model simulates steady state behavior without variation in metabolite concentration.

Research studies, which utilize isotope labeling and kinetic-based frameworks, are limited for central metabolic networks or whole-cell analysis [82]. In contrast, solely constraint-based frameworks have been formally studied at the genome scale for a comprehensive representation of metabolic fluxes as seen in [85], [86] and [87]. Literature on constraint-based frameworks has mapped and simulated intracellular metabolism specific to individual organelles or compartments for oleaginous microalgal cells. Wu et al. [88] deduced the optimal status for cell growth and lipid accumulation by reconstructing and simulating the primary metabolism of *A. protothecoides* through genome annotation and flux balanced analysis. Alternatively, an earlier study by Xiong et al. [89] carried out a metabolomic study of *A. protothecoides* through the isotope labelling approach which produced flux estimation of lower accuracy. This approach necessitates augmentation of dynamic isotope-labelled pathways of the central carbon metabolism to further strengthen the accuracy of metabolic flux estimation [88].

Kinetic based models incorporate a large number of parameters for reactions mechanisms such as the Michaelis-menten reaction, mass action and inhibitive activity [90]. In detail, Michaelis-menten reactions are characterized through the catalytic constant (k_{cat}), maximal reaction rate (V_{max}) and Michaelis-Menten constant (k_m) [83]. Kinetic models enable simulation of quantitative and dynamic variations in metabolite concentrations and intracellular fluxes with respect to time. Research studies have designed dynamic metabolic models at pathway-scale of glycolysis [91], Entner-Doudoroff pathways [92] and central carbon metabolism [93] through kinetic modeling.

2.2.2 Metabolic modelling constraints

Physicochemical constraints: In all modelling approaches, constraints are applied for the analysis of specific microorganisms or experimental conditions. General constraints constitute the mass conservation principle and an overall energy balance in an isolated system. Kinetic modelling adopts a steady-state assumption for the metabolism, where the intermediary metabolite concentrations are constant while flux of metabolic products, biomass constituents and substrates has non-zero values [69], [58]. The logic enforces the metabolic model to sustain the biological activity involved in the process design for a long period instead of reaching it for a transient phase [83]. The transition phase must occur for a long duration before it reaches steady state. This ensures a realistic and feasible modelling structure where the transition phase of the metabolites does not surpass lifespan of the organism. On the other hand, thermodynamic constraints are placed to curb the number of reversible reactions, which can significantly amplify the solution space.

Biological constraints: Organism level constraints consider biological limitations such as the metabolic pathways and the physiological limitations of the specific organism. An example of the physiological aspect is the limitation on enzyme-building resources, which places a caveat on

the total enzyme activity [83]. Magnus et al. [95] implemented flux control coefficients to curb the influence of enzyme level on variable flux rates. The assumption basis is to limit the production of proteins in the modified modelling structure to simulate organism performance with higher accuracy [83]. Moreover, certain metabolites can have cytotoxic effects on the organism above an upper limit. Hence, constraints have to be placed on intracellular metabolic concentrations for feasible results.

Homeostatic constraints curb the effect of substantial variations in metabolite concentration on reactions beyond the kinetic model scope through reaction flux, direction and gene expression [96]. The constraint limits the optimized objective values to a specific range around the initial conditions of the steady state metabolite concentrations. Magnus et al. [95], among others [58], [72] and [99], introduced homeostatic constraints to the mathematical model, which ensured the average change in metabolite level was lower than 10%.

Experimental constraints: The system environment and availability of nutrients varies with experimental conditions, which limit the cellular resources such as mass, energy, surface, volume and others [83]. Biomass synthesis largely depends on the production of macromolecules from the available substrates for feasible cellular growth in the metabolic models. This characteristic constraint maintains biomass composition throughout the organism's lifetime. Hence, this does not consider increasing cytosolic mass to cell mass ratio for cells with fast growth rate [100]. Several research studies argue biomass yield is unaffected by changes in a single biomass precursor. On the other hand, a 10% increase in primary energy carriers such as ATP and NADH can lower biomass yield by 2% [83]. A summary of different types of constraints can be seen in Table 2.5.

Table 2.5: Descriptive examples of metabolic modelling constraints and descriptions for enzyme and metabolite concentrations.

Modelling constraint	Constraint type	Objective	Mathematical formulation	Ref.
All reactions are feasible	Thermodynamic	The constraint ensures feasibility by restricting the flux through each reaction to equal or greater than zero.	$0 \leq v_i \leq z_i . \ v_{\max}$, $\{i = 1, \dots, r\}$	[101]
Concentration constraint	Experimental	This restricts the intracellular concentration (c_i) of the nutrient below the extracellular concentration (c_{ext}) in the media. The intermediate metabolites do not exceed the highest measured cellular concentration, which also limits nutrient uptake for the cell.	$10^{-7} < c_i < c_{ext}$	[83], [101]
Enzyme constraint	Biological	This constraint is associated with the limited enzyme resource pool. Increase in a singular enzyme concentration influences the individual concentrations of other enzymes in the pool.	$c_{\Sigma}^{K} := \sum_i w_i^K e_i \leq 1$	[102]

2.2.3 Metabolic network analysis

According to Kim et al. [103], the quantitative assessment of a kinetic model is defined through two different strategies:

(1) Steady-state kinetic models, which consider a minimal amount of reaction kinetics with metabolite flux in pseudo steady state.

(2) Dynamic kinetic models, which consider reaction kinetics for all enzymes in the metabolic network.

At the crux of the design, a dynamic model represents the interaction mechanisms of a cellular factory through a select mathematical strategy for the kinetic rate expressions. Ultimately, a dynamic model is rendered as an assembly of ordinary differential equations (ODEs) that exemplify the cellular processes as a function of time. The ODEs are validated through experimental outcomes in a time series. DiStefano [104] elucidated the network construction,

initial statements, boundary conditions and mathematical framework for reaction rates through Eq. 1.

$$\frac{dx(t)}{dt} = S.r(x(t), u(t), p) \quad (1)$$

$$y(t) = g(x(t), u(t), p)$$

$$\text{with } x(0) = x_0(p)$$

In Eq. 1, *S* is an *i*x*j* dimensional matrix, which stores the stoichiometric information for all the biochemical reactions in the metabolic model. *x(t)* is a vector representing the state variables as a function of time. *r* is a vector with dimension *j*, which encompasses reaction rates, initial conditions *u(t)* and kinetic parameters *p*. *g* connects the output *y(t)* to the input *x(t)* [103]. The mass balance equation, as shown in Eq. 1, disregards the dilution of intracellular metabolites. According to Knorr et al. [105], the change in metabolite concentration through dilution has a negligible effect in comparison to enzymatic reactions hence this assumption is justified.

Secondly, flux balance analysis assumes pseudo steady-state because the enzymatic activity is considered transient, which enables a fast response of metabolite concentrations to external disturbances [5], [105]. Stephanopoulos et al. [5] subsumed the pseudo steady-state assumption by qualifying Eq. 2, summation of reaction fluxes, to Eq. 3, which entails a series of linear algebraic equations.

$$\frac{dx_i}{dt} = \sum_j S_{ij}.\emptyset_j \quad (2)$$

$$S.\emptyset = 0 \quad (3)$$

In Eq. 2 and 3, *S* is the *i*x*j* dimensional matrix, which stores the stoichiometric coefficients of all the *i* metabolites in all *j* metabolic fluxes and ø is the vector of reaction rates [105].

2.2.4 Rate law expressions

Kinetic rate expressions rely on rate laws for representation of elementary or enzymatic reactions. A series of mathematical expressions are listed below for different reaction types.

2.2.4.1 Michaelis-Menten model

Michaelis-Menten kinetics involve elementary level reactions through separation of fast and slow dynamics. This method is suited for biochemical reactions with lower enzyme concentration in comparison to substrate concentration [103]. It is represented through the mathematical expression shown in Eq. 4.

$$r = \frac{d[X]}{dt} = r_{max} \frac{[S]}{[S]+k_m} \tag{4}$$

In Eq. 4, r is the rate of the reaction, [S] is the substrate concentration, [X] is the product concentration, r_{max} is the maximal reaction rate, and k_m is the substrate concentration at half the maximal reaction rate. Bertolazzi [106] appended supplemental information such as limitation of nutrients and inhibitors in the reaction rate formula to account for the complexity of the system. Osvaldo et al. [103] contends experimental means are essential for parameter determination in order to lower the analytical uncertainty of kinetic modelling.

2.2.4.2 Hill rate laws

Hill rate law models the fast dynamic responses of the genetic regulatory circuits within a microorganism [107]. The mathematical expression for the transcription activity is illustrated through Eq. 5 and 6.

$$\frac{dx_{act}(t)}{dt} = f_{act}[x(t,p)] = \lambda \frac{x^n}{x^n+k^n} \tag{5}$$

$$\frac{dx_{inh}(t)}{dt} = f_{inh}[x(t,p)] = \lambda \frac{k^n}{x^n+k^n} \tag{6}$$

In Eq. 5 and 6, the transcription activity is represented by accounting for the rate of activated (x_{act}) and inhibited (x_{inh}) substrates, λ is the maximal regulation rate, k is the Hills coefficient

representing activation or inhibition, and *x* is the substrate concentration [103]. In the special case of *n*=1, the Hill function for activation is similar to the Michaelis-Menten equation. Perez-Correa et al. [107] argued the limitations of the Hill rate law for process control applications and added integrative action for minimization of transient effects.

2.2.4.3 Approximated kinetic expressions

Borger et al. [108] devised universal and condensed mathematical formula to approximate kinetics for enzymatic reactions, which curbed the need to quantify a great many reaction parameters through experimental validation. This results in relatively similar model predictions in comparison to mechanistic expressions despite the generalization of several parameters. Literature studies that have derived approximated reaction kinetics for dynamic modelling are listed in Table 2.6.

Table 2.6: Mathematical formulation and description of approximated rate expressions for kinetic modelling of dynamic systems.

Approximate kinetic expresssion	Mathematical formulation	Description	Ref.
Lin-log kinetics	$r_j = \frac{e_f}{e_f^0} J_j^0 \left(1 + \sum_{k=1}^{M} \varepsilon_{j,k}^{0} \log \frac{N_k}{N_k^0}\right)$	A linear expression of logarithms for mechanisms involving high enzyme content. r represents rate law for j^{th} reaction in a network with M metabolite species.	[109]
Power laws	$r = \lambda \prod_{j=1}^{n_{subs}} \left(\frac{S_f}{S_f^0}\right)^{m_f} - \mu \prod_{k=1}^{n_{prod}} \left(\frac{P_k}{P_k^0}\right)^{n_k}$	In power law, the coefficients λ and μ represent the summation of forward and reverse rates, which specifically interact with the substrate S and product P.	[103]
Modular rate laws	$r = T \frac{E_0 . f_r}{D + D^{reg}}$	Modular rate laws primarily account for allosteric regulation of enzymes through the terms f_r, D and D^r and considers T as the stoichiometric parametrization.	[110]

2.2.5 Model refinement and optimization

A suitable objective function has to be implemented to refine the modelling performance and prediction accuracy. In kinetic systems, the metabolic models are underdetermined because the number of fluxes are greater than the metabolites [5], [105]. For instance, S is typically a non-square matrix where reaction fluxes (*j*) greatly outnumber the metabolites (*i*). Hence, the computer model requires an optimization strategy in the form of linear programming to solve for the vector of reaction fluxes (ø) [105]. Linear programming recognizes optimal solutions by maximizing or minimizing an objective function while placing caveats on the variability of the reaction fluxes [105], [111]. The linear programming optimization model for a series of reaction fluxes (i) and metabolites (j) in a steady-state metabolic network can be seen in Eq. 7.

$$\begin{aligned} &\text{Maximize/Minimize:} && Z_p = \textstyle\sum_{j \in P}\, c_j v_j \qquad \forall\, i \,\in\, N \\ &\text{Subject to:} && \textstyle\sum_{j=1}^{M} S_{ij} v_j = 0 \end{aligned} \tag{7}$$

In Eq. 7, S_{ij} is the stoichiometric matrix for a metabolic network, which is made of metabolites (*i*) and reaction fluxes (*j*). c_j represents the weight factor assigned to each reaction flux in reference to its importance for the specific objective function [112].

Table 2.7: Description and application of various objective functions towards optimization of metabolic models.

Objective function	Mathematical expression	Purpose	Biological explanation	Ref.
Max biomass	$\max \frac{v_{biomass}}{v_{glucose}}$	Maximization of growth rate	Evolutionary drive for maximising biomass yield	[113]
Max ATP	$\max \frac{v_{ATP}}{v_{glucose}}$	Maximisation of ATP uptake efficiency	Evolutionary drive for maximising energy efficiency	[114]
Min $\sum v^2$	$\min \sum_{i=1}^{n} v_i^2$	Minimization of the overall flux rates within the cell	Maximising efficient performance of enzymes for cellular growth	[115]
Min glucose	$\min \frac{v_{glucose}}{v_{biomass}}$	Minimization of glucose uptake	Evolutionary drive for efficient consumption of glucose	[116]
Min reaction steps	$\min \sum_{i=1}^{n} y_i^2, y_i \in [0,1]$	Minimization of steps required for each reaction	Cells reduce reaction steps involved in biomass production	[111]

Objective function	Mathematical expression	Purpose	Biological explanation	Ref.
Min redox potential	$\min \frac{\sum_N v_{NADH}}{v_{glucose}}$	Minimization of redox potential	Cells reduce oxidisation reactions for higher energy efficiency	[114]
Min ATP production	$\min \frac{\sum_N v_{ATP}}{v_{glucose}}$	Minimization of fluxes involved in ATP production	Cellular growth occurs through minimal energy production and usage	[105]

Research studies, as seen in Table 2.7, have explored objective function in the form of maximization of biomass growth and ATP production or minimization of glucose uptake and NADH/NADPH production [117]. Angione [118] disputes the assumption that states a cell would optimize the metabolic network towards a higher growth rate. On a biological and evolutionary basis, cellular functionality does not always necessitate maximum biomass as seen in human cells [119]. However, metabolic models considering microorganisms can safely assume the cellular goal is to maximize growth rate [120].

2.3 Metabolic regulation and biosynthesis pathways

2.3.1 Central Carbon Metabolism

Several research studies have been conducted on elucidating the pathways involved in the central carbon metabolism of oleaginous microalgae as seen in [121], [122], [114], [3], [123] and [124]. Within the central carbon metabolism, research studies have expanded on glycolysis, pentose-phosphate pathway (PPP), tricarboxylic acid (TCA) cycle, and the Calvin cycle under mixotrophic, autotrophic and heterotrophic conditions [82].

Glucose is a preferred source of carbon and energy for microalgae except for species such as *C. reinhardtii*, which lack the capacity to uptake complex compounds containing more than two carbon units [121]. When glucose is transported to the cytosol, it undergoes oxidation through the glycolytic route to form pyruvate, oxidation through PPP pathway to form ribose 5-phosphate or accumulated in the form of lipids or polysaccharides [125]. The glycolytic route includes the

Embden-Meyerhof pathway (EMP) and PPP pathway for carbon catabolism, which differ by transpiring solely in light and dark conditions respectively [126]. Under anaerobic and light conditions, glucose catabolism results in the formation of lactate through the EMP route [82].

Glycerol assimilates into the cell through passive transport and renders biochemical and structural transformations in the photosynthetic functionality of the cell. It reduces phycoerythrin content, degree of thylakoid packing and the number of thylakoid discs present in an individual cell [40]. Glycerol plays the role of an osmoregulatory molecule, which undergoes phosphorylation to form glycerophosphate in the presence of ATP and subsequent oxidization into triose phosphate [127]. Consequently, the intermediates transform into glyceraldehyde 3-phosphate and glycerate, which form pyruvate that proceeds to the TCA cycle for fatty acid synthesis [128].

In the presence of organic carbon substrate, carbon trickles through the TCA cycle for respiration and production of energy compounds such as ATP and NADPH, which limits flux through the Calvin cycle. Henceforth, the enzymes in the TCA cycle are most active at energy production in heterotrophic growth phase as opposed to photosynthetic conditions, where production of biosynthetic precursors alone is observed [82]. Since the TCA cycle is responsible for production of metabolic intermediates, which lead to lipid, and amino acid production such as acetyl-CoA, oxaloacetate and alpha-ketoglutarate (AKG) [129]. Along with the TCA cycle taking place in the mitochondria, oxidative phosphorylation generates glucose 6-phosphate (G6P), a biomass precursor and imperative towards respiration [40].

In autotrophic growth conditions, the electron transport chain (ETC) uses protons from light to amass energy in the form of ATP and NADPH in the thylakoid membrane of a chloroplast [82]. The energy compounds, ATP and NADPH, undertake conversion of CO_2 molecules into

triose phosphates (G3P) in the Calvin cycle [130]. Further reactions transform G3P into glucose 6-phosphate (G6P), sucrose, starch and other complex carbohydrates in the chloroplast [125].

2.3.2 Amino acid metabolism

In this research, glycine is integrated into the system as a nitrogen source and the metabolic pathway of glycine assimilation mapped based on literature studies [131], [132]. Glycine dehydrogenase converts glycine into Methylenetetrahydrofolate (MEETHF), which has a single carbon unit [132]. MEETHF coalesces with some of the glycine to form an amino acid serine. Some of the glycine undergoes transamination and the glyoxylate formed flows to the glyoxylate shunt [131]. The residual glycine content is utilized for protein formation.

An observable drop in the activity of glycine dehydrogenase occurs in nitrogen deficient conditions as most of the glycine is directed to the glyoxylate shunt [132]. The reduction in the activity of glycine dehydrogenase results in lower consumption of energy compounds ATP and NADPH [133], [134]. Glycine dehydrogenase also releases nitrogen from the glycine molecule in the form of ammonia [132]. Hence, the cell maintains nitrogen content by regulating glycine assimilation through transamination without requiring energy. This energy is conserved by lipid accumulation through fatty acid synthesis and the pool of lipids is reserved in the cell during the high stress conditions [134].

2.3.3 Fatty acid synthesis

Fatty acids involve organic acids with a carboxylic functional group and an aliphatic chain in saturated (SFA), monounsaturated (MUFA) or polyunsaturated (PUFA) form [135]. According to Zuniga et al. [136], oleaginous microalgae generate lipids in the form of triacylglycerol (TAG), phosphatidylglycerol (PG), phosphatidylinositol (PI), phosphatidylethanolamine (PE), sulfoquinovosyldiglycerol (SQDG), monogalactosyldiacylglycerol (MGDG),

digalactosyldiglycerol (DGDG) and phosphatidylcholine (PC). Several research studies, such as [137]–[141], have explored the influence of nitrogen deficient conditions on enhancing lipid accumulation. In a high stress environment, the carbon flux is directed away from biomass growth towards fatty acid synthesis in order to store energy through lipid accumulation [82].

Initially, an intermediate formed from glycolysis in the cytosol, pyruvate, is transported to the chloroplast for an oxidative reaction. Acetyl-CoA (coenzyme A) is a primary precursor for fatty acid synthesis and transpires from the oxidative decarboxylation of pyruvate [142]. Fatty acid synthesis entails the formation of malonyl-CoA from acetyl-CoA and bicarbonate in the presence of the enzyme acetyl-CoA carboxylase (ACCase) [143], [144]. Further catalysis steps are carried out on elongation of fatty acids by enzymes known as beta-ketoacyl-ACP reductase (KAR), hydroxyacyl-ACP dehydrase (HAD), and enoyl-ACP reductase (EAR) [145]. Subsequently, the elongated fatty acids enter the cytosol for triacylglycerol (TAG) synthesis [135]. Aside from other storage compounds, TAG forms a significant portion of the dry cell weight (30-60 %) [146].

2.3.4 Terpenoid backbone and Carotenoid biosynthesis

Carotenoids are a category of terpenoids or isoprenoids, which are formed from two distinct biosynthetic pathways known as the mevalonate (MVA) and the 2-C-methyl-D-erythritol 4-phosphate (MEP) pathway [147]. Microorganisms differ from higher plants in that only a singular pathway can be facilitated based on the respective cellular activity. Prokaryotes such as cyanobacteria and eukaryotes such as microalgae can only perform terpenoid synthesis through the MVA and MEP pathway respectively [147], [148]. While Chlorophyta (green algae) derived the MVA pathway by a eukaryotic host cell through endosymbiosis, the pathway became inactive over time in subgroups of algae. The genetic information was rendered inessential to the survival

of the organism for species such as *Chlamydomonas reinhardtii*, *Scenedesmus obliquus* and *Chlorella fusca* [149].

The MEP pathway produces an intermediary DXP from a condensation reaction involving pyruvate and glyceraldehyde 3-phosphate [150]. Subsequent transformations of the intermediaries involve reduction and several catalytic reactions, which lead to 1-hydroxy-2-methyl-2-(E)-butenyl-4-diphosphate (HMBPP) [151]. HMBPP reductase regulates the conversion of HMBPP to a 6:1 ratio of isopentenyl pyrophosphate (IPP) and dimethylallyl pyrophosphate (DMAPP) depending on the cellular functionality [148].

A condensation reaction combines IPP and DMAPP into either geranyl diphosphate (GPP) or farnesyl diphosphate through two distinct enzymes GPP synthase and FPP synthase [150]. GPP leads to the formation of geranyl geranyl pyrophosphate (GGPP), which is a primary precursor for the synthesis of carotenoids, gibberellins, tocopherols and chlorophylls [152]. GGPP is condensed to form phytoene, the first carotenoid in the biosynthetic pathway, in order to produce lycopene [153]. Several catalysis reactions transform lycopene into β-carotene, γ-carotene, torulene, torularhodin and astaxanthin [154]. Carotenoid diversity and accumulation can be enhanced by modulating the carbon sources in the media. Several studies have reported glycerol as a significant contributor due to the overexpression of enzymes involved in the synthesis of primary precursors phosphoenolpyruvate and glycerate 3-phosphate [151], [155]. Alternatively, succinate enhances astaxanthin production when introduced as a supplemental carbon source [156].

2.3.5 Biomass formation

The metabolic reconstruction of biomass formation involves concentrating on primary biomass constituents such as carbohydrates, lipids, proteins, nucleotides and pigments [82]. The stoichiometry of the reactions is defined by the composition of precursor metabolites, such as

amino acids, nucleotides, fatty acids, and sugars, which make up the cellular mass [157]. Research has exhibited variations of the biomass reaction through genome scale models of multiple species such as *Bacillus subtilis, Escherichia coli, Klebsiella pneumoniae, Salmonella typhimurium, Mycobacterium tuberculosis, Thermotoga maritima, Synechocystis* [158]–[164]. Xavier et al. [165] contends discrepancies in biomass composition studies create unreliability in metabolic models. He reasons the reactions neglect essential cofactor synthesis since the compounds do not appear in the literature data [165].

A review of current literature informs best cultivation practices, which is heterotrophic cultivation, to obtain high production yields with low process economy. Since nutrient feed can largely contribute to the production costs of large-scale system, literature reports prove the biomass and product yields can be modulated by employing low-cost substrates such as glycerol. Optimization of these process conditions can enhance production yields due to the combinatory effect of optimal nutrient (organic carbon substrate proportion and nitrogen) levels. *A. protothecoides* is studied to utilize its robust abilities in synthesizing high lipid and antioxidant content.

The review of metabolic studies deduces the caveats and scope of the intracellular structure of the microalgal cell. Specific pathways dominate the dynamics of a microalgal cell's primary functions such as cellular growth and maintenance. Calvin-Benson cycle, TCA cycle, nitrogen assimilation, fatty acid synthesis are essential pathways that contribute to accumulation of macronutrients and biomass formation. An evolutionary study elucidates solely the MEP pathway is active in the *Chlorella* species.

Chapter 3: Materials and Methods

In this chapter, a description of the experimental setup and analytical methods employed in the research is included with the corresponding materials and equipment. The analytical stages study the biomass yield, lipid content, nutrient assimilation, specific antioxidant content, total antioxidant content of the batch level experiments.

3.1 Microalgal strain

Experiments were conducted with the microalgal strain *Auxenochlorella protothecoides* (UTEX 25), which was retrieved from University of Texas at Austin, USA [14]. The microalgal culture was maintained under heterotrophic conditions in 4x basal medium with organic carbon substrate at 25^{o}C, 100 rpm and a light/dark cycle of 16/8 hours.

3.2 Chemical Reagents

The chemical reagents involved in the cultivation, experiments and analysis are listed in Table 3.1 with their respective CAS ID and supplier.

Table 3.1: Description of chemical reagents utilized in culture medium and experimental analysis.

Molecular formula	Chemical name	CAS ID	Supplier
Potassium phosphate dibasic	K_2HPO_4	7758-11-4	Fisher-Scientific
Potassium phosphate monobasic	KH_2PO_4	7778-77-0	Fisher-Scientific
Iron sulfate	$FeSO_4.7H_2O$	7720-78-7	Fisher-Scientific
Magnesium sulfate	$MgSO_4.7H_2O$	7487-88-9	Fisher-Scientific
Thiamine hydrochloride	$C_{12}H_{17}N_4OS+$	67-03-8	Sigma-Aldrich
Calcium chloride	$CaCl_2.2H_2O$	10043-52-4	Fisher-Scientific
Glycine	$C_2H_5NO_2$	56-40-6	Fisher-Scientific
Glucose	$C_6\ H_{12}O_6$	50-99-7	Amresco
Glycerol	$C_3H_8O_3$	56-81-5	Fisher-Scientific

Molecular formula	Chemical name	CAS ID	Supplier
Hexane	C_6H_{14}	110-54-3	Fisher-Scientific
Acetone	C_3H_6O	67-64-1	Fisher-Scientific
Ethanol	C_2H_5OH	64-17-5	Merck Canada
Nitrogen	N_2	7727-37-9	Praxair
Methanol	CH_3OH	67-56-1	Fisher-Scientific
Ethyl acetate	$CH_3COOC_2H_5$	141-78-6	Fisher-Scientific
Acetonitrile	CH_3CN	75-05-08	Fisher-Scientific
Sodium hydrogen phosphate monobasic	H_4NaO_5P	7558-79-4	Fisher-Scientific
OPA	$C_8H_6O_2$	643-79-8	Fisher-Scientific
Borate buffer	Na_2B_4O	1303-96-4	Fisher-Scientific
Sodium hydroxide	NaOH	1310-73-2	Fisher-Scientific
Sulfuric acid	H_2SO_4	7664-93-9	Anachemia Canada Co.
Trolox	$C_{14}H_{18}O_4$	53188-07-1	Fisher-Scientific
ABTS	$C_{18}H_{18}N_4O_6S_4$	30931-67-0	Fisher-Scientific
Sodium Chloride	NaCl	7440-23-5	Fisher-Scientific
Potassium Chloride	KCl	7440-09-7	Fisher-Scientific
Sodium hydrogen phosphate dibasic	Na_2HPO_4	10028-24-7	Fisher-Scientific

3.3 Microalgal cultivation

3.3.1 Inoculum cultivation conditions

The microalgal culture was maintained in aerated 1000 ml flasks with an equal proportion of both carbon substrates glucose and glycerol at an overall concentration 20 $g.L^{-1}$ in 300 ml of total culture medium. Prior to inoculation, the flask containing the culture medium was sealed and sterilized at 120°C and 103 kPa in an autoclave. The flasks were maintained on tabletop orbital shaker (Thermo Scientific^{TM} MaxQ416^{TM}) at 100 rpm. The culture was placed in a 16/8 hour light-

dark cycle under 110-130 V, 60 Hz and 0.4 A fluorescent lamps (Genuine sun blaster) at 25°C for a five-day period before inoculating the experiment at 10% volume.

3.3.2 Microalgal growth medium

A four times concentrated basal (4x basal) solution, which consists of glucose, glycerol, glycine and vitamin B1 was prepared for the growth medium. The nutrient content of the growth medium for microalgal cultivation is listed in Table 3.2.

Table 3.2: Chemical composition of the 4x basal media used for microalgal cultivation.

Chemical composition	Chemical formula	Concentration in culture medium ($g.L^{-1}$)
Potassium phosphate dibasic	K_2HPO_4	1.2
Potassium phosphate monobasic	KH_2PO_4	2.8
Iron sulfate	$FeSO_4.7H_2O$	0.048
Magnesium sulfate	$MgSO_4.7H_2O$	1.2
Thiamine hydrochloride (vit B1)	$C_{12}H_{17}N_4OS+$	4×10^{-5}
Calcium chloride	$CaCl_2.2H_2O$	0.01
Nitrogen source (Glycine)	NH_2CH_2COOH	Variable
Arnon 5		
Boric acid	H_3BO_3	1.16×10^{-5}
Manganese chloride	$MnCl_2.4H_2O$	7.2×10^{-6}
Zinc sulfate	$ZnSO_4.7H_2O$	8.8×10^{-7}
Copper sulfate	$CuSO_4.5H_2O$	3.2×10^{-7}
Molybdenum oxide	MoO_3	7.2×10^{-8}

3.4 Experimental analysis

3.4.1 Dry weight analysis

Microalgal growth was assessed using dry weight analysis through daily samples collected from the experiments. During the experiment, 2 ml samples of the microalgal culture were

collected daily in pre-weighted micro-centrifuge tubes (PP Natural, 2 ml). The supernatant was separated from the microalgal biomass using a centrifuge (Beckman Coulter Allegra X-22R) for 12 minutes at 3901 rcf. The supernatant was carefully stored in HPLC vials after filtration for analysis of nutrient consumption. The remaining biomass pellets were washed with Phosphate buffered saline (PBS), containing 17.5 $g.L^{-1}$ KH_2PO_4 and 7.5 $g.L^{-1}$ K_2HPO_4, to remove the residual salts from the culture. After separation of fluids using the centrifuge, the tubes were placed under vacuum conditions at -50°C in freeze dryer (TOPT-10C Toption group Co. Ltd.) for 24 hours. After drying, the mass of the microcentrifuge tubes with and without biomass pellets, m_t and m_{t+p} respectively, was weighed using an analytical balance (Kern ABT 120-5DM) and substituted in Eq. 8 to determine the biomass growth in $g.L^{-1}$.

$$\frac{(m_{t+p}-m_t)\ g}{1\ ml} \cdot \frac{1000\ ml}{1} \tag{8}$$

3.4.2 Substrate consumption

The supernatant was separated from the daily samples and filtered for the analysis of glucose and glycerol content present in the medium. Hence, the consumption of organic carbon substrate was determined through high-performance liquid chromatography (Agilent 1260) with the Hi-plex H column (p/n PL1170-6830). The method details are included in Table 3.3.

Table 3.3: HPLC column methodology for analysis of glucose and glycerol consumption using the Agilent HPLC system.

Method settings	Description
HPLC column	Agilent Hi-Plex H
Column dimensions	7.7 x 300 mm
Particle diameter	8 µm
Eluent	0.005 M H_2SO_4
Eluent flowrate	0.5 $ml.min^{-1}$
Injection volume	20 µL
Column temperature	65°C

Method settings	Description
Column pressure	60 bar
Detection method	RI (35°C)

3.4.2.1 Calibration curve for glucose and glycerol

Glucose and Glycerol calibration was carried out using five proportions of standard solutions in concentration range of 5-25 $g.L^{-1}$. The standard solutions were run through the HPLC analysis method and the results used to plot a calibration curve.

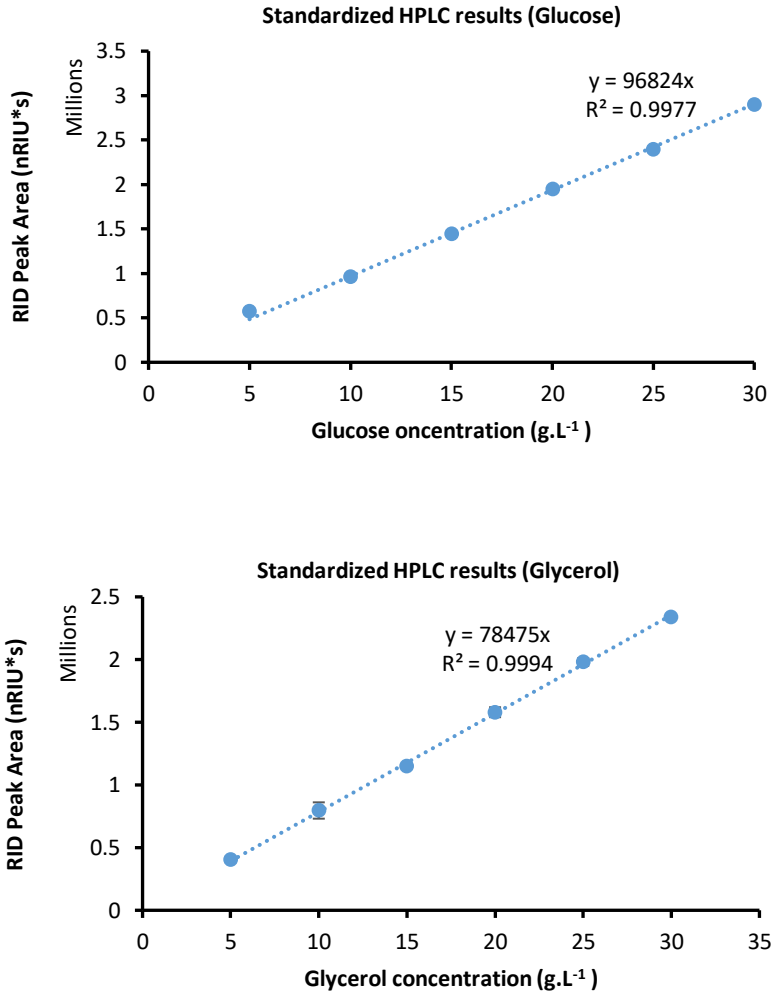

Figure 3.1: Standard calibration curve for glucose and glycerol using standard concentrations 5-25 $g.L^{-1}$.

In Figure 3.1, the graph crossing the origin is used to derive Eq. 9 and 10, which determines the carbon content in experimental samples.

$$C_{glucose}\ (g.L^{-1}) = \frac{sample\ area}{96824} \quad (9)$$

$$\mathrm{C_{glycerol}\ (g.L^{-1})} = \frac{\mathrm{sample\ area}}{78475} \quad (10)$$

3.4.3 Glycine assimilation

3.4.3.1 Derivatization of amino acids for HPLC analysis of glycine

Glycine assimilation is evaluated using the ortho-phthalaldehyde (OPA) chemistry protocol, which derivatizes amino acids for high-performance liquid chromatographic (HPLC) analysis with the Agilent 1260 system. The method protocol for the amino acid analysis is shown in Table 3.4.

Table 3.4: HPLC column methodology for analysis of glycine assimilation using Agilent HPLC system.

Method settings	Description
HPLC column	ZORBAX Eclipse AAA
Column dimensions	4.6 x 150 mm
Particle diameter	3.5 µm
Eluent	Solvent A: 40 mM NaH_2PO_4 pH 7.8 Solvent B: Acetonitrile: Methanol: water (45:45:10, v/v)
Eluent flowrate	2 ml/min
Injection volume	Refer to injection program
Column temperature	35°C
Column pressure	220 bar
Detection method	UV/Vis detection 338 nm, 10 nm bandwidth Reference: 390 nm, 20 nm bandwidth

According to the method for Eclipse Zorbax AAA column, the injector program for the derivatization of amino acids is entered into the HPLC autosampler G1313A.

1. Draw 2.5 µL from the borate buffer vial.
2. Draw 0.5 µL from sample
3. Mix 3 µL "in air" at maximum speed and repeat twice.
4. Wait 0.5 min.
5. Draw 0 µL from uncapped vial of water for needle wash.
6. Draw 0.5 µL from the vial containing OPA reagent.
7. Mix 3.5 µL "in air" at maximum speed and repeat six times.
8. Draw 32 µL from the capped vial containing water.
9. Mix 18 µL "in air" at maximum speed and repeat twice.

The variation in gradient elution for the analytical method is listed in Table 3.5. The solvents vary from the sodium hydrogen phosphate monobasic buffer to the solvent mixture of acetonitrile, methanol and water.

Table 3.5: Gradient flow ratio of Eluent A and B through the ZORBAX Eclipse AAA column for glycine analysis.

Time (min)	Eluent A	Eluent B
0	100	0
1.9	100	0
18.1	43	57
18.6	0	100
22.3	0	100
23.2	100	0
26	100	0

3.4.3.2 Calibration curve for glycine

Glycine calibration was carried out using standard solutions for a concentration range of 0.005 – 0.1 mol.l^{-1} in five proportions. The resulting values from the chromatographic analysis were plotted on Figure 3.2.

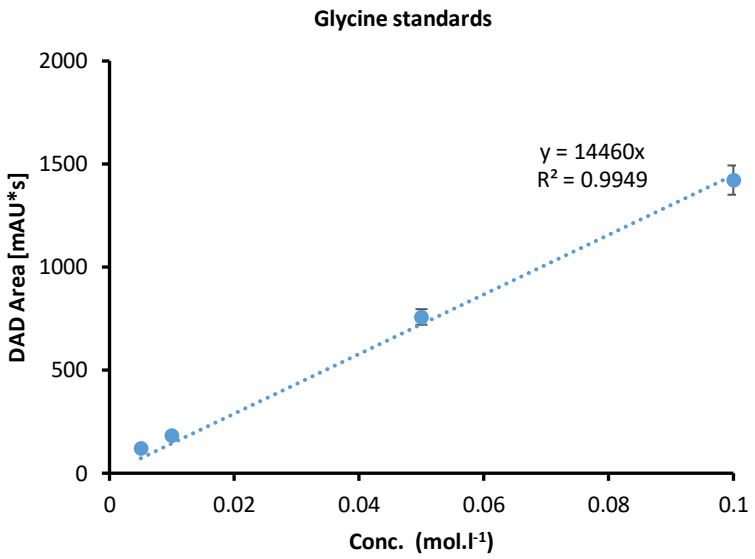

Figure 3.2: Standard calibration curve for glycine using standard concentrations of 0.005-0.1 mol.l^{-1}.

The graph crosses the origin for a zero intercept and the straight-line equation helps determine the glycine content in experimental samples as seen in Eq. 11.

$$C_{glycine}\ (g.l^{-1}) = \frac{sample\ area\ .75}{14460} \quad (11)$$

3.4.4 Recovery of microalgal products

The total biomass from the experiment was freeze dried for 48 hours at -50°C vacuum conditions using the freeze dryer (TOPT-10C Toption Group Ltd.). Subsequently, 200 mg of the dried biomass was measured and collected for cell disruption. The cell disruption was carried out using a homogenizer (PT 2500 E system) with a 7 mm probe at 25000 rpm in a small portion of hexane.

3.4.4.1 Product recovery (Solvent extraction)

The homogenized sample undergoes solvent extraction to recover polar and non-polar antioxidants. The sample was dissolved in 2 ml of an individual solvent and separated using the centrifuge (Beckman Coulter Allegra X-22R) for 12 minutes at 3901 rcf. The antioxidant recovery followed a series of solvent extractions using hexane, ethyl acetate and water. The hexane and ethyl acetate extracts were dried with nitrogen gas while the water assay was immediately used towards total antioxidant analysis.

3.4.4.2 Lipid content analysis

The hexane extract, from the solvent extraction method, was transferred to a pre-weighed glass tube and dried in a nitrogen gas environment. The residual extract was weighed on an analytical balance (Kern ABT 120-5DM) and substituted in Eq. 12.

$$\text{Lipid content } (g.gDW^{-1}) = \frac{(m_f - m_i)}{m_b} \tag{12}$$

3.4.4.3 Total antioxidant evaluation (Trolox equivalent antioxidant capacity)

Trolox equivalent antioxidant capacity (TEAC) is a proven and reliable method for antioxidant evaluation [166] . The scavenging effect of the extracts in comparison to Trolox on an $ABTS^+$ radical determines the total antioxidant content of the solvent extracts. An $ABTS^+$ stock solution is prepared by mixing equal proportions of solution A containing 7mM ABTS (7.18 mg in 1 ml of distilled water) and solution B containing 2.45 mM potassium persulfate (13.2 mg in 10 ml of water). The stock solution was left for 12-16 hours in the dark and used up within two days. A working solution was developed by adding ethanol and adjusting absorbance to 0.700 ± 0.05 at 734 nm in the UV spectrophotometer (VWR UV-3100 PC). A calibration curve was prepared using a 1.5 mM stock solution of Trolox and the final concentrations are listed in Table 3.6.

Table 3.6: Standard solutions used for Trolox equivalent antioxidant calibration (TEAC) assay.

Trolox stock solution (µL)	PBS (µL)	Final concentration (µM)
0	1000	0
30	970	75
40	960	100
50	950	125
60	940	150
90	910	225
120	880	300

From the concentrations prepared in Table 3.6, 40 µL of Trolox solution was introduced to the disposable cuvettes in addition to 800 µL of ABTS radical cation working solution. The Trolox solution was allowed to react with the ABTS cation for 15 minutes at room temperature. After the designated time, the absorbance was measured for each cuvette and plotted to obtain a calibration curve as seen in Figure 3.3.

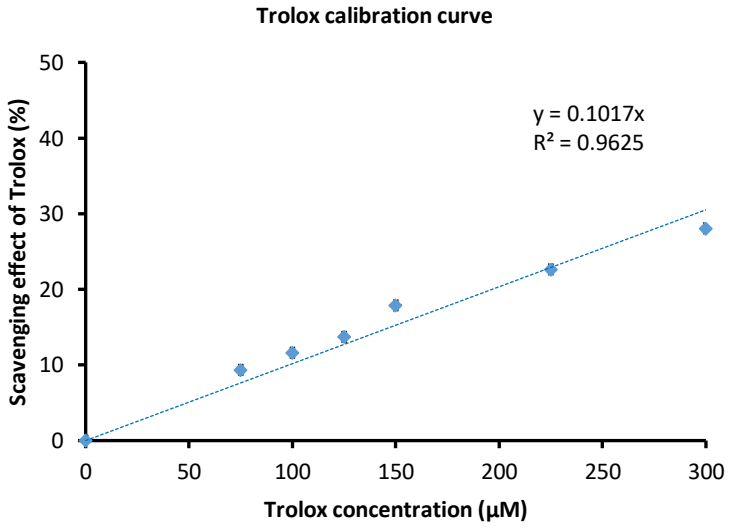

Figure 3.3: Trolox calibration curve by investigating the scavenging effect of Trolox at various concentrations.

Subsequently, ethanol was introduced to the dried hexane and ethyl acetate extracts. About 40 µL of the sample was mixed with 800 µL of the ABTS working solution and allowed to react for 15 minutes at room temperature. The absorbance of the reaction mixture was tested at 734 nm to investigate the scavenging effect of the antioxidant assay. Hence, the hexane, ethyl acetate and water assay were tested and expressed as µmol Trolox.gDW^{-1} of microalgae.

3.4.4.3.1 Specific antioxidant compound analysis

The hexane extract from the solvent extraction method was dried in nitrogen gas. The residual extract was dissolved in 1 ml of a solution of acetone and methanol (50:50 v/v). This sample is analyzed using the specific antioxidant analysis method as seen in Table 3.7.

Table 3.7: HPLC column methodology for analysis of lutein and zeaxanthin through the Agilent HPLC system.

Method settings	Description
HPLC column	Poroshell 120 EC-C18
Column dimensions	4.6 x 50 mm
Particle diameter	2.7 µm
Eluent	Solvent A: Water:Methanol 1:4 v/v Solvent B: Acetone:Methanol 1:1 v/v
Eluent flowrate	2 $ml.min^{-1}$
Injection volume	5 µL
Column temperature	35°C
Column pressure	260 bar
Detection method	UV/Vis detection 425 ± 3 nm, 446 ± 3 nm, 474 ± 3 nm

The gradient elution levels are listed in detail in Table 3.8 as the solvents switch between aqueous and organic elements for enhanced separation of the lipophilic antioxidants.

Table 3.8: Gradient flow ratio of eluent A and B through the Poroshell EC-C18 column for antioxidant analysis.

Time (min)	Eluent A	Eluent B
2	75	25
5	25	75
6	10	90
8	0	100
9	75	25

3.5 Batch reactor setup

The batch reactor experiment was carried out at five different settings for the glucose and glycerol proportion but the overall carbon concentration remained 20 $g.L^{-1}$ for all experiments. The glycerol content was adjusted to ensure the number of moles of carbon were equivalent to glucose as seen in Table 3.9. The nitrogen content was varied on a molar basis at six different settings of Carbon to Nitrogen ratio (C:N 10:1, 40:1, 60:1, 80:1, 240:1 and 480:1) with reference to the total moles of carbon. The culture medium was sterilized in an autoclave at 120°C and 103 kPa before the addition of 10% inoculum.

Table 3.9: Carbon source proportion in five different settings for the batch level operation of *A. protothecoides*.

Batch reactor setting Glucose:Glycerol	Culture medium	Volume added of glucose (0.2 $g.ml^{-1}$)	Volume added of glycerol (0.2 $g.ml^{-1}$)	10% inoculum	Total
100:0	80	10	0	10	100
75:25	80	7.5	2.5	10	100
50:50	80	5	5	10	100
25:75	80	2.5	7.5	10	100
0:100	80	0	10	10	100

Daily samples were collected from the batch reactors to analyze the biomass growth, organic substrate and glycine consumption over the experimental duration. At the end of the experiment, the total biomass was washed with Phosphate buffered saline solution and placed at -50°C in freeze dryer (TOPT-10C Toption group Co. Ltd.) for 24 hours to remove moisture content. The dried biomass was used to study total antioxidant, specific antioxidants, lipid content and overall biomass growth. The experimental setup, as seen in Figure 3.4, includes a sampler system and filtered air was used to avoid residue buildup in the sampling tubes.

Figure 3.4: Batch level operation of *A. protothecoides* at varying proportions of carbon source and nitrogen content.

Chapter 4: Study effect of nutrients on product composition

In this chapter, the observations and production yields are discussed comprehensively from the batch level operation of the microalgal system at varying proportion of carbon source and nitrogen content. The biological structural changes that result in chloroplast disintegration explain the discoloration of the microalgal culture in glucose rich and nitrogen deprivation conditions. The optimal conditions for lipid and antioxidant yield are observed to be glucose rich and glycerol rich conditions respectively. However, there is a threshold for nitrogen deprivation conditions after which high product yields are considered redundant with the stunted growth of microalgal biomass. With regards to product synthesis, the glycerol rich conditions resulted in significantly high lutein and zeaxanthin content in comparison to current literature. The biomass yield with respect to the consumption of carbon source is much higher for *A. protothecoides* as opposed to bacterial cultures due to the complexity of its metabolic pathways.

4.1 Modulation of photo-bleaching effect with addition of glycerol

Different carbon sources have varying effects on the physiological structure of the cell as the heterotrophic microorganism assimilates the compounds. Liao [167] explains the glucose-induced reduction in chlorophyll, which is a nitrogen-rich component, causes the discoloration of microalgal cultures in nitrogen deficient conditions. As seen in Figure 4.1, *A. protothecoides* experiences degeneration of chloroplasts, known as the glucose-induced bleaching effect, when grown in the presence of glucose [168].

Figure 4.1: Discoloration of *A. protothecoides* culture with variation in carbon source at five settings of glucose and glycerol (100:0, 75:25, 50:50, 25:75, 0:100 from left to right).

According to Oshio et al., the degradation of chlorophyll pigment is induced by the presence of an organic carbon substrate in *A. protothecoides* in nitrogen starvation [169]. The disappearance of chlorophyll concurrently results in the excretion of red bile pigments to the culture medium. The pigment formation is further explained by the chlorin ring opening up through an enzymatic process [170]. The presence of carotenoids, specifically lutein, remains constant or increases with the bleaching effect [169], [170]. On the other hand, the disappearance of chlorophyll pigment unmasks the characteristic color of such pigments which were not visually prominent in the prior case. The introduction of a nitrogen source to the cultivation medium reverses this process and results in the synthesis of chloroplasts. This phenomenon is known as re-greening in algal cultivation [171].

4.2 Assimilation of glucose and glycerol as organic carbon source

The consumption of glucose and glycerol was studied for the duration of the batch experiments. As seen in Figure 4.2 and Figure 4.3, the substrates were consumed rapidly in the experiments conducted with higher nitrogen content (C:N 10:1 and 40:1) since increasing cell density heightens assimilation of the organic carbon. Particularly, majority of glucose, the preferred source of carbon, was predominantly assimilated from the cultivation medium for all

carbon to nitrogen ratios. The microorganism derives a substantial amount of energy from the glucose source.

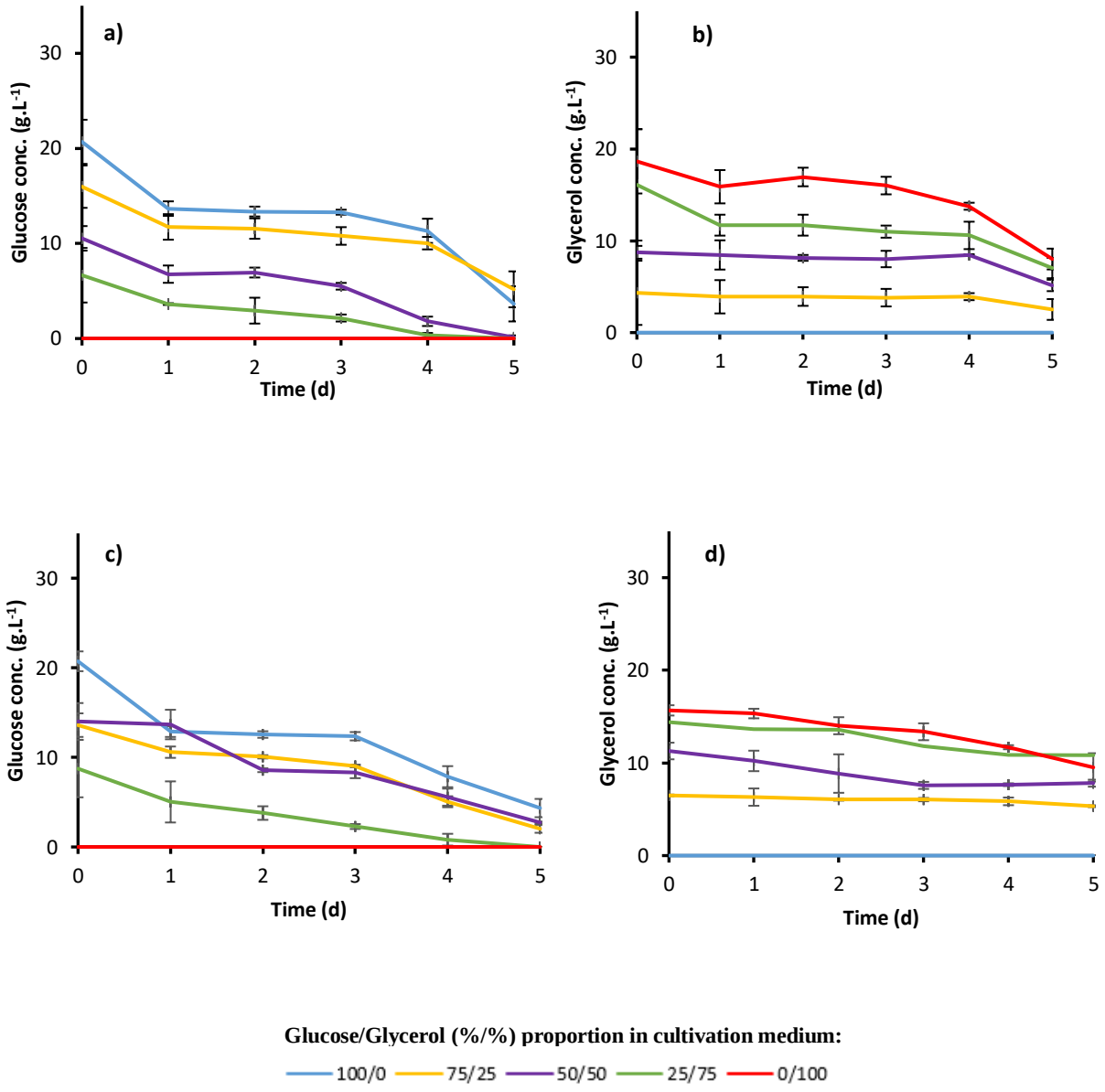

Figure 4.2: Substrate consumption analysis for glucose and glycerol in batch level operation of *A. protothecoides* at C:N content of 10:1 and 40:1. Images represent a) C:N 10:1 glucose, b) C:N 10:1 glycerol, c) C:N 40:1 glucose and d) C:N 40:1 glycerol consumption. Error bars represent ± σ.

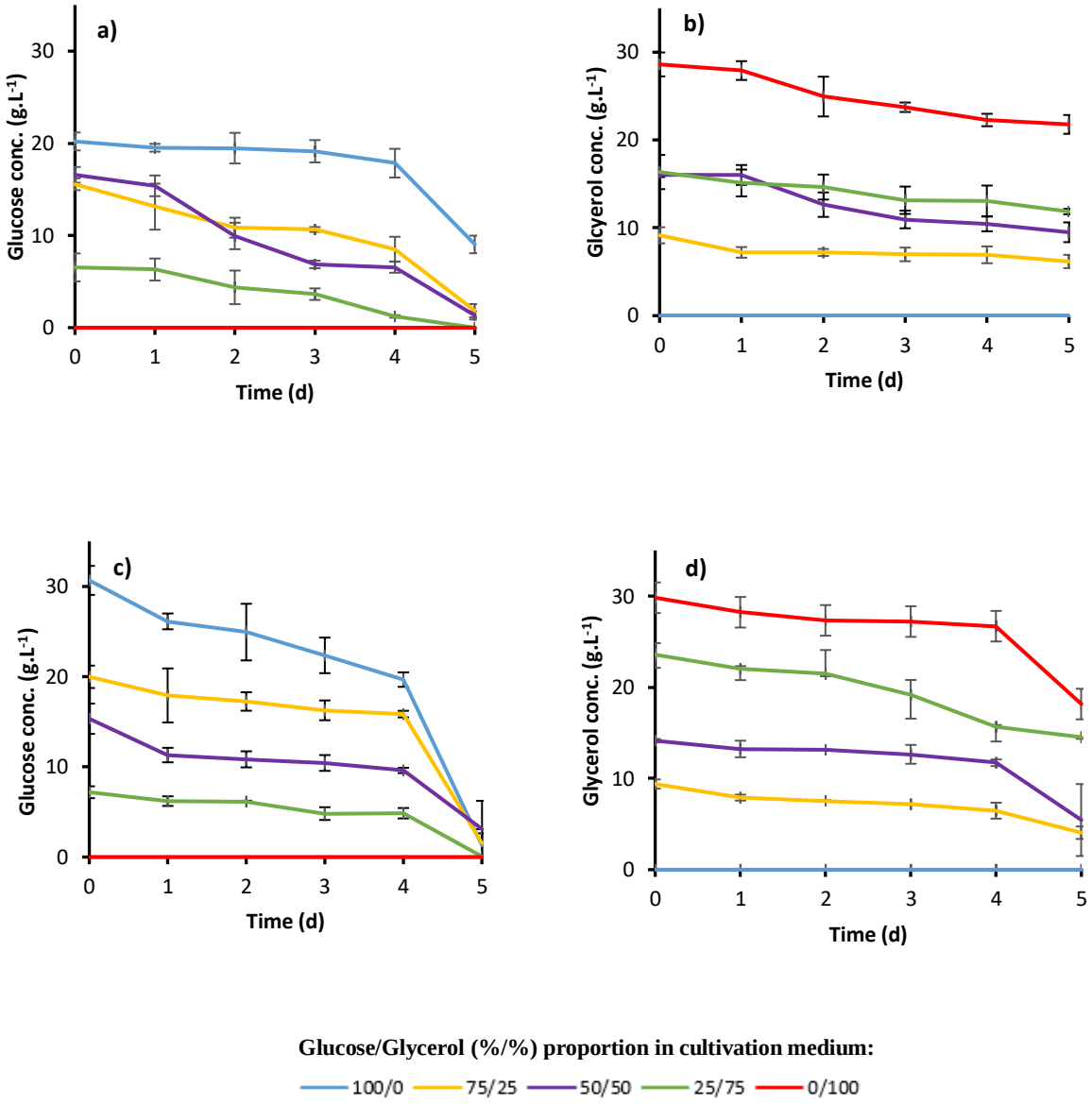

Figure 4.3: Substrate consumption analysis for glucose and glycerol in batch level operation of *A. protothecoides* at C:N content of 60:1 and 80:1. Images represent a) C:N 60:1 glucose, b) C:N 60:1 glycerol, c) C:N 80:1 glucose and d) C:N 80:1 glycerol consumption. Error bars represent ± σ.

On the other hand, glycerol consumption is at a slower rate in comparison to glucose. Specifically, the glycerol content experiences a substantial drop in C:N 10:1 ratio since more cells are available to consume energy from the medium. Furthermore, C:N 80:1 consumes a large amount of glycerol

due to the nitrogen deprived conditions placing the cell under duress. Alternatively, the C:N 40:1 and 60:1, which contain a higher nitrogen content despite the nitrogen limited conditions, assimilate a small amount of glycerol.

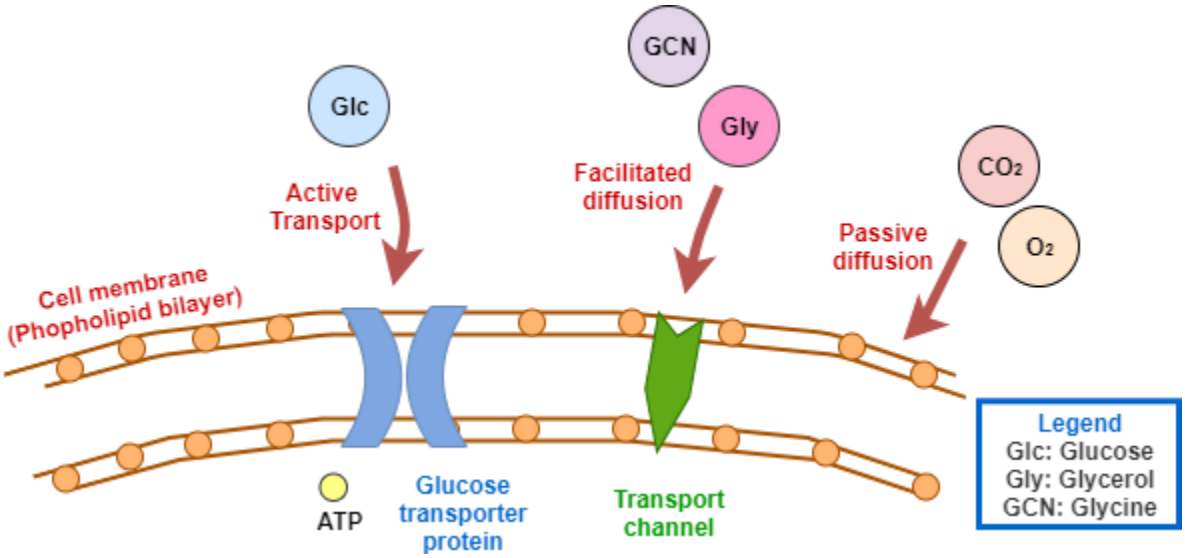

Figure 4.4: Active transport of glucose and passive diffusion of glycerol across cell membrane.

It is imperative to understand the transport kinetics of the carbon sources in order to explain their metabolism in microalgal cells. Active transport, which has an energy requirement, allows the transfer of glucose across the cell membrane through a transporter protein as observed in Figure 4.4 [172]. Glycerol, a smaller, osmoregulatory and lipid soluble molecule, is transported across the cell membrane through facilitated diffusion by aquaporin transport channels and subsequently prevents loss of nutrients in osmotic stress [173]. While glycerol is not a preferred source of carbon, the cell increases metabolism of glycerol as a compatible solute under salt stress [174]. The metabolism of glycerol promotes carotenoid biosynthesis, which enhances the presence of photo-protective receptors in the thylakoid membrane of chloroplasts [151], [155]. Hence, the presence of glycerol in cultivation medium modulates the pigment content and prevents the photo-bleaching effect.

4.3 Assimilation of glycine as source of nitrogen

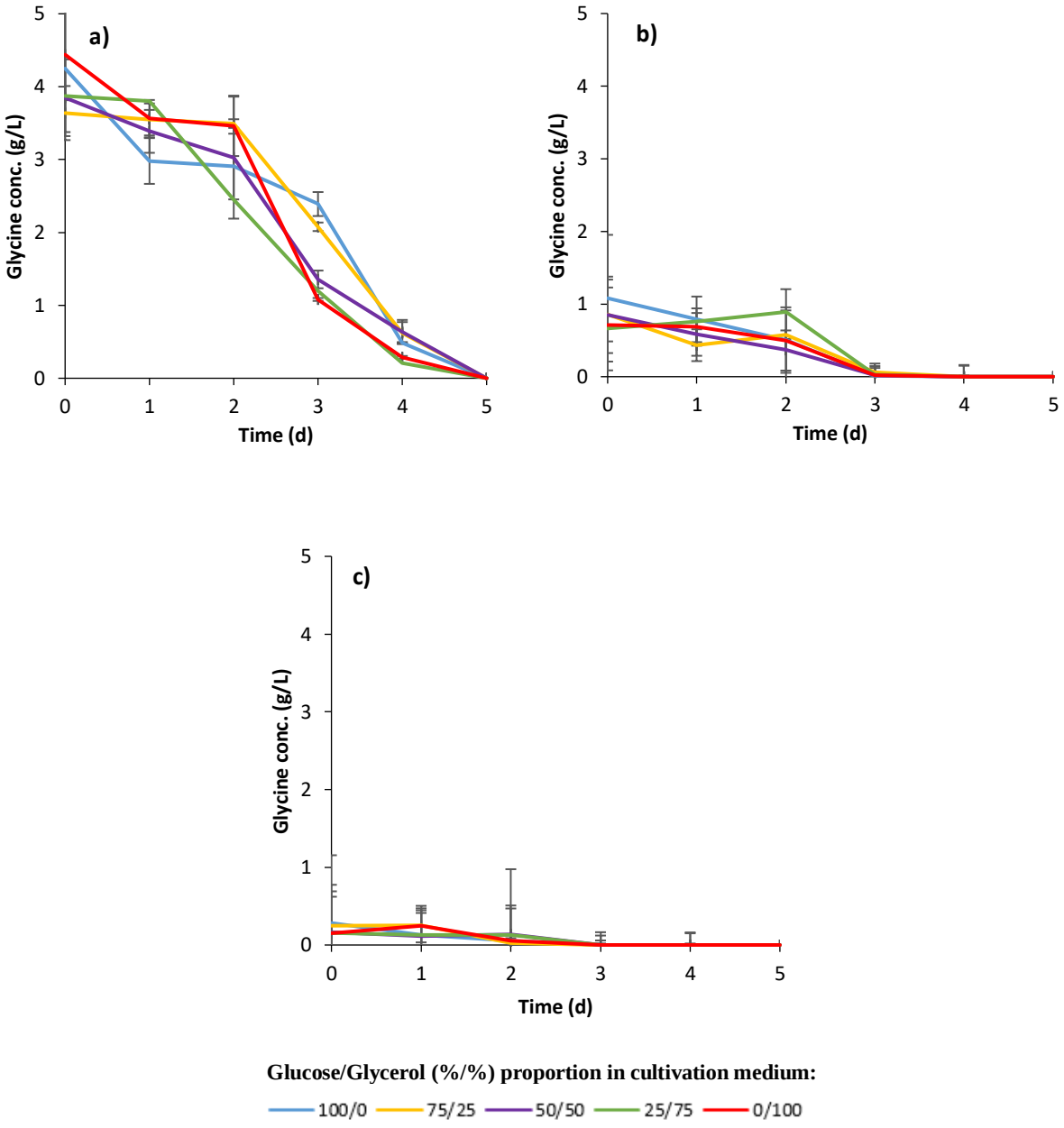

Figure 4.5: Glycine consumption in the batch level cultivation of *A. protothecoides* for C:N ratio of a) 10:1, b) 40:1 and c) 80:1. Error bars represent ± σ.

Glycine is a readily available free amino acid in the cultivation medium and immediately available for uptake by the microalgae [175]. A free amino acid is directly integrated in the synthesis of proteins but undergoes several metabolic reactions, involving ammonium formation,

towards synthesis of nitrogen-based compounds and other amino acids [176]. The integration of glycine involves intermediate metabolites from the carbon fixation stage (Calvin-Benson cycle). In Figure 4.5, the kinetics of amino acid integration are relatively slow in comparison to glucose. This behavior is attributed to the involvement of the intermediates from the carbon fixation stage. Once the intermediaries are acquired from photosynthetic functionality, the amino acid pool reaches maximal levels within the cell and inhibits transport of additional amino acids [175]. Hence, a reduction in amino acid uptake should be expected during daylight period and assimilation should resume in the darker period as amino acid pool depletes from growth.

4.4 Influence of nutrient variation on biomass growth

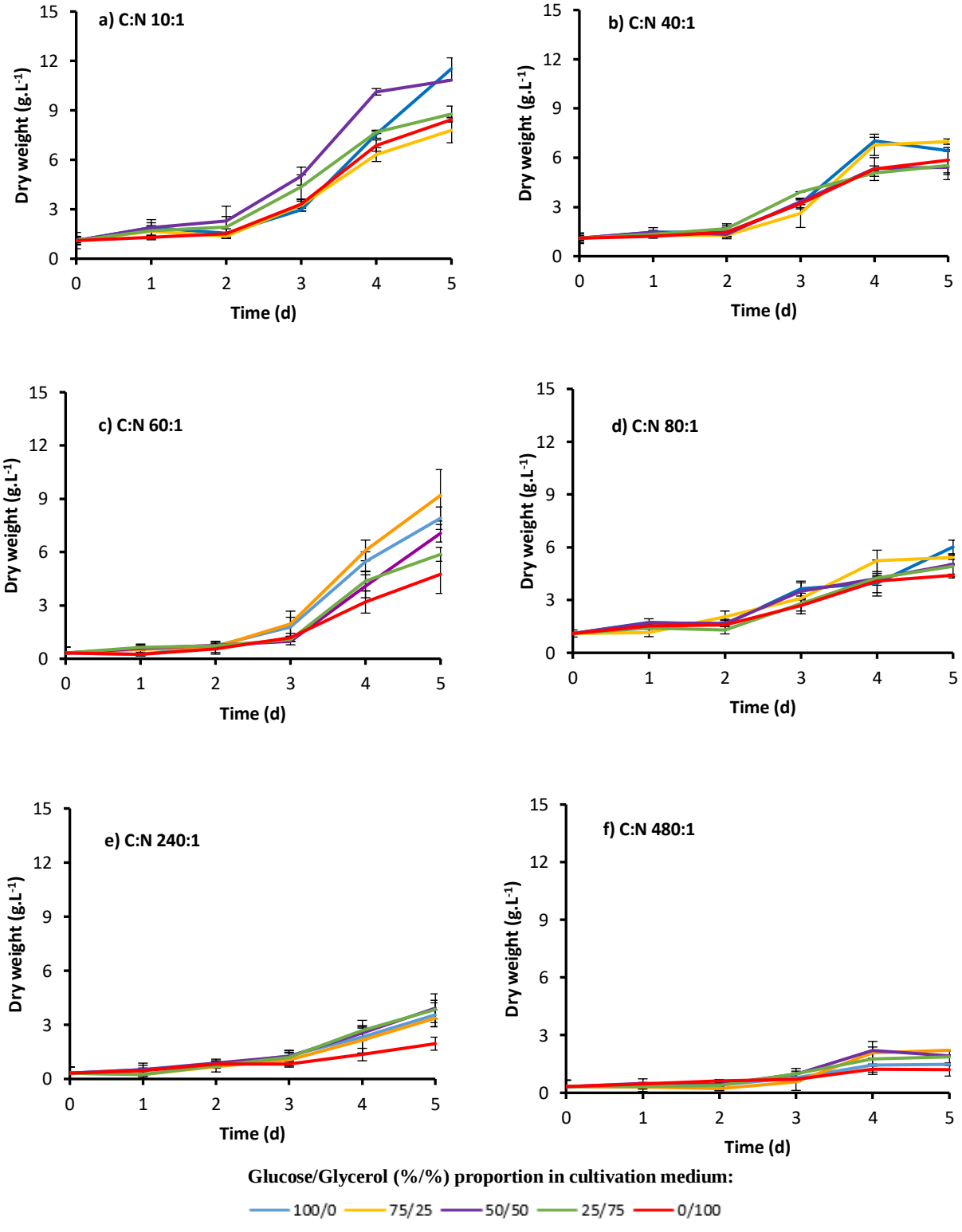

Figure 4.6: Influence of variation in type of carbon source and nitrogen on biomass growth of *A. protothecoides* in batch level operation for C:N ratio of a) 10:1, b) 40:1, c) 60:1, d) 80:1, e) 240:1 and f) 480:1. Error bars represent ± σ.

Reportedly, for the growth of *Chlorella* species, glycine consumption results in the second highest biomass density in comparison to utilization of nitrates and urea as a nitrogen source [175]. The glycine content was varied on a molar basis with respect to the total moles of carbon in the cultivation medium. In Figure 4.6, the highest biomass growth (11.53 $g.L^{-1}$) is observed for greater nitrogen content (C:N 10:1) within the nitrogen deplete conditions tested for batch experiments. According to literature, microalgae demonstrate enhanced growth under nitrogen deplete conditions as it promotes metabolism of intracellular pools of nitrogen, for instance, pigment proteins [175]. However, the enhanced growth can result in a significant drop in bioactive compounds and pigments. Hence, a trade-off is reached between the biomass growth and intracellular pigment content by studying the product yields at nitrogen deplete conditions.

On the other hand, cultivation medium containing greater glucose content (100:0 and 75:25 glucose to glycerol ratio) resulted in higher biomass growth due to the faster kinetics of glucose metabolism. Despite this, solely glucose and glycerol cultivation mediums resulted in a 28% discrepancy in biomass growth, which is not significant at the batch level but can substantially influence the results of a large-scale fed-batch production system.

4.5 Influence of nutrient variation on antioxidants

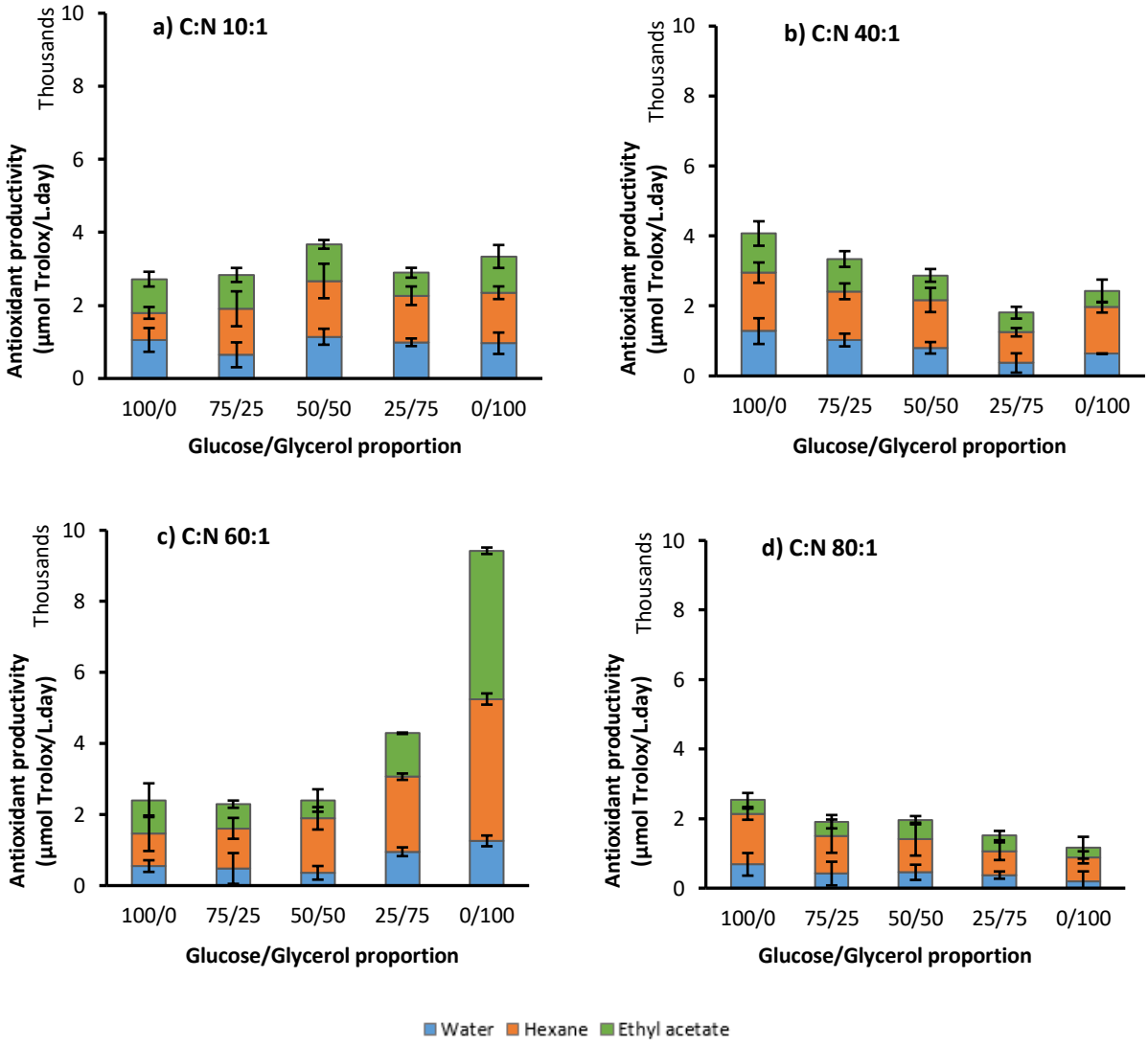

Figure 4.7: Effect of carbon source and nitrogen content on total antioxidant productivity of *A. protothecoides* at batch level operation for C:N ratio of a) 10:1, b) 40:1, c) 60:1 and d) 80:1. Error bars represent ± σ.

The total antioxidant activity was analyzed to study the effect of carbon source and nitrogen content on composition of antioxidants and pigments within the microalgae. Literature reports the overproduction of antioxidant molecules within microalgae in the presence of stressful conditions [177]. A primary stress factor is nutrient deprivation, which causes the cell to enhance antioxidant production in order to resist damage from buildup of oxidizing agents [175], [177]. The scavenging effect of antioxidants was studied through the trolox equivalent antioxidant capacity method. For

C:N ratios of 10:1, 40:1 and 60:1, total antioxidant activity from hexane, ethyl acetate and water assays resulted in an average range of 2950 µmol Trolox.L^{-1}.d^{-1}. However, the C:N 80:1 ratio experienced a large drop in antioxidant activity (1810 µmol Trolox.L^{-1}.d^{-1} average) as seen in Figure 4.7. This can be attributed to the significantly low nitrogen content of the cultivation medium, which drives the disintegration of chloroplasts and primary antioxidants. Remarkably, the cultivation of microalgae under solely glycerol and C:N 60:1 ratio resulted in the highest antioxidant activity. The presence of glycerol enhances carotenoid biosynthesis by overexpression of enzymes involved in the formation of primary terpenoid precursors glycerol 3-phosphate and pyruvate [151], [155]. Moreover, the high stress experienced by the microalgae in nitrogen deplete conditions promotes production of powerful antioxidants [178]. Hence, the antioxidant activity of this specific cultivation condition has a higher scavenging effect on the ABTS radical.

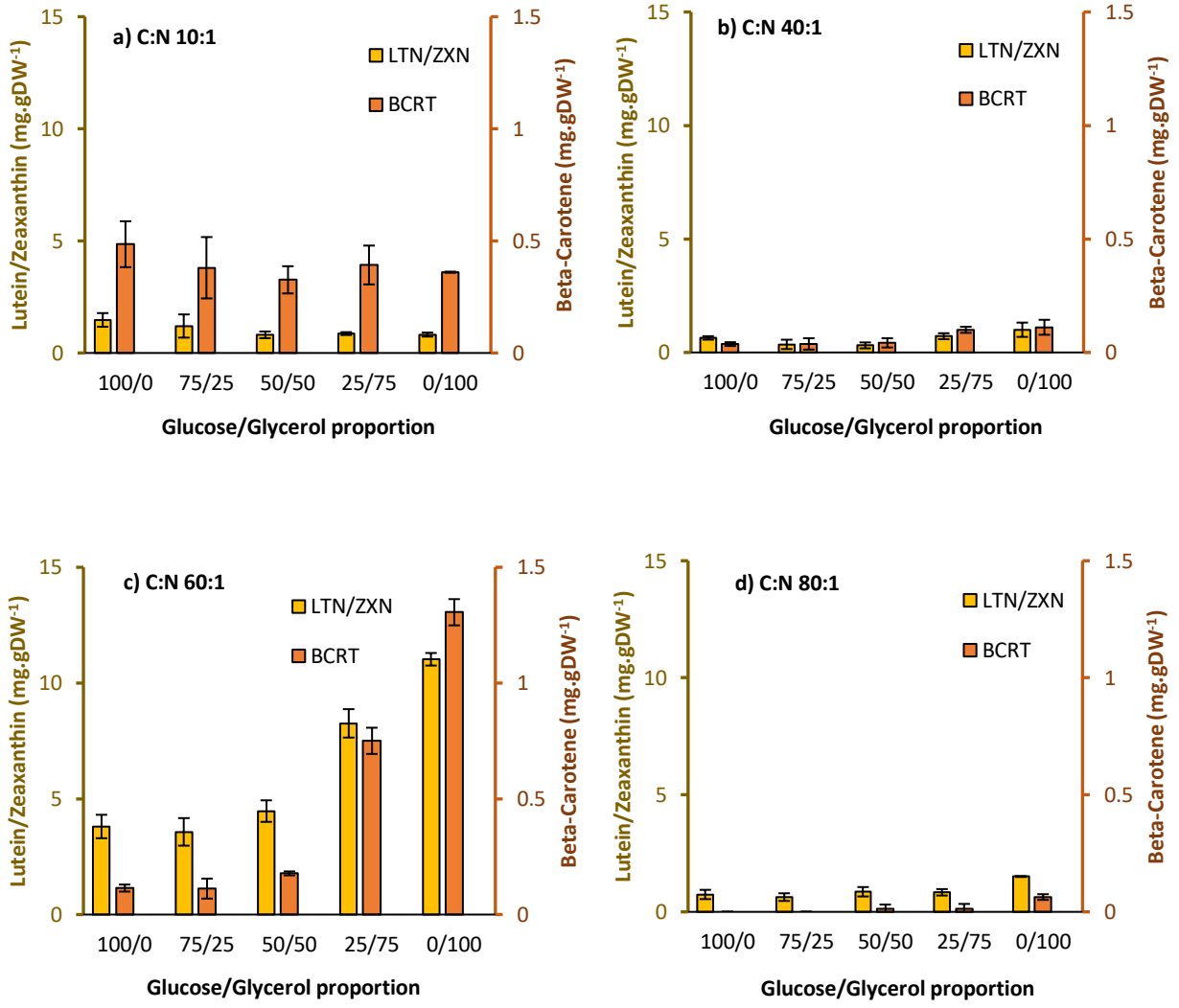

Figure 4.8: Effect of carbon source and nitrogen content on carotenoid biosynthesis of lutein, zeaxanthin and beta-carotene of *A. protothecoides* at batch level operation for C:N ratio of a) 10:1, b) 40:1, c) 60:1 and d) 80:1. Error bars represent ± σ.

The carotenoid biosynthesis was further studied by evaluating the presence of lutein, zeaxanthin and beta-carotene in the batch-level experiments as seen in Figure 4.8. Beta-carotene content, 1.31 mg.gDW^{-1} (6.21 mg.L^{-1}), was reportedly the highest for C:N 60:1 under high glycerol levels. On the other hand, lutein and zeaxanthin were observed to accumulate to 11.02 mg.gDW^{-1} (52.43 mg.L^{-1}) in batch culture operation for C:N 60:1 ratio at solely glycerol cultivation. This is the highest reported product yield of lutein/zeaxanthin in comparison to current literature, which

shows 2-4 mg.gDW^{-1} lutein content, 34.13 mg.L^{-1} and 36.79 mg.L^{-1} zeaxanthin production [179]–[181]. These are primary carotenoids, which are distinctly affected by a combination of stress factors in the environment. Stress factors such as nutrient limitation, high light intensity, and salt content influence the electron transfer in the cell, which causes oxidative damage [182]. While lutein disintegrates under oxidative stress, beta carotene content increases in high stress conditions [182].

4.6 Influence of nutrient variation on lipid content

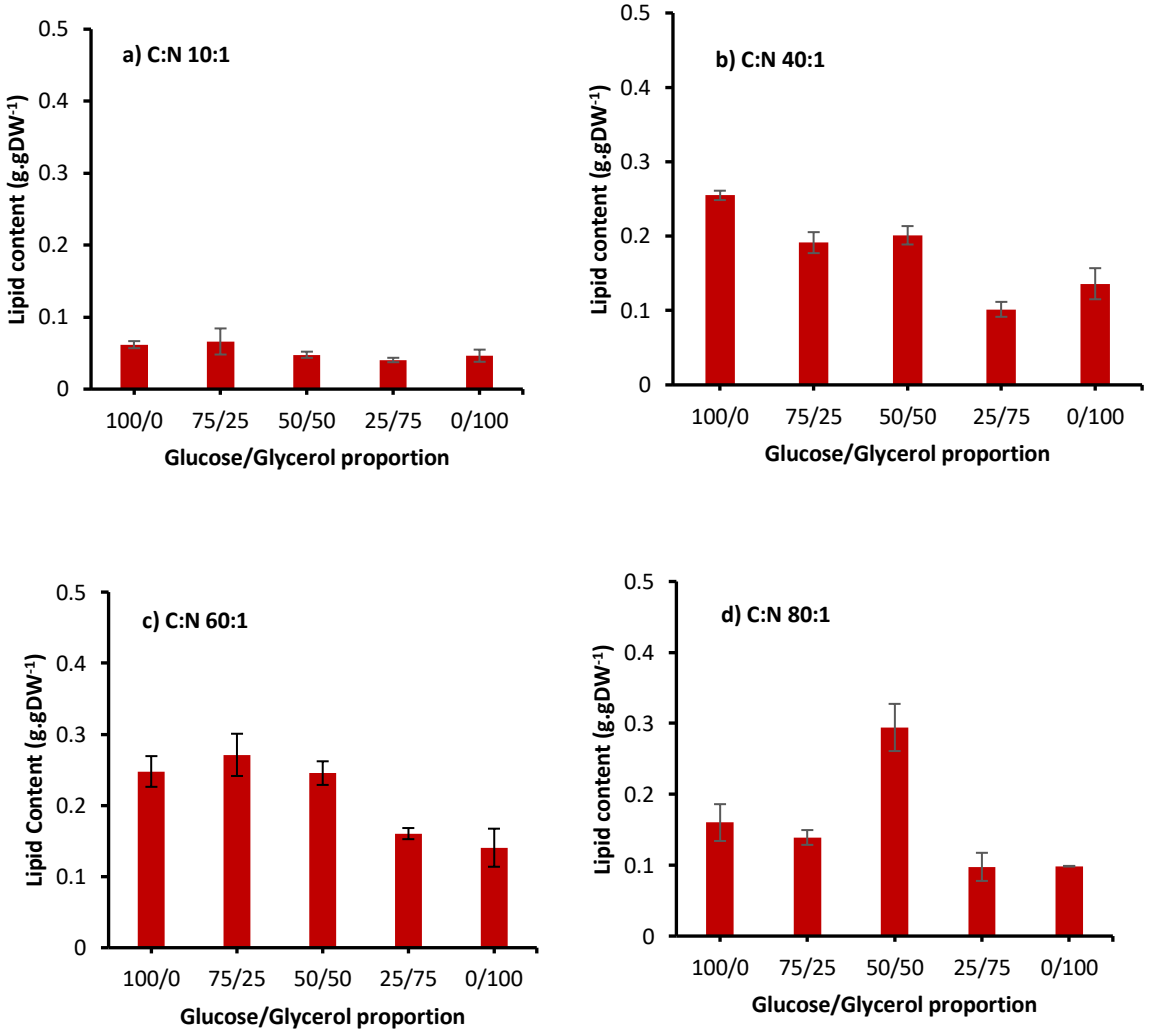

Figure 4.9: Influence of variation in carbon source and nitrogen content on lipid yield (g.gDW^{-1}) of *A. protothecoides* at batch level operation for C:N ratio of 10:1, 40:1, 60:1 and 80:1. Error bars represent ± σ.

Microalgae carry out lipid and carbohydrate accumulation in nitrogen deplete conditions while the cellular growth rate largely declines in order to reduce energy consumption in protein synthesis [183]. In this research, neutral lipids were recovered as a result of the solvent extraction stage. As seen in Figure 4.9, C:N 10:1 ratio has not pushed the cell into the high stress mode of energy conservation, which explains the low lipid yields. Subsequently, the highest lipid yield, 0.27-0.29 $g.gDW^{-1}$, were observed for C:N 40:1 and 60:1 with high glucose content (100:0, 75:25 and 50:50). Glucose promotes overexpression of the enzyme responsible for lipid accumulation and results in higher lipid yields in comparison to glycerol [184]. At C:N 80:1, the biomass growth is severely affected by the low nitrogen content, which significantly lowers the reported lipid content when biomass growth is taken into account.

4.7 Yield and productivity of heterotrophic growth conditions

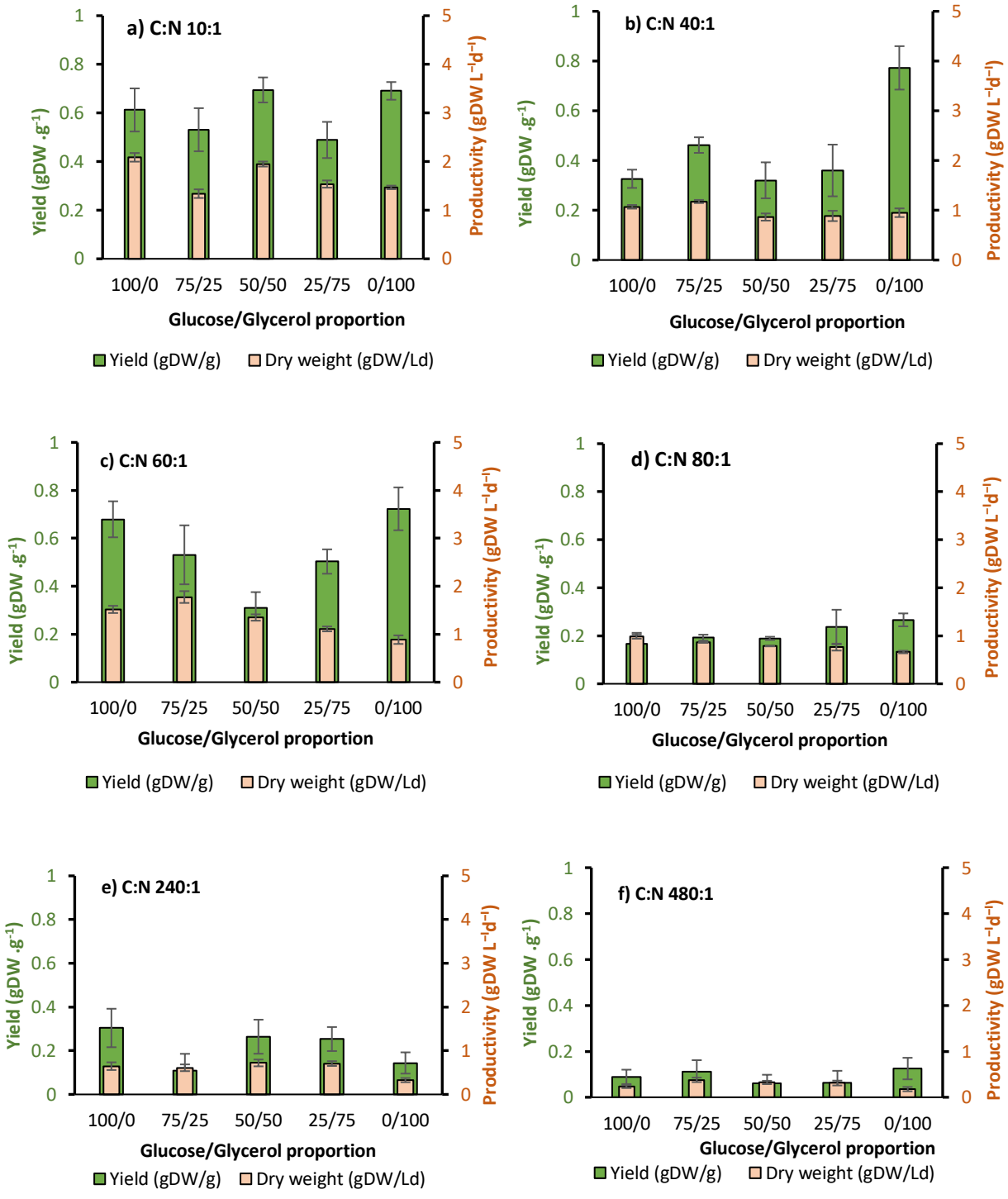

Figure 4.10: Study of yield and productivity of batch operation of *A. protothecoides* for C:N ratio of a) 10:1, b) 40:1, c) 60:1, d) 80:1, e) 240:1 and f) 480:1. Error bars represent ± σ.

The cultivation efficiency was evaluated by studying the yield (dry weight per mass of carbon substrate consumed $gDW.g^{-1}$) and productivity (daily biomass growth $gDWL^{-1}d^{-1}$) of the batch level operation. Overall, the yield and productivity are significantly higher for increased nitrogen content in the cultivation medium as seen in Figure 4.10. The yield did not exceed 0.77 $gDW.g^{-1}$ and a similar peak value was observed for high glycerol content in C:N 10:1, 40:1 and 60:1 ratio. Since, the majority of the energy for cell division derives from higher nitrogen content, the carbon source have a less significant impact on the productivity of the microalgal cultivation. Evidently, a substantial drop is observed in the yield at C:N 80:1, 240:1, 480:1 ratios.

Most importantly, the range of yields for *A. protothecoides* is 0.6-0.8 $gDW.g^{-1}$, which is much higher than the reported yield (0.3-0.4 $gDW.g^{-1}$) for bacterial cultivation on glucose [185]. Specifically, *A. protothecoides* shows better performance results in diauxic growth conditions because of its ability to simultaneously assimilate two different carbon sources and maintain photosynthetic function. The synthesis of precursors from three different metabolic pathways, albeit at different rates, yields an increase in macromolecule content and biomass growth.

4.8 Optimal cultivation strategy based on batch operation

The batch level operation informs the two-stage cultivation strategy for the fed-batch bioreactor system. The variation in biomass growth and product composition was successfully investigated through changes in carbon substrate and nitrogen content of the cultivation medium. It can be seen that biomass growth does not significantly alter with changes in carbon substrate. Nevertheless, high glucose content derives increased growth in microalgal cultivation. High nitrogen in nitrogen limited conditions promotes high cell densities. Hence, the first stage of the cultivation strategy focuses on biomass growth and the second stage focuses on product accumulation. The first stage maintains nutrient conditions at a C:N ratio of 40:1 and high glucose

content (75:25) for dense cell culture. The second stage enriches and recovers the pigments by switching to 60:1 ratio and high glycerol content (25:75). The dense cell culture from the first stage will allow lipid accretion at 60:1 nitrogen conditions without compromising the pigment content.

The batch level cultivation of *A. protothecoides* enables a comprehensive understanding of the microalgal performance with variation in carbon source and nitrogen content. The chloroplast bleaching effect evidently appears for the high glucose conditions but is effectively modulated with the presence of glycerol in the cultivation medium. High biomass growth of 11.53 $g.L^{-1}$ was achieved for high nitrogen content (C:N 100:0) but variation between glucose and glycerol resulted in less than 28% discrepancy in the final biomass growth at a given C:N ratio. Antioxidant productivity was significantly high for high glycerol content at C:N ratio of 60:1. Specifically, carotenoids (lutein, zeaxanthin and beta-carotene) reached an increased accumulation of 11.02 $mg.gDW^{-1}$ (52.43 $mg.L^{-1}$) at high glycerol conditions and C:N ratio of 60:1. Subsequently, the highest lipid yield, 0.27-0.29 $g.gDW^{-1}$, were observed for C:N 40:1 and 60:1 with high glucose content (100:0, 75:25 and 50:50). The results agree with the initial assumption whereby glucose leads to high lipid accumulation and glycerol promotes antioxidant production in microalgae. The biomass yield with respect to the carbon source consumed is much higher in comparison to bacterial cultivation. From these results, an optimal cultivation strategy can be derived for a two-stage fed-batch process that promotes biomass growth in the first stage (C:N 40:1) and product accumulation in the second stage (C:N 60:1).

Chapter 5: Metabolic reconstruction and calibration

In this chapter, the genome-specific metabolic pathways, that play an essential role in the cellular maintenance and growth of the microalgal system, are assembled from current literature. The chapter provides an overview on all the modelling assumptions, underlying mathematical model, biochemical reactions and the kinetic parameters of the enzymes. The metabolic pathways elucidate similar precursors in the synthesis of both lipids and antioxidants. This means a trade-off should be identified in the selection of optimal conditions in order to achieve high product yields for both lutein and lipid content. On the other hand, three metabolic pathways from the central carbon metabolism are responsible for the generation of the precursors. The complexity of the metabolic pathways in the cellular structure yields improved performance results for the microalgal production system.

5.1 Reconstruction of metabolic model

Heterotrophic microalgae have the ability to substitute their photosynthetic functionality with the simultaneous assimilation of different carbon sources present in the culture media through ‘dark metabolism’, which allows them to grow in the absence of light [186]. The consumption of glucose is limited by the transport kinetics across the cellular membrane after that glucose undergoes the glycolysis reactions for energy production including an initial stage of oxidative phosphorylation and parallel oxidation through the Pentose Phosphate Pathway (PPP). Alternatively, glucose metabolism also occurs through the Embden-Meyerhof-Parnas (EMP) pathway, part of glycolysis, in the presence of light and aerobic conditions [187].

The metabolites formed from carbon assimilation in the glycolysis reactions trickle down into the terpenoid backbone biosynthesis. The biosynthesis pathways involved in the terpenoid

backbone biosynthesis generate building blocks such as geranyl diphosphate (GPP), farsenyl diphosphate (FPP), and geranylgeranyl diphosphate (GGPP), which are important precursors of sterols and carotenoids [188]. Specifically, FPP and GGPP lead to the biosynthesis of xanthophyll carotenoids such as lutein and zeaxanthin, found in the lipid phase of the thylakoid membrane of chloroplasts. They function as photo-protective receptors within the chloroplast to provide protection against the damaging effect of high light intensity [189]. Consequently, the reactions for the metabolic model account for the metabolic assimilation of glucose and glycerol in the intracellular organelles, among other nutrients, for the formation of antioxidants through the terpenoid backbone and carotenoid biosynthesis pathways.

Table 5.1: Online databases used for data collection of enzyme-specific metabolic pathways and kinetics.

Database abbreviation	Name of database	Objective	Ref.
KEGG	Kyoto Encyclopedia of Genes and Genomes	Contains genome annotations and complete metabolic pathways	[190]
BRENDA	The Comprehensive Enzyme Information System	Contains information on enzyme activity, molecular structure and limiting factors.	[191]

The design of the metabolic model incorporates essential metabolic pathways involved in nutrient assimilation, carbon fixation and biosynthesis of metabolic products. These pathways are namely glycolysis of the intermediates formed from glucose and glycerol, Calvin-Benson cycle, glycine assimilation, fatty acid synthesis, terpenoid backbone synthesis and carotenoid biosynthesis. Auxiliary metabolic pathways, such as Tri-carboxylic acid (TCA) cycle and pentose phosphate pathway, append the metabolic model by sustaining the production of intermediate precursors. In this research, literature on heterotrophic microalgae, [88], [186], [192], was employed to inform the enzyme-led reaction pathways. Genome specific information on the enzymes involved in the biochemical reaction was assembled from the databases KEGG and

BRENDA as listed in Table 5.1. The list of biochemical reactions assembled for the metabolic pathways are listed in Table 5.2.

Table 5.2: Metabolic reactions specific to *A. protothecoides* for carbon source assimilation, oxidative pathways, carbon-fixation, glycine assimilation, TCA cycle, terpenoid and carotenoid synthesis.

EC Abb.	EC No.	Enzyme	Reaction Equation
		Glucose metabolism (Glycolysis) [186], [190]–[192]	
GK	2.7.1.199	Gluco-kinase	ATP + D-Glucose => ADP + D-Glucose 6-phosphae
G6PI	5.3.1.9	Glucose-6-phosphate isomerase	D-Glucose 6-phosphate <=> D-Fructose 6-phosphate
6PFK	2.7.1.11	6-Phosphofructokinase	ATP + D-Fructose 6-phosphate <=> ADP + D-Fructose 1,6-biphosphate
FBPA	4.1.2.13	Fructose-biphosphate aldolase	D-Fructose 1,6-biphosphate <=> Glycerone phosphate + D-Glyceraldehyde-3-phosphate
GY3PD	1.2.1.12	Glyceraldehyde-3-phosphate dehydrogenase-NAD	D-Glyceraldehyde-3-phosphate + Orthophosphate + NAD+ => 1,3-Biphosphoglycerate + NADH + H+
		Glycerol metabolism (Glycolysis) [186], [190]–[192]	
GYK	2.7.1.30	Glycerol kinase	ATP + Glycerol <=> ADP + sn-Glycerol 3-phosphate
SG3PO	1.1.1.8	sn-glycerol-3-phosphate NAD+ oxidoreductase	sn-glycerol 3-phosphate + NAD+ <=> Glycerone phosphate + NADH + H+
TPI	5.3.1.1	Triose-phosphate isomerase	Glycerone phosphate <=> D-Glyceraldehyde-3-phosphate
		Pentose phosphate pathway [186], [190]–[192]	
PPHD	4.2.1.11	phosphopyruvate hydratase	2 1,3-Bisphosphoglycerate + 2 ADP = 2phosphoenolpyruvate + H2O +2 ATP
PYK	2.7.1.40	pyruvate kinase	2ADP + 2phosphoenolpyruvate = 2ATP + 2pyruvate
G6PD	1.1.1.49	Glucose-6-phosphate dehydrogenase	D-Glucose 6-phosphate + NADP+ <=> D-Glucono-1,5-lactone 6-phosphate + NADPH + H+
6PGA	3.1.1.3	6-phosphogluconolactonase	D-Glucono-1,5-lactone 6-phosphate + H2O <=> 6-Phospho-D-gluconate
6PGD	1.1.1.44	6-phosphogluconate dehydrogenase	6-Phospho-D-gluconate + NADP+ <=> D-Ribulose 5-phosphate + CO2 + NADPH + H+

		Calvin-Benson Cycle [186], [190]–[192]	
RP3E	5.1.3.1	Ribulose-phosphate 3-epimerase	D-Ribulose 5-phosphate <=> D-Xylulose 5-phosphate
RBPC	4.1.1.39	ribulose-bisphosphate carboxylase	D-ribulose 1,5-bisphosphate + CO2 + H2O = 3-phospho-D-glycerate + 2 H+
G3PD	1.2.1.59	glyceraldehyde-3-phosphate dehydrogenase	3-phospho-D-glycerate + NADH + H+ <=> D-Glyceraldehyde 3-phosphate + Orthophosphate + NAD+
PPKT	4.1.2.9	phosphoketolase	D-glyceraldehyde 3-phosphate + H2O = D-xylulose 5-phosphate
R5PK	2.7.1.19	phosphoribulokinase	ATP + D-xylulose 5-phosphate = ADP + D-ribulose 1,5-bisphosphate
		Tricarboxylic acid cycle (Krebb cycle) [186], [190]–[192]	
PYAT	1.2.4.1	pyruvate dehydrogenase	CoA + pyruvate = acetyl-CoA + formate
ATCS	2.3.3.8	ATP citrate synthase	ADP + acetyl-CoA + Oxaloacetate = ATP + citrate + CoA
AH	4.2.1.3	Aconitate Hydratase	Citrate <=> Isocitrate
ICDN1	1.1.1.41	Isocitrate dehydrogenase-NADH dependent	Isocitrate + NAD+ <=> alpha-Ketoglutarate + CO2 + NADH + H+
KGD	1.2.4.2	Ketoglutarate dehydrogenase	alpha-Ketoglutarate + CoA + NAD+ <=> (S)-Malate+ CO2 + NADH + H+
MDN	1.1.1.37	Malate Dehydrogenase-NADP dependent	(S)-Malate + NADP+ <=> Oxaloacetate + NADPH + H+
		Glycine assimilation [186], [190]–[192]	
GYND	1.4.4.2	Glycine dehydrogenase	Glycine <=> S-Aminomethyldihydrolipoylprotein + CO2
AMT	2.1.2.10	Aminomethyltransferase	S-Aminomethyldihydrolipoylprotein <=> 5,10-Methylenetetrehydrofolate + Ammonium
GS	6.3.1.2	Glutamine synthetaste (GS)	ATP + Glutamate + Ammonium => ADP + Orthophosphate + L-Glutamine
ACAC	6.4.1.2	acetyl-CoA carboxylase	ATP + acetyl-CoA = ADP + malonyl-CoA

Terpenoid backbone synthesis [149], [151], [190], [191]			
1XPS	2.2.1.7	1-deoxy-D-xylulose-5-phosphate synthase	Pyruvate + D-Glyceraldehyde 3-phosphate <=> 1-Deoxy-D-xylulose 5-phosphate + CO2
1XPR	1.1.1.267	1-deoxy-D-xylulose-5-phosphate reductoisomerase	2-C-Methyl-D-erythritol 4-phosphate + NADP+ <=> 1-Deoxy-D-xylulose 5-phosphate + NADPH + H+
2E4PC	2.7.7.60	2-C-methyl-D-erythritol 4-phosphate cytidylyltransferase	2-C-Methyl-D-erythritol 4-phosphate + CTP <=> 4-(Cytidine 5'-diphospho)-2-C-methyl-D-erythritol + Diphosphate
MDEK	2.7.1.148	4-(cytidine 5'-diphospho)-2-C-methyl-D-erythritol kinase	ATP + 4-(cytidine 5'-diphospho)-2-C-methyl-D-erythritol <=> ADP + 2-phospho-4-(cytidine 5'-diphospho)-2-C-methyl-D-erythritol
MDECL	4.6.1.12	2-Phospho-4-(cytidine 5'-diphospho)-2-C-methyl-D-erythritol CMP-lyase (cyclizing)	2-Phospho-4-(cytidine 5'-diphospho)-2-C-methyl-D-erythritol <=> 2-C-Methyl-D-erythritol 2,4-cyclodiphosphate + CMP
FLAV	1.17.7.1	(E)-4-hydroxy-3-methylbut-2-enyl-diphosphate synthase (flavodoxin)	2-C-Methyl-D-erythritol 2,4-cyclodiphosphate + 2 Reduced ferredoxin <=> 1-Hydroxy-2-methyl-2-butenyl 4-diphosphate + H2O + 2 Oxidized ferredoxin
MDFO	1.17.7.4	dimethylallyl diphosphate:ferredoxin oxidoreductase	Dimethylallyl diphosphate + 2 Oxidized ferredoxin + H2O <=> 1-Hydroxy-2-methyl-2-butenyl 4-diphosphate + 2 Reduced ferredoxin + 2 H+
IFO		isopentenyl-diphosphate:ferredoxin oxidoreductase	isopentenyl diphosphate + 2 oxidized ferredoxin [iron-sulfur] cluster + H2O <=> (E)-4-hydroxy-3-methylbut-2-en-1-yl diphosphate + 2 reduced ferredoxin [iron-sulfur] cluster + 2 H+

Carotenoid biosynthesis [190], [191]			
PDS	2.5.1.32	prephytoene-diphosphate synthase	Geranylgeranyl diphosphate <=> Diphosphate + Prephytoene diphosphate
CPS	2.5.1.32	15-cis-phytoene synthase	Prephytoene diphosphate <=> Diphosphate + 15-cis-Phytoene
CPS	2.5.1.32	15-cis-phytoene synthase	2 Geranylgeranyl diphosphate <=> 15-cis-Phytoene + 2 Diphosphate
PD	1.3.99.28	phytoene desaturase	15-cis-Phytoene + Acceptor <=> all-trans-Phytofluene + Reduced acceptor
CPD	1.3.5.5	15-cis-phytoene desaturase	all-trans-Phytofluene + Acceptor <=> all-trans-zeta-Carotene + Reduced acceptor
ZCD	1.3.5.6	zeta-carotene desaturase	all-trans-Neurosporene + Reduced acceptor + Oxygen <=> Lycopene + Acceptor + 2 H2O
LEC	5.5.1.18	lycopene epsilon-cyclase	Lycopene <=> delta-Carotene
LBC	5.5.1.19	lycopene beta-cyclase	delta-Carotene <=> alpha-Carotene
BCH	1.14.15.24	beta-carotene 3-hydroxylase	alpha-Carotene + 2 Reduced ferredoxin + H+ + Oxygen <=> Zeinoxanthin + 2 Oxidized ferredoxin + H2O
CEMO	1.14.99.45	carotene epsilon-monooxygenase	Zeinoxanthin + Reduced acceptor + Oxygen <=> Lutein + Acceptor + H2O
CEMO	1.14.99.45	carotene epsilon-monooxygenase	alpha-Carotene + Oxygen + Reduced acceptor <=> alpha-Cryptoxanthin + Acceptor + H2O
BCH	1.14.15.24	beta-carotene 3-hydroxylase	beta-Cryptoxanthin + 2 Reduced ferredoxin + H+ + Oxygen <=> Zeaxanthin + 2 Oxidized ferredoxin + H2O

5.2 Localization of intracellular components

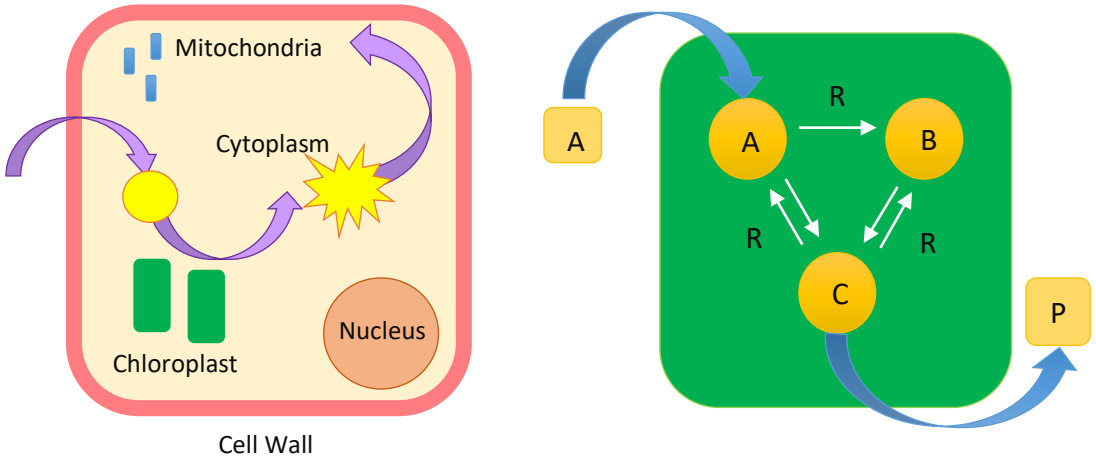

Figure 5.1: Cellular models for metabolic engineering 1) Compartmentalized cellular model 2) Simplified cellular model.

Microalgae are eukaryotic organisms, which contain several intracellular organelles such as mitochondria, nucleus, glyoxysome, chloroplast, vacuole and cell membrane as briefly seen in Figure 5.1 [82]. The localization of these organelles is specific to the microalgal strain. In order to account for compartmentalization, additional details such as transport kinetics between compartments, specific concentration levels of energy components and metabolites in each organelle are required for a comprehensive metabolic model.

In this research, a simplified cellular model is adopted to reduce the quantity of kinetic parameters. The transport kinetics of smaller nutrients, such as glycine and glycerol, are considered to have negligible effect on the overall metabolism within the microorganism. The kinetics of the glucose transporter protein GLUT1 were incorporated into the model [193]. Synthesis of energy molecules, such as ATP and NADP, was assigned to the metabolism of substrates [186]. All cells within a cultural medium are considered to grow with a singular aim instead of individualistic objectives [194]. The biochemical reactions within the cell are assumed to be all enzyme catalyzed. The reactions for the lipid production were streamlined to the synthesis of a global lipid pool in the

form of Malonyl CoA [186]. Malonyl CoA is utilized in elongation of substrate for fatty acid synthesis [88].

5.3 Cellular growth

Similar to Cloutier et al. [195], the biomass growth rate is derived from the synthesis of essential components that make up the composition of a cell. These components include nucleotides, such as Ribulose 5-phosphate and Xylulose 5-phosphate, which contribute to synthesis of genetic molecules such as DNA and RNA [82], [186]. Other components include Glucose 6-phosphate for the synthesis of carbohydrate storage pools, L-Glutamine for protein synthesis and lastly Acetyl CoA for the synthesis of lipid pools [186]. The reactions for biomass growth rate were derived as enzyme led reactions with the parameters listed in Table 5.3.

Table 5.3: Biochemical reactions for cellular growth in the metabolic model.

Biomass precursor	Reaction
Xylulose 5-phosphate	$X5P \rightarrow Biomass$
Glucose 6-phosphate	$G6P \rightarrow Biomass$
L-Glutamine	$LGTM \rightarrow Biomass$
Acetyl CoA	$ACoA \rightarrow Biomass$

5.4 Mathematical modelling (Mechanistic expression)

Michaelis-Menten rate law was primarily derived for analytical evaluation of enzyme led biochemical reactions *in vitro*. The mathematical representation of the method exhibits the reaction kinetics of reversibly forming an intermediate conjugate between the enzyme and substrate [187]. The application of Michaelis-Menten is limited towards microorganisms *in vivo* as it does not fully represent the kinetics of all enzymes in an integrated biochemical environment [196]. However, vast literature studies have measured characteristic Michaelis-Menten parameters of isolated enzyme kinetics. Secondly, the Michaelis Menten model is also attractive as it has an embedded

saturation component in the nonlinear function [187]. The Michaelis-Menten approach, as seen in Eq. 13 [196], [197], has been widely applied to represent metabolic modelling.

$$v = V_{max} \cdot \frac{S}{K_m + S'} \tag{13}$$

In Eq. 13, S is the substrate concentration, K_m is the substrate concentration at half the maximal reaction rate, Vmax is the specific activity of the enzyme with respect to the enzyme quantity [186].

5.5 Kinetic and parameter estimation

The model consists of 63 metabolites and 88 reactions from the 9 metabolic pathways. This model would require 88 values for specific activity, approximately 120 values for K_m and 88 values for enzyme content. The initial conditions comprise of initial metabolite concentrations collected from literature [186] and initial kinetic parameters (V_{max} and K_m) from enzyme databases BRENDA and KEGG as listed in Table 5.1. The system of units are $mmol.s^{-1}.mgE^{-1}$ and $mmol.L^{-1}$ for specific activity of the enzyme and saturated constant respectively.

Table 5.4: Michaelis-Menten kinetic parameters for the enzyme-specific reactions involved in the metabolic model [193] [191] [198]**.**

EC Abb.	EC No.	Enzyme	Vmax_EC ($mmol.d^{-1}.mgE^{-1}$)	Km_EC_m1 ($mmol.gDW^{-1}$)	Km_EC_m2 ($mmol.gDW^{-1}$)
GLUT1		Hexose carriers (glucose transporter protein)	0.0035	4.3	
GK	2.7.1.199	Glucokinase	3250	25	0.015
G6PI	5.3.1.9	Glucose-6-phosphate isomerase	21.2	0.28	
6PFK	2.7.1.11	6-Phosphofructokinase	18.9	0.005	0.006
FBPA	4.1.2.13	Fructose-biphosphate aldolase	20	0.45	
GY3PD	1.2.1.12	Glyceraldehyde-3-phosphate dehydrogenase-NAD	51.1	0.081	0.0066
GYK	2.7.1.30	Glycerol kinase	4500	0.006	2
SG3PO	1.1.1.8	sn-glycerol-3-phosphate NAD+ oxidoreductase	53.6	0.12	0.41
TPI	5.3.1.1	Triose-phosphate isomerase	7193	0.88	
PPHD	4.2.1.11	Phosphopyruvate hydratase	675	0.27	0.035
PYK	2.7.1.40	Pyruvate kinase	8.16	99.98	
G6PD	1.1.1.49	Glucose-6-phosphate dehydrogenase	100	0.0075	0.07
6PGA	3.1.1.3	6-phosphogluconolactonase	68	0.038	
6PGD	1.1.1.44	6-phosphogluconate dehydrogenase	21	0.0102	0.0041
RP3E	5.1.3.1	Ribulose-phosphate 3-epimerase	11610	0.00033	3.3e-4

EC Abb.	EC No.	Enzyme	Vmax_EC ($mmol.d^{-1}.mgE^{-1}$)	Km_EC_m1 ($mmol.gDW^{-1}$)	Km_EC_m2 ($mmol.gDW^{-1}$)
RBPC	4.1.1.39	Ribulose-bisphosphate carboxylase	1.21	0.0015	0.015
G3PD	1.2.1.59	Glyceraldehyde-3-phosphate dehydrogenase	18.6	0.0625	0.22
PPKT	4.1.2.9	Phosphoketolase	0.083	0.19	0.19
R5PK	2.7.1.19	Phosphoribulokinase	16	0.0053	0.0053
PYAT	1.2.4.1	Pyruvate dehydrogenase	40.5	0.0221	0.00077
ATCS	2.3.3.8	ATP citrate synthase	108	0.00225	0.0021
AH	4.2.1.3	Aconitate Hydratase	1.9	0.12	
ICDN1	1.1.1.41	Isocitrate dehydrogenase-NADH dependent	0.084	0.2	0.12
KGD	1.2.4.2	Ketoglutarate dehydrogenase	0.2	0.1	0.041
MDN	1.1.1.37	Malate Dehydrogenase-NADP dependent	1920	0.178	0.00012
GYND	1.4.4.2	Glycine dehydrogenase	0.25	2.84	0.47
AMT	2.1.2.10	Aminomethyltransferase	1.08	0.0037	0.17
GS	6.3.1.2	Glutamine synthetaste (GS)	33.9	0.79	5.71
ACAC	6.4.1.2	Acetyl-CoA carboxylase	1047	0.9640	0.0068
1XPS	2.2.1.7	1-deoxy-D-xylulose-5-phosphate synthase	1.6	0.53	0.64
1XPR	1.1.1.267	1-deoxy-D-xylulose-5-Phosphate reductoisomerase	2.1	0.47	0.972
DMAT	2.5.1.1	Dimethylallyltranstransferase	0.636	0.125	0.001
FDS	2.5.1.10	Farnesyl-diphosphate synthase	0.04	0.036	0.048
FT	2.5.1.29	Farnesyltranstransferase	0.0087	0.0028	0.0003
PDS	2.5.1.32	Prephytoene-diphosphate synthase	0.067	0.003	68
CPS	2.5.1.32	15-cis-phytoene synthase	0.067	0.0027	2.8
PD	1.3.99.28	Phytoene desaturase	0.00029	0.0048	0.0331
LEC	5.5.1.18	Lycopene epsilon-cyclase	60	0.4830	
LBC	5.5.1.19	Lycopene beta-cyclase	0.356	0.035	
BCH	1.14.15.24	Beta-carotene 3-hydroxylase	0.001	0.0025	
XB1	N/A	Biomass formation reaction 1	150	4	
XB2	N/A	Biomass formation reaction 2	203	0.05	
XB3	N/A	Biomass formation reaction 3	22	0.05	
XB4	N/A	Biomass formation reaction 4	108	3	

For compatibility of metabolite content with biomass growth, the metabolite concentrations ($mmol.L^{-1}$) were divided with the average biomass content ($gDW.L^{-1}$) of the given nutrient conditions from the experimental data. The initial conditions are listed in Table 5.4 while the kinetic parameters are listed in Table 5.5.

Table 5.5: Initial conditions for the concentration of the metabolites and extracellular nutrients.

Abb.	Metabolite	Concentration	Physical unit
ATP	Adenosine triphosphate	1.43E-02	mmol.gDW^{-1}
ADP	Adenosine diphosphate	2.22E-03	mmol.gDW^{-1}
NADx	Nicotinamide adenine dinucleotide	2.22E-03	mmol.gDW^{-1}
NADH	Nicotinamide adenine dinucleotide hydrogen	2.22E-03	mmol.gDW^{-1}
NADPH	Nicotinamide adenine dinucleotide phosphate hydrogen	2.22E-03	mmol.gDW^{-1}
NADPx	Nicotinamide adenine dinucleotide phosphate	2.22E-03	mmol.gDW^{-1}
GLC	D-glucose	5.55E+01	mmol.L^{-1}
GLY	Glycerol	1.08E+02	mmol.L^{-1}
H2O	Water	5.50E+01	mmol.gDW^{-1}
GCN	Glycine	1.38E+00	mmol.L^{-1}
G6P	D-Glucose-6-Phosphate	2.36E-04	mmol.gDW^{-1}
F6P	D-Fructose-6-Phosphate	4.72E-05	mmol.gDW^{-1}
F16BP	D-Fructose 1,6-biphosphate	2.00E-04	mmol.gDW^{-1}
GCNP	Glycerone phosphate	2.00E-04	mmol.gDW^{-1}
G3P	D-glyceraldehyde 3-phosphate	2.00E-04	mmol.gDW^{-1}
OP	Orthophosphate	2.00E-04	mmol.gDW^{-1}
3BPG	1,3-Biphosphoglycerate	2.00E-04	mmol.gDW^{-1}
Hx	Hydrogen ion	2.00E-04	mmol.gDW^{-1}
SG30	sn-Glycerol 3-phosphate	2.00E-04	mmol.gDW^{-1}
OA	Oxaloacetate	2.00E-04	mmol.gDW^{-1}
PEP	Phosphoenolpyruvate	2.00E-04	mmol.gDW^{-1}
GL6P	Glucono-1,5-lactone 6-phosphate	2.00E-04	mmol.gDW^{-1}
6PG	6-phospho-D-gluconate	2.00E-04	mmol.gDW^{-1}
R5P	D-Ribulose 5-phosphate	2.26E-05	mmol.gDW^{-1}
X5P	D-Xylulose 5-phosphate	2.26E-05	mmol.gDW^{-1}
CT	Citrate	2.00E-04	mmol.gDW^{-1}
CoA	Coenzyme A	2.00E-04	mmol.gDW^{-1}
IC	Isocitrate	2.00E-04	mmol.gDW^{-1}
AKG	alpha-Ketoglutarate	1.43E-02	mmol.gDW^{-1}
MCoA	Malonyl-CoA	2.00E-04	mmol.gDW^{-1}
SM	(S)-Malate	2.00E-04	mmol.gDW^{-1}
R15B	D-Ribulose 1,5-biphosphate	2.00E-04	mmol.gDW^{-1}
3PG	3-phospho-D-glycerate	2.00E-04	mmol.gDW^{-1}
PY	Pyruvate	2.00E-04	mmol.gDW^{-1}
SAMP	S-Aminomethyldihydrolipoylprotein	2.00E-04	mmol.gDW^{-1}
METF	5,10-Methylenetetrehydrofolate	2.00E-04	mmol.gDW^{-1}

Abb.	Metabolite	Concentration	Physical unit
NH3	Ammonia	2.00E-04	$mmol.gDW^{-1}$
GTM	Glutamate	2.00E-04	$mmol.gDW^{-1}$
LGM	L-Glutamine	2.00E-04	$mmol.gDW^{-1}$
DX5P	1-Deoxy-D-xylulose 5-phosphate	2.00E-04	$mmol.gDW^{-1}$
DPH	Diphosphate	2.00E-04	$mmol.gDW^{-1}$
PPDP	Prephytoene diphosphate	2.00E-04	$mmol.gDW^{-1}$
15cP	15-cis-phytoene	3.80E+01	$mmol.gDW^{-1}$
LYC	Lycopene	3.80E+01	$mmol.gDW^{-1}$
LTN	Lutein	3.80E+01	$mmol.gDW^{-1}$
BCRT	Beta-Carotene	2.00E-04	$mmol.gDW^{-1}$
ZXN	Zeaxanthin	2.00E-04	$mmol.gDW^{-1}$
MADP	Dimethylallyl diphosphate	2.00E-04	$mmol.gDW^{-1}$
IPP	isopentenyl diphosphate	2.00E-04	$mmol.gDW^{-1}$
BCRT	(E)-4-hydroxy-3-methylbut-2-en-1-yl diphosphate	2.00E-04	$mmol.gDW^{-1}$
GDP	Geranyl diphosphate	2.00E-04	$mmol.gDW^{-1}$
FDP	Farnesyl diphosphate	2.00E-04	$mmol.gDW^{-1}$
CO2	Carbon dioxide	1.20E-04	$mmol.L^{-1}$
ACoA	Acetyl-Coenzyme A	2.56E-04	$mmol.L^{-1}$
GGDP	Geranylgeranyl diphosphate	3.80E-04	$mmol.L^{-1}$
X_b	Biomass	0.30E+00	$gDW.L^{-1}$

5.6 Model refinement

In order to simplify the evaluation of the metabolic model, certain biochemical reactions were lumped together to reduce the quantity of parameters. The lumped reactions are illustrated in Figure 5.2-5.4, where certain intermediates were removed if irrelevant pathways were required to sustain their synthesis. Reactions that led to the formation of insignificant intermediates and reactions with instantaneous kinetics were lumped together. Moreover, reactions that lead to synthesis of metabolic end-products through a singular route were lumped together [5]. Consequently, Figure 5.2 constitutes the simplified metabolic pathways for metabolism of glucose and glycerol, Calvin-Benson cycle and pentose phosphate pathway. Figure 5.3 summarizes the simplified routes taken for TCA cycle, nitrogen assimilation and fatty acid synthesis. Figure 5.4

includes the simplified pathways for the biosynthesis of carotenoids through the terpenoid backbone and carotenoid synthesis.

The metabolic pathways are assembled by prioritizing relevance to the growth and maintenance of *A. protothecoides*. The databases are utilized to obtain enzyme-specific kinetics of the biochemical reactions in the metabolic pathways. Modelling assumptions towards the metabolic model simplify the modelling process by adopting a unique compartment approach. In this model, biomass reactions are hypothesized based on macronutrient precursors. This will tie the biomass growth to the metabolites derived from nutrient assimilation.

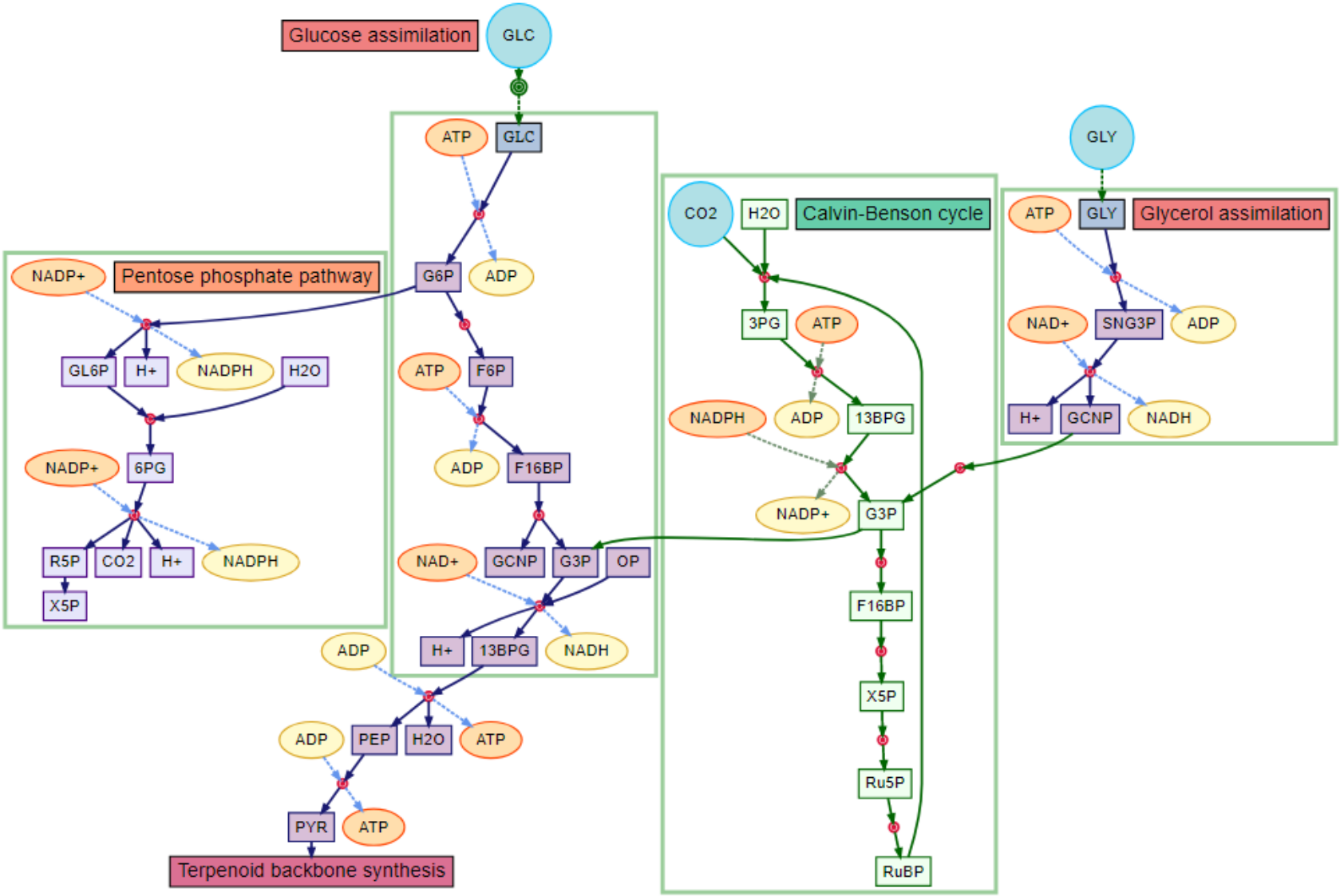

Figure 5.2: Metabolic reconstruction of glucose and glycerol assimilation through glycolytic pathways, carbon fixation through Calvin-Benson cycle and oxidation through Pentose Phosphate pathway.

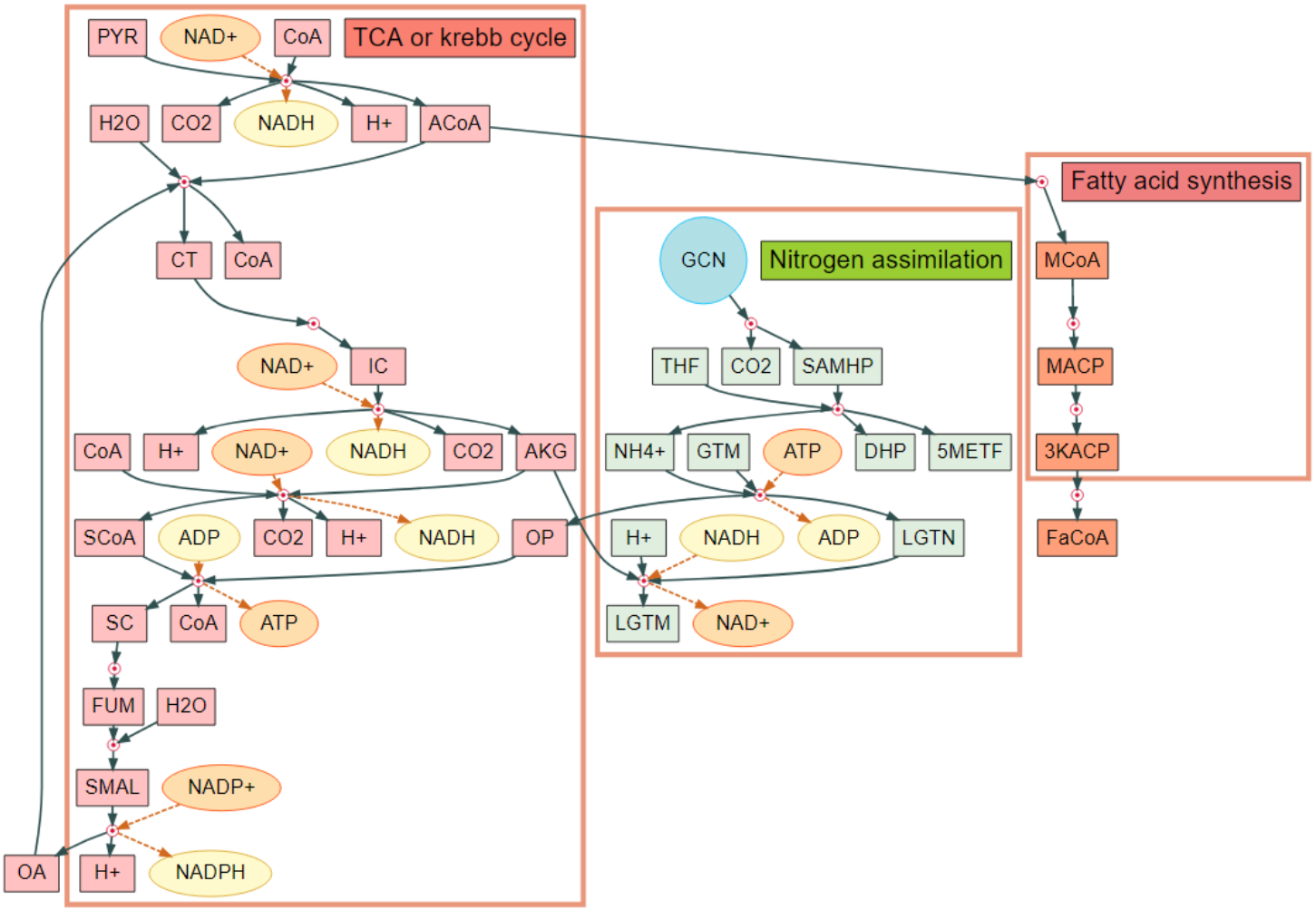

Figure 5.3: Metabolic reconstruction for oxidation of acetyl-CoA through tricarboxylic acid or the Krebs cycle, nitrogen assimilation and fatty acid synthesis.

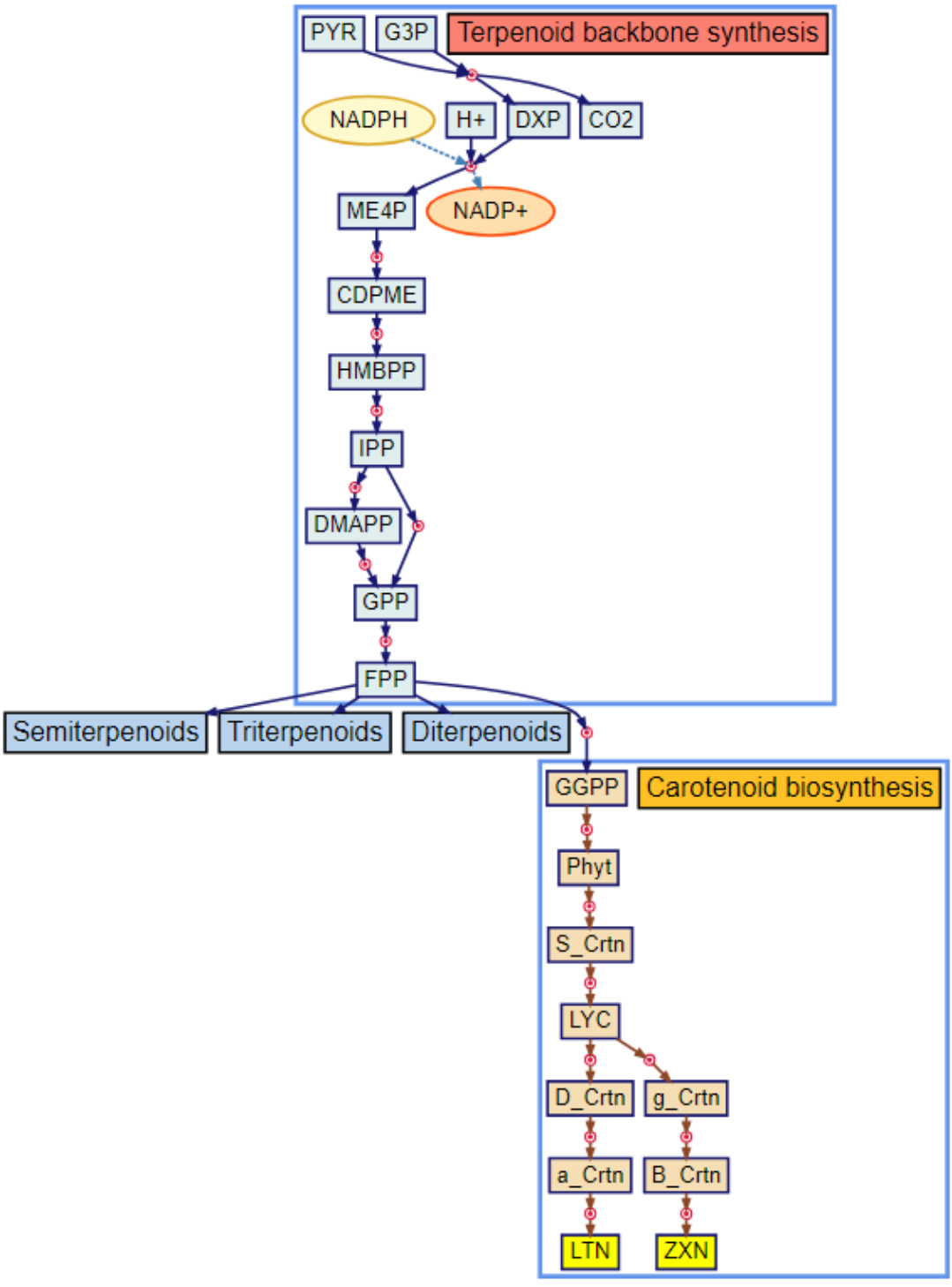

Figure 5.4: Metabolic products from the glycolytic pathway enter the terpenoid backbone synthesis, which leads to carotenoid biosynthesis

Chapter 6: Dynamic metabolic modelling

This chapter provides an overview of the modelling framework in Matlab for optimization and refinement of the metabolic model. The decisions towards the selection of the in-built functions and solvers are also covered to explain the framework of the model. Subsequently, experimental validation of the model informs the sections of the metabolic model that require improvement in future works. In the scenarios discussed in this chapter, increased complexity in the carotenoid biosynthesis pathway and the relationship between TCA cycle and nitrogen assimilation is required to obtain more reliable estimation of the microalgal performance.

6.1 Framework of the dynamic model

The enzyme specific information and reaction equations, listed in Table 5.2 in section 5.2, were employed towards developing a non-linear programming framework in Matlab [188]. The biochemical reactions from Table 5.2 were fitted into the Michaelis-Menten equation to derive a vector assembly of reactions rates. The reaction rates are then multiplied with a matrix containing stoichiometric information for individual metabolites in the respective reactions. The stoichiometric information for the biochemical reactions was retrieved from literature studies such as [128], [186]. The information assembled from literature data was stored in an Excel file and Visual Basic for Applications (VBA) was employed to generate the Matlab code. The reaction rates were stored within a function file, 'Enz_rates.mat', and subsequently called by another function file, 'Enz_dynmod.mat', which stores stoichiometric information. 'Enz_dynmod.mat' was used to multiply the stoichiometric matrix with the vector of reaction rates. The stoichiometric matrix for the lumped metabolic model was stored as a sparse matrix using the sparse function in Matlab [188].

The sparse function syphons out the zero elements from the stoichiometric matrix in order to substantially minimize the file size and accelerate programming time.

The mathematical representation of the consumption and generation of the metabolites, as seen in Eq. 14, is stored in the stoichiometric matrix in binary values of 1 or -1 as seen in appendix A.3.

$$\frac{dM_i}{dt} = (\sum_{m=1}^{a} V_{input_i} - \sum_{m=1}^{b} V_{output_j}) \quad (14)$$

In Eq. 14, M represents the concentration of the metabolites, a and b represents the reaction number for input and output flux rates respectively, V_{input} and V_{output} are the reaction rates for each enzyme [186].

6.2 ODE solver

A set of ordinary differential equations (ODE) was developed for the evaluation of the metabolite concentrations with respect to their consumption or generation based on the 'Enz_dynmod.mat' function file. An ODE solver embedded in Matlab software was used to evaluate the metabolite concentrations in the form of ODEs stored in the function file 'Enz_ODE_mod.mat'. The ODE solver uses initial conditions for the metabolite concentrations as listed in section 5.5.

$$\frac{dM_i}{dt} = \sum_j S_{ij}.r_j \quad (15)$$

In Eq. 15, M represents the concentration of the metabolites, S represents the *ixj* matrix containing stoichiometric information on 68 metabolites for 53 reactions, r represents the vector containing the reaction rates for each enzyme involved in the 9 metabolic pathways [5].

The dynamic metabolic model forms implicit non-linear ODEs of the changing metabolite concentrations as a function of time [197]. ODE problems often involve stiffness or complexity in numerical determination. Stiffness arises when the time factor substantially differs on a large scale for individual components of the given problem [188]. Evidently, the metabolic model involves

large variation between the kinetics of individual enzymes [5]. This necessitates the implementation of an appropriate ODE solver. The ODE solvers embedded within the Matlab software for a variety of applications are listed in Table 6.1.

Table 6.1: Description and application of ODE solvers embedded in Matlab software for a variety of differential equations [188]**.**

ODE solver	Type of differential equation	Application
Ode45	Non-stiff	Evaluation of a function dependent on time and state variables.
Ode23	Non-stiff problem	Evaluation of a function dependent on time and state variables with moderate stiffness and non-restrictive tolerances.
Ode113	Non-stiff problem	Employed in place of ode45 when a problem involves strict tolerance constraints.
Ode15s	Fully implicit with non-negativity constraint and stiffness	Evaluation of a problem with high level of stiffness and when ode45 is ineffective at determining the solution productively.
Ode23s	Stiffness	Replaces ode15s when tolerances are non-restricting and low accuracy is required in the solution
Ode23t	Stiffness in differential algebraic equations	Evaluation of differential algebraic equations at high frequencies.
Ode15i	Fully implicit and stiff	Fully implicit ODE system

Since the metabolic model involves implicit differential equations, which exhibit stiffness due to the massive discrepancy in enzyme kinetics, ode15s is employed for evaluation of the dynamic model [188]. Ode15s provides an efficient framework to evaluate the metabolic model since ode45 failed to return a solution within a reasonable period of time. Ode15s is a solver of changeable orders derived from the numerical differentiation methods [199]. Gear's method, a backward differentiation method can also be utilized in certain scenarios. Ode15s is capable of solving problems at multiple steps where the solution has to be determined from earlier data points [188]. Specifically, ode15s offers the functionality to integrate non-negativity constraints in the solver [188]. Non-negativity constraints are essential in substrate modelling since metabolite concentration cannot biologically fall below null values [200]. Hence, a nonnegative constraint is

placed on the ode solver by using the options functions as shown in appendix 1.1. The nonnegative constraint precludes the integration problem from descending into negative infinity.

6.3 Optimization of kinetic parameters

The metabolic model possesses kinetic parameters from literature studies, which investigated the enzyme kinetics in isolated conditions *in vitro* [191]. Hence, these kinetic parameters have to be optimized for improved fitting on the experimental data. Optimal solutions of enzyme kinetics are explored through linear and non-linear objective functions. A primary example of a linear objective function is maximizing the production of cell density [14]. On the other hand, cellular goals change with varying environmental conditions. For instance, cells focus on increasing biomass growth rate in nitrogen rich conditions but switch to energy conservation in nitrogen deplete conditions [201]. The gene regulatory networks within the cell will upregulate enzymes responsible for energy storage in the form of carbohydrates and lipids [70], [132]. Hence, a set of discrete objective functions are taken into account to study the impact on metabolic behavior. These objective functions are discussed in greater detail in section 2.2.5.

For optimization of biomass growth, objective functions will tend towards directly minimizing the specific activity of the enzymes that lead to formation of intermediate metabolites irrelevant to biomass growth. Therefore, constraints have to be implemented to maintain the specific activity of these enzymes and ensure it does not fall below a threshold to contradict biological theory. In order to maintain a threshold of enzymatic activity, the enzyme content is optimized for the given objective function. The initial enzyme quantity is set as 0.0001 $mmol.L^{-1}$, which is constrained between 0 and 0.01 since enzyme content does not exceed intracellular protein content [96].

The Matlab optimization toolbox is employed to evaluate optimal solutions for the enzyme content. The optimization toolbox, as seen in Table 6.2, contains a variety of solvers, which can be applied for linear, non-linear, scalar or vector problem sets.

Table 6.2: Description and example of optimization algorithms embedded in Matlab software with specific applications [188]**.**

Solver type	Type of problems	Example solver	Description
Minimization	• Scalar or unconstrained minimization. • Mixed integer linear programming • Semi-infinite minimization	Fminbnd Linprog Quadprog Fmincon Fseminf	Searches for a local minimum of the objective function near an initial value.
Multi-objective	• Goal attainment • Minimaz	Fgoalattain Fminimax	Searches for an optimal solution by minimizing the maximal values of a function set.
Equation solving	• Linear and non-linear equations	Mldivide Fzero Fsolve	Searches a solution for a scalar or vector valued non-linear equation at an initial value.
Least-squares (model-fitting)	• Linear least-squares • Non-negative or constrained linear least squares • Non-linear curve fitting	Mldivide Lsqlin Lsqnonneg lsqnonlin	Searches for optimal solution by fitting a model to data.

The minimization function was applied for the set of implicit non-linear ODEs from the metabolic model in order to obtain the optimal values of enzyme content for enhanced biomass growth, lipid accumulation and antioxidant production. A negative objective function is adopted for maximizing a goal through the fmincon function. Fmincon function in Matlab is typically used to find minimum or maximum of constrained nonlinear multivariable functions. The optimset function was integrated into the fmincon optimization function in order to implement the interior point algorithm. The interior point algorithm searches for an approximation of an optimal solution in linear and non-linear programming models within a constrained feasible space over several iterations [188]. In the metabolic model, the objective functions listed in Eq. 16 were used to achieve the kinetics for the metabolic model under varying environmental conditions.

$$\frac{X_b}{C_{glc}+C_{gly}} \ , \frac{C_{AcoA}}{C_{glc}+C_{gly}}, \frac{C_{LTN}}{C_{glc}+C_{gly}} \tag{16}$$

6.4 Experimental validation of metabolic pathways at different nitrogen ratios

A dynamic modelling framework has the capacity for reduced quantity of parameters as opposed to a steady-state flux balance analysis method. The metabolic modelling framework incorporates a simplified network, which is augmented after calibrating the initial kinetic parameters. In this research, the glycolysis reactions are initially calibrated as they play an essential role in biomass growth. Once these metabolic pathways are found to have robust kinetics, then the terpenoid backbone and carotenoid biosynthesis pathways are introduced to the metabolic model. Ultimately, the optimal solutions for the enzyme content from the set of objective functions were validated with the experimental data. The metabolic model simulated the behavior of the microalgae at variation in nitrogen content and carbon source proportions. Hence, the following section includes the experimental validation for C:N ratio of 10:1, 40:1 and 80:1 as seen in Figure 6.1, Figure 6.2 and Figure 6.3.

The model generally agrees well with the experimental data specifically the uptake of glycine for low nitrogen content as seen in Figure 6.2 and Figure 6.3. The metabolic model was tied to the precursors generated from the assimilation of glycine. Hence, microalgal biomass is directly impacted by the reduced or increased production of L-Glutamine, which is an essential amino acid towards cell maintenance and growth. As seen in the experimental validation for C:N 80:1 ratio in Figure 6.3, there is an early onset of saturation observed in biomass growth, since nitrogen is a primary source of energy for cellular growth. This shows reliable prediction of biomass growth from experimental data where the biomass growth reaches a plateau due to the intensity of nitrogen limitation in this C:N ratio. The range of final biomass growth attained from the model

prediction at different nitrogen conditions is close to the experimental data. However, the model underestimates the biomass growth in each of the three scenarios in Figure 6.1, 6.2 and 6.3 explored for experimental validation. This can be attributed to the depletion of intracellular pools of nitrogen, which are not incorporated in the metabolic model. Particularly, the experimental nitrogen uptake at C:N 10:1 ratio, plateaus in Figure 6.1 but the model is unable to capture the effect of nitrogen rich storage pools in the microalgal cell. The metabolic pathways integrated a singular amino acid but the intermediates generated from phosphates are not taken into account within this model.

The model exhibits a rapid increase in lipid production at C:N 80:1 ratio. This is in agreement with the microalgal response in high stress conditions. However, the model requires further improvement in the kinetics of the TCA cycle. The TCA cycle is responsible for the breakdown of ACoA, which ultimately leads to the production of Malonyl CoA, a primary precursor in the unidirectional elongation of fatty acids. The TCA cycle is maintained by intermediates generated from the nitrogen assimilation pathway while the nitrogen assimilation requires an intermediate produced from the TCA cycle. The complex interconnected relationship between the TCA cycle and the nitrogen assimilation pathway needs to be further refined to improve the prediction of lipid accumulation. Moreover, experimental validation of lipid accumulation in time series would improve the validation results. Alternatively, the changes in antioxidant production at lower nitrogen content are in line with the experimental data. Orthophosphate, an intermediate required in the glycolytic pathway for pyruvate production, is generated from the metabolism of glycine. Hence, minimizing nitrogen content lowers the intracellular antioxidant content.

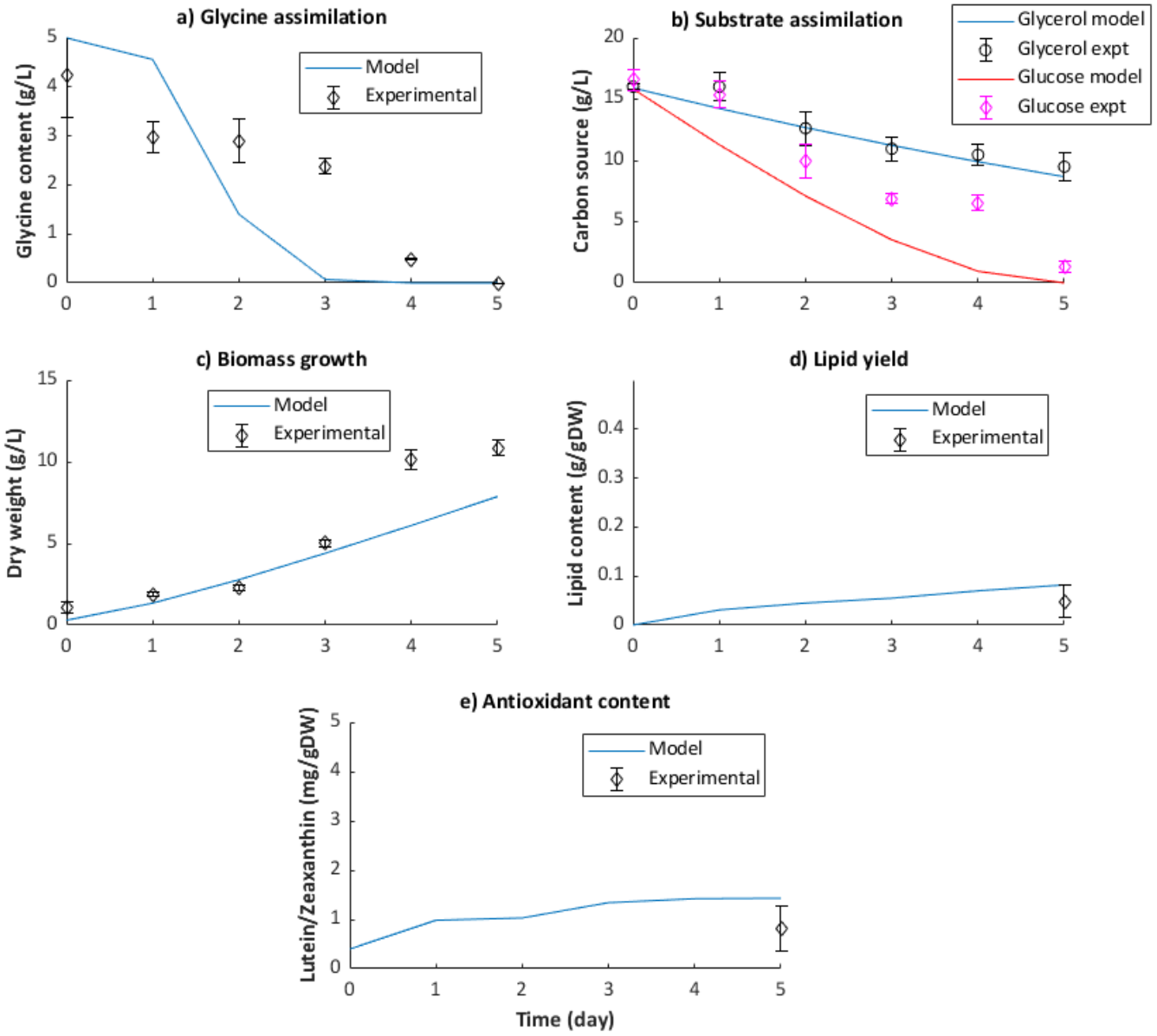

Figure 6.1: Simulation of metabolic model and results validation of a) glycine, b) carbon substrates, c) biomass growth, d) lipid yield and e) antioxidant content for batch level operation of *A. protothecoides* at C:N 10:1 ratio.

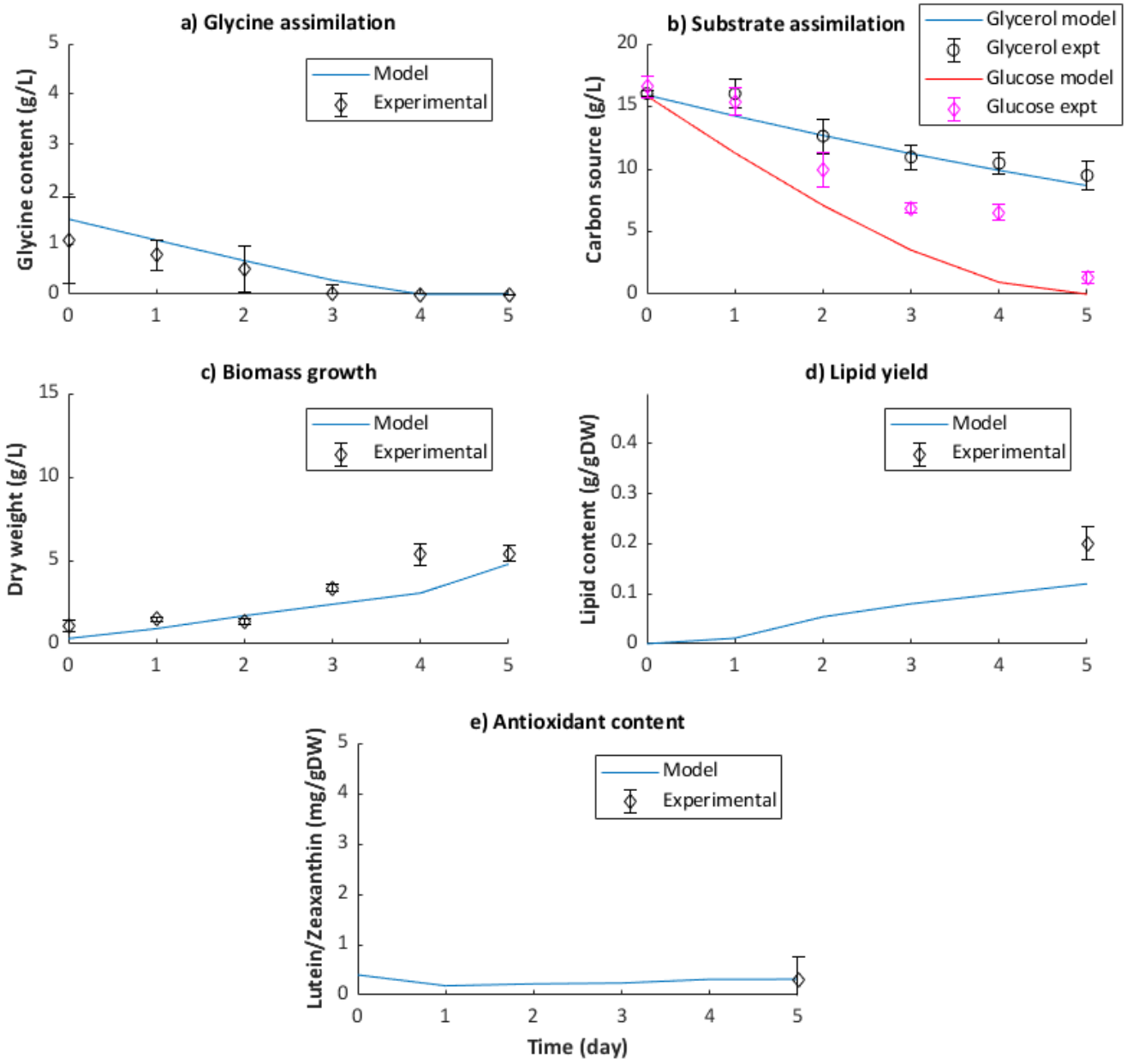

Figure 6.2: Simulation of metabolic model and results validation of a) glycine, b) carbon substrates, c) biomass growth, d) lipid yield and e) antioxidant content for batch level operation of *A. protothecoides* at C:N 40:1 ratio.

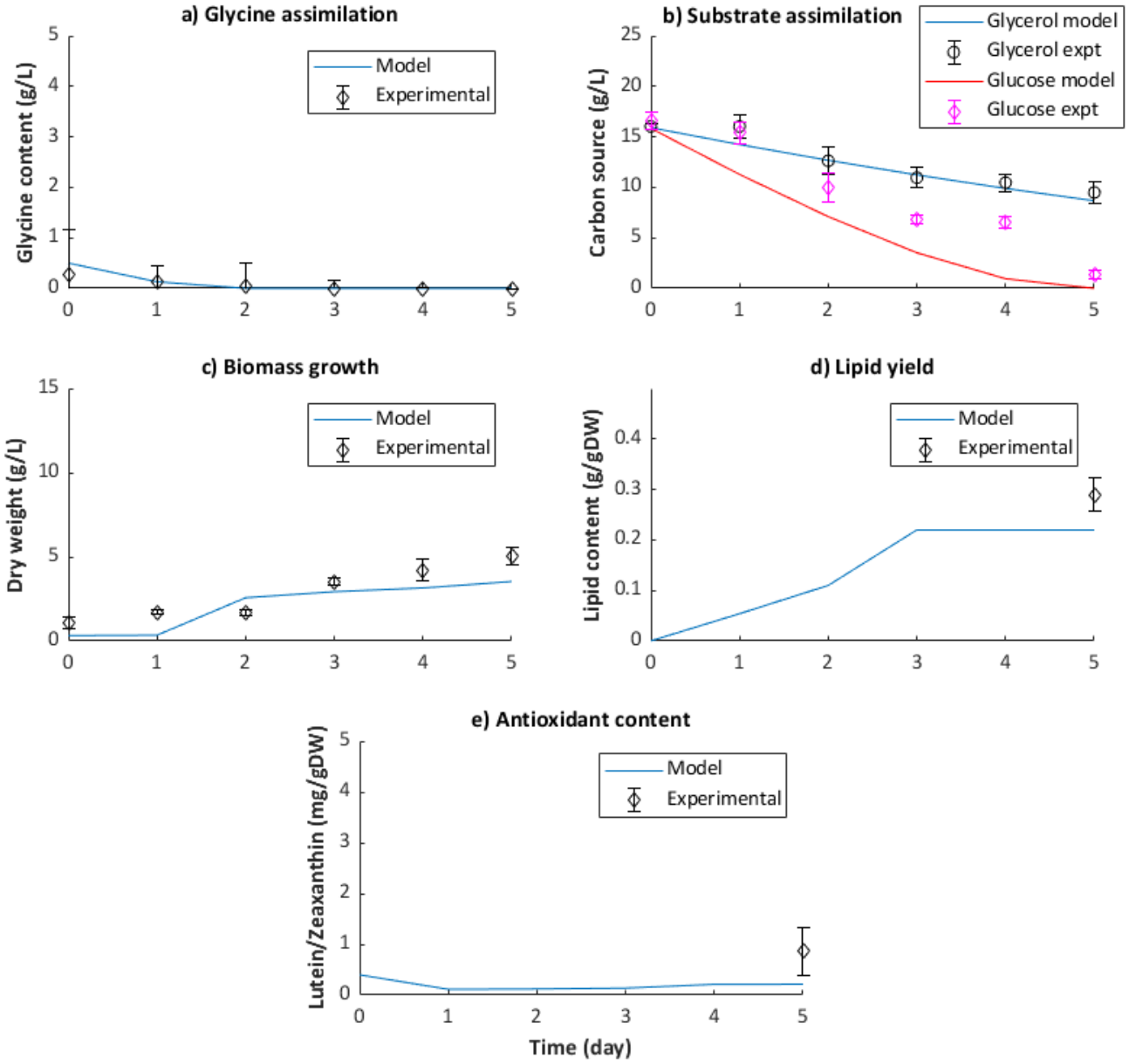

Figure 6.3: Simulation of metabolic model and results validation of a) glycine, b) carbon substrates, c) biomass growth, d) lipid yield and e) antioxidant content for batch level operation of *A. protothecoides* at C:N 80:1 ratio.

6.5 Experimental validation of metabolic pathways at different proportions of carbon sources

Additionally, the model was also used to simulate for variation in carbon source proportions at high glucose (75:25 for glucose to glycerol ratio) and high glycerol content (25:75 for glucose to glycerol ratio) at the same C:N 40:1 ratio as seen in Figure 6.4 and Figure 6.5. The enzymes responsible for the formation of Glucose 6-phosphate have faster kinetics from the glucose assimilation pathway as opposed to the metabolism of glycerol. This is observed in the initial plateau in biomass growth at higher glycerol content, which agrees with the experimental data. The assimilation of glycine is unaffected by the variation in proportions of carbon source since the required metabolites were not connected to the glycolytic pathway. The assimilation of glycerol achieves better agreement with the experimental data in both Figure 6.4 and Figure 6.5. The discrepancies with the experimental validation of glucose can be associated with the limited understanding of the glucose transporters in microalgal cells. The enzyme databases don't store genome specific information on glucose transporters which influences the accuracy of glucose assimilation.

Similarly, the lipid accumulation rapidly increases in high glucose content as opposed to high glycerol content where a slower buildup in the initial stage was observed as seen in Figure 6.4 and Figure 6.5. The intermediates required for fatty acid synthesis are generated with faster kinetics in higher glucose conditions. Alternatively, antioxidant production is significantly higher in glycerol rich conditions; this can be attributed to the upregulation of genes that control the enzyme content for Glyceraldehyde 3-phosphate (G3P) formation within the chloroplast. The enhanced production of G3P promotes production of antioxidants.

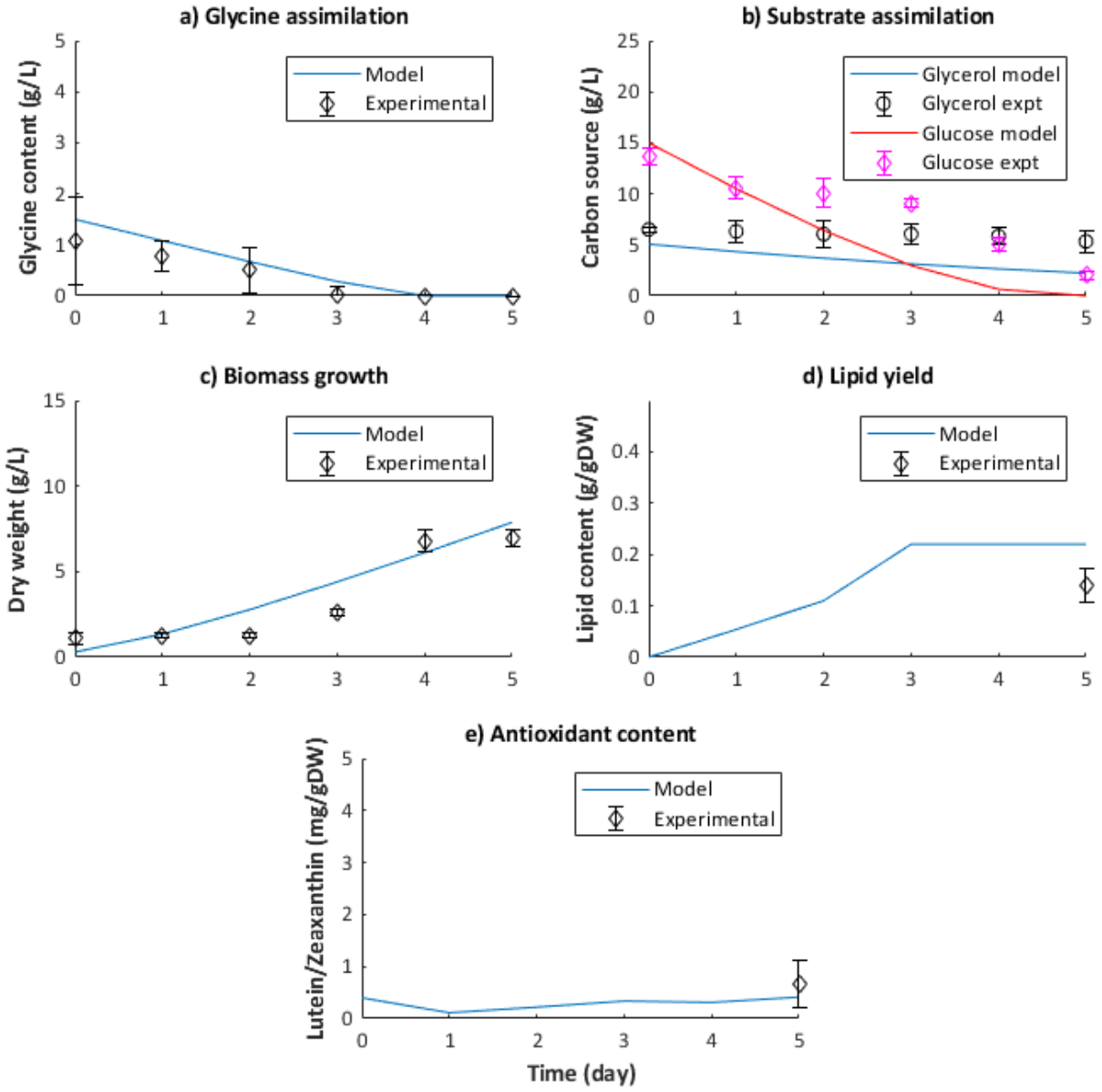

Figure 6.4: Simulation of metabolic model and results validation of a) glycine, b) carbon substrates, c) biomass growth, d) lipid yield and e) antioxidant content for batch level operation of *A. protothecoides* at high glucose nutrient conditions.

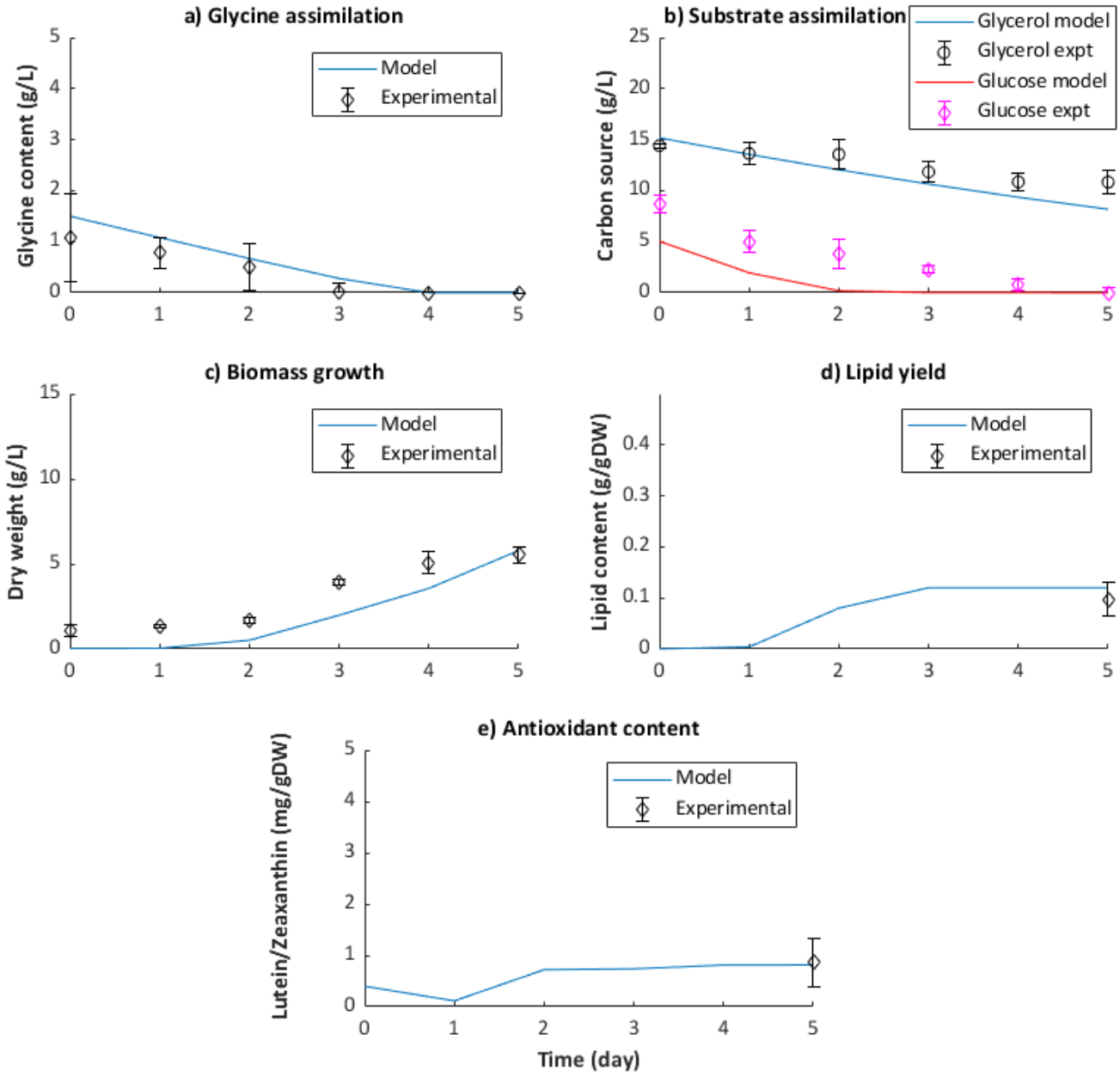

Figure 6.5: Simulation of metabolic model and results validation of a) glycine, b) carbon substrates, c) biomass growth, d) lipid yield and e) antioxidant content for batch level operation of *A. protothecoides* at high glycerol nutrient conditions.

In summary, the metabolic model achieves good agreement for biomass growth in all five scenarios as seen in Figure 6.1-6.5. Evidently, interlinking biomass growth and the relevant metabolites for macronutrient formation has built a reliable relationship. Additional experimental data in time series is required to validate lipid content and the specific carotenoids produced in the microalgal system. While glycine assimilation reaches good agreement at low C:N ratio, intracellular storage pools have to be considered to enhance the model's ability to predict nitrogen uptake at higher C:N proportions. Moreover, glycerol uptake is simpler and easier to simulate due to the absence of transporter proteins. On the other hand, kinetic information on glucose transporter proteins should be improved to enhance simulation results for glucose consumption.

Chapter 7: Conclusions and Recommendations

In this chapter, the summary of conclusions is reported for each investigative study conducted in the research project. This section provides highlights and recommendations for the batch level operation, metabolic reconstruction and metabolic model design.

7.1 Effect of nutrients on product composition

The batch level operation of the microalgae shows simultaneous assimilation of both organic carbon substrates. Glycerol uptake is controlled by its osmoregulatory capability for the microorganism against high salinity environment, the enzymes within the cell metabolize the molecule, which enables modulation of other pigments and bioactive compounds. The high glycerol nutrient conditions enabled production of significantly high levels of lutein, zeaxanthin and beta-carotene at about 52.43 $mg.L^{-1}$ and 6.2 $mg.L^{-1}$ respectively. High biomass growth of 11.53 $g.L^{-1}$ was reported for C:N ratio of 10:1 at high glucose conditions. Since biomass growth is higher with high glucose and nitrogen content, bi-substrate cultivation ensures high product yields in order to not compromise the biomass growth. While batch level operation informs the strategies utilized for a fed-batch system, the biomass results are an indicator of substantially higher biomass yields that can be obtained in a larger system. Nitrogen deprivation promotes lipid accumulation in microalgae but there is an upper threshold where the biomass growth is stunted and thus reduces the viability of the system entirely. Moreover, the biomass yield based on the consumption of carbon source is much higher for the microalgal system in comparison to bacterial cultures.

7.2 Metabolic reconstruction

The metabolic reconstruction of the metabolic pathways enables the research to further understand the microalgal response to changes in nutrient conditions. The pathway for glycerol assimilation helps explain the modulation of pigment content within the microalgae. Glucose is seen to circumvent the carbon fixation pathway and render the chloroplast inactive, which leads to its degeneration. Further investigation highlight the pathways taken by microalgae for carotenoid biosynthesis, which differ from microalgal strains outside of Chlorella species due to evolutionary changes. Nevertheless, the central carbon metabolism for the microalgae integrates the glucose and glycerol metabolism as well as the Calvin-Benson cycle for the synthesis of primary precursors. Since, the complexity of the central carbon metabolism is enhanced in the microalgal system, this strengthens their case to support an integrated biorefinery system. Alternatively, both products share the precursors G3P and pyruvate, that means the product yields of the antioxidants are affected when the cell tends towards lipid accumulation for energy storage.

7.3 Dynamic metabolic modelling

The dynamic metabolic model enables a simulation of microalgal response to changing process conditions. The model was calibrated within a small threshold of feasible enzyme quantities within a cell. This allows the metabolic model to make predictions based on the enzyme kinetics and the network of pathways without limiting the decision making to experimental results. Hence, the metabolic model provides more reliable results than a kinetic model, which is driven on experimental results. Similar to several other models, increasing complexity can be introduced to the dynamic metabolic model after the given pathways have been calibrated appropriately. Specifically, the carotenoid biosynthesis should be expanded in order to explain the low product

yields of lutein and zeaxanthin in certain conditions. The low product yields could be attributed to the production of other carotenoids.

Bibliography

[1] M. Bilal, T. Rasheed, I. Ahmed, and H. M. N. Iqbal, "High-value compounds from microalgae with industrial exploitability - A review.," *Front. Biosci. (Schol. Ed).*, vol. 9, pp. 319–342, Jun. 2017.

[2] M. Zuluaga, V. Gueguen, G. Pavon-Djavid, and D. Letourneur, "Carotenoids from microalgae to block oxidative stress," *Bioimpacts*, vol. 7, no. 1, pp. 1–3, Feb. 2017.

[3] N. G. Grant, M. H. Hommersand, J. Dai, and Q. Wu, "The Respiratory Chain of *Chlorella protothecoides*: I. Inhibitor Responses and Cytochrome Components of Whole Cells.," *Plant Physiol.*, vol. 54, no. 1, pp. 50–6, Jul. 1974.

[4] W. B. Kong, H. Yang, Y. T. Cao, H. Song, S. F. Hua, and C. G. Xia, "Effect of Glycerol and Glucose on the Enhancement of Biomass, Lipid and Soluble Carbohydrate Production by *Chlorella vulgaris* in Mixotrophic Culture," *Food Technol. Biotechnol.*, vol. 51, 2013.

[5] G. Stephanopoulos, A. A. Aristidou, and J. H. Nielsen, *Metabolic engineering: principles and methodologies*. Elsevier Inc., 1998.

[6] S. I. B. Blackburn and K. J. Lee-Chang, "Blue biotechnology," in *The Dictionary of Genomics, Transcriptomics and Proteomics*, First., Stéphane La Barre and Stephen S. Bates., Ed. Hobart: Wiley, 2015, pp. 1–1.

[7] S. M. A. Mobin, H. Chowdhury, and F. Alam, "Commercially important bioproducts from microalgae and their current applications – A review," *Energy Procedia*, vol. 160, pp. 752–760, 2019.

[8] D. Parlevliet and N. R. Moheimani, "Efficient conversion of solar energy to biomass and electricity," *Aquat. Biosyst.*, vol. 10, p. 4, Jun. 2014.

[9] S. Sigamani, D. Ramamurthy, and H. Natarajan, "A Review on Potential Biotechnological applications of Microalgae," *J. Appl. Pharm. Sci.*, pp. 179–184, 2016.

[10] M. I. Khan, J. H. Shin, and J. D. Kim, "The promising future of microalgae: current status, challenges, and optimization of a sustainable and renewable industry for biofuels, feed, and other products," *Microb. Cell Fact.*, vol. 17, p. 36, Mar. 2018.

[11] M.-H. Liang, L. Wang, Q. Wang, J. Zhu, and J.-G. Jiang, "High-value bioproducts from microalgae: Strategies and progress," *Crit. Rev. Food Sci. Nutr.*, pp. 1–19, Apr. 2018.

[12] S. Mostafa, *Microalgal Biotechnology: Prospects and Applications*. IntechOpen, 2012.

[13] S. Mobin and F. Alam, "Some Promising Microalgal Species for Commercial Applications: A review," *Energy Procedia*, vol. 110, pp. 510–517, 2017.

[14] H. De la Hoz Siegler, W. C. McCaffrey, R. E. Burrell, and A. Ben-Zvi, "Optimization of microalgal productivity using an adaptive, non-linear model based strategy," *Bioresour.*

Technol., vol. 104, pp. 537–546, 2012.

[15] Y. Li, M. Horsman, B. Wang, N. Wu, and C. Q. Lan, "Effects of nitrogen sources on cell growth and lipid accumulation of green alga *Neochloris oleoabundans*.," *Appl. Microbiol. Biotechnol.*, vol. 81, no. 4, pp. 629–636, Dec. 2008.

[16] H. Rismani-Yazdi, K. H. Hampel, C. D. Lane, B. A. Kessler, and N. M. White, "High-productivity lipid production using mixed trophic state cultivation of *Auxenochlorella (Chlorella) protothecoides*.," *Bioprocess Biosyst. Eng.*, vol. 38, no. 4, pp. 639–650, Apr. 2015.

[17] M. Paul Abishek, J. Patel, and A. Prem Rajan, "Algae oil: a sustainable renewable fuel of future.," *Biotechnol. Res. Int.*, vol. 2014, p. 272814, May 2014.

[18] J. Benemann, "Opportunities and challenges in algae biofuels production," *Algae World*, 2008.

[19] H. Karan, C. Funk, M. Grabert, M. Oey, and B. Hankamer, "Green Bioplastics as Part of a Circular Bioeconomy," *Trends Plant Sci.*, vol. 24, no. 3, pp. 237–249, Mar. 2019.

[20] M. Hernández-Lepe, A. Wall-Medrano, J. A. López-Díaz, M. A. Juárez-Oropeza, and A. Ramos-Jiménez et al., "Hypolipidemic Effect of *Arthrospira (Spirulina)* maxima Supplementation and a Systematic Physical Exercise Program in Overweight and Obese Men: A Double-Blind, Randomized, and Crossover Controlled Trial.," *Mar. Drugs*, vol. 17, no. 5, May 2019.

[21] M. P. Caporgno and A. Mathys, "Trends in Microalgae Incorporation Into Innovative Food Products With Potential Health Benefits.," *Front. Nutr.*, vol. 5, p. 58, 2018.

[22] J. Hermawan, E. D. Masithah, W. Tjahjaningsih, and A. A. Abdillah, "Increasing β-carotene content of phytoplankton *Dunaliella salina* using different salinity media," *IOP Conf. Ser. Earth Environ. Sci*, vol. 137, p. 12034, 2018.

[23] R. Sathasivam, R. Radhakrishnan, A. Hashem, and E. F. Abd-Allah, "Microalgae metabolites: A rich source for food and medicine," *Saudi J. Biol. Sci.*, vol. 26, no. 4, pp. 709–722, May 2019.

[24] J. S. Singh, A. Kumar, A. N. Rai, and D. P. Singh, "Cyanobacteria: A Precious Bio-resource in Agriculture, Ecosystem, and Environmental Sustainability.," *Front. Microbiol.*, vol. 7, p. 529, 2016.

[25] C. Gonzalez-Fernandez, S. Barreiro-Vescovo, I. de Godos, M. Fernandez, and M. Ballesteros et al., "Biochemical methane potential of microalgae biomass using different microbial inocula," *Biotechnol. Biofuels*, vol. 11, p. 184, 2018.

[26] L. Delgadillo-Mirquez, F. Lopes, B. Taidi, and D. Pareau, "Nitrogen and phosphate removal from wastewater with a mixed microalgae and bacteria culture," *Biotechnol. Reports*, vol. 11, pp. 18–26, Sep. 2016.

[27] A. R. J. Lima, A. S. Siqueira, J. M. de Vasconcelos, J. S. Pereira, J. S. N. de Azevedo, and P. H. G. Moraes, "Insights Into *Limnothrix sp.* Metabolism Based on Comparative Genomics," *Front. Microbiol.*, vol. 9, p. 2811, Nov. 2018.

[28] Indrayani and A. Haslianti, "Isolation and screening of marine microalgae from Kendari waters, Southeast Sulawesi, Indonesia suitable for outdoor mass cultivation in hypersaline media," *AACL Bioflux*, vol. 11, no. 5, pp. 1445–1455, 2018.

[29] F. Bumbak, S. Cook, V. Zachleder, S. Hauser, and K. Kovar, "Best practices in heterotrophic high-cell-density microalgal processes: achievements, potential and possible limitations," *Appl. Microbiol. Biotechnol.*, vol. 91, no. 1, pp. 31–46, Jul. 2011.

[30] F. K. El-Baz and H. H. A. El Baky, "Pilot Scale of Microalgal Production Using Photobioreactor," in *Photosynthesis - From Its Evolution to Future Improvements in Photosynthetic Efficiency Using Nanomaterials*, InTech, 2018.

[31] Y. R. Cruz, D. A. G. Aranda, P. R. Seidl, G. C. Diaz, and M. M. Fortes et al., *Cultivation Systems of Microalgae for the Production of Biofuels*. InTechOpen, 2018.

[32] J. Masojídek, M. Sergejevová, J. R. Malapascua, and J. Kopecký, "Thin-Layer Systems for Mass Cultivation of Microalgae: Flat Panels and Sloping Cascades," in *Algal Biorefineries*, Cham: Springer International Publishing, 2015, pp. 237–261.

[33] S. Huo, Z. Wang, S. Zhu, Q. Shu, and L. Qin et al., "Biomass Accumulation of *Chlorella Zofingiensis* G1 Cultures Grown Outdoors in Photobioreactors," *Front. Energy Res.*, vol. 6, p. 49, Jun. 2018.

[34] H. N. P. Vo, H. H. Ngo, W. Guo, T. M. H. Nguyen, and Y. Liu et al., "A critical review on designs and applications of microalgae-based photobioreactors for pollutants treatment," *Sci. Total Environ.*, vol. 651, pp. 1549–1568, Feb. 2019.

[35] M. A. Alam and Z. Wang, *Microalgae biotechnology for development of biofuel and wastewater treatment*, 1st ed. Springer Singapore, 2019.

[36] N. Sreekumar, M. S. Giri Nandagopal, A. Vasudevan, R. Antony, and N. Selvaraju, "Marine microalgal culturing in open pond systems for biodiesel production—Critical parameters," *J. Renew. Sustain. Energy*, vol. 8, no. 2, p. 023105, Mar. 2016.

[37] X. Wen, H. Tao, X. Peng, Z. Wang, and Y. Xu, "Sequential phototrophic–mixotrophic cultivation of oleaginous microalga *Graesiella sp.* WBG-1 in a 1000 m^2 open raceway pond," *Biotechnol. Biofuels*, vol. 12, no. 1, p. 27, Dec. 2019.

[38] O. Perez-Garcia and Y. Bashan, "Microalgal Heterotrophic and Mixotrophic Culturing for Bio-refining: From Metabolic Routes to Techno-economics BT - Algal Biorefineries: Volume 2: Products and Refinery Design," A. Prokop, R. K. Bajpai, and M. E. Zappi, Eds. Cham: Springer International Publishing, 2015, pp. 61–131.

[39] D. Morales-Sanchez, O. A. Martinez-Rodriguez, J. Kyndt, and A. Martinez, "Heterotrophic growth of microalgae: metabolic aspects.," *World J. Microbiol. Biotechnol.*, vol. 31, no. 1, pp. 1–9, Jan. 2015.

[40] O. Perez-Garcia, F. M. E. Escalante, L. E. de-Bashan, and Y. Bashan, "Heterotrophic cultures of microalgae: metabolism and potential products.," *Water Res.*, vol. 45, no. 1, pp. 11–36, Jan. 2011.

[41] H. Chansang and K. E. Cooksey, "The glucose transport system of *Amphora Coffeaeformis*

(Bacillariophyceae),” *J. Phycol.*, vol. 13, no. 1, pp. 51–57, Mar. 1977.

[42] J. Feng, Y. Guo, X. Zhang, G. Wang, and Q. Liu et al., “Identification and characterization of a symbiotic alga from soil bryophyte for lipid profiles.,” *Biol. Open*, vol. 5, no. 9, pp. 1317–23, Sep. 2016.

[43] S. Keerthi, U. D. Koduru, S. S. Nittala, and N. R. Parine, “The heterotrophic eubacterial and archaeal co-inhabitants of the halophilic *Dunaliella salina* in solar salterns fed by Bay of Bengal along south eastern coast of India,” *Saudi J. Biol. Sci.*, vol. 25, no. 7, pp. 1411–1419, Nov. 2018.

[44] J. Roostaei, Y. Zhang, K. Gopalakrishnan, and A. J. Ochocki, “Mixotrophic Microalgae Biofilm: A Novel Algae Cultivation Strategy for Improved Productivity and Cost-efficiency of Biofuel Feedstock Production,” *Sci. Rep.*, vol. 8, no. 1, p. 12528, Dec. 2018.

[45] K. U. Devi, G. Swapna, and S. Suneetha, “Microalgae in Bioremediation: Sequestration of Greenhouse Gases, Clearout of Fugitive Nutrient Minerals, and Subtraction of Toxic Elements from Waters,” *Microb. Biodegrad. Bioremediation*, pp. 433–454, Jan. 2014.

[46] A. Richmond, *Handbook of Microalgal Culture.* John Wiley & Sons, 2007.

[47] Y. Xiao, Y. Lu, J. Dai, and Q. Wu, “Industrial Fermentation of *Auxenochlorella protothecoides* for Production of Biodiesel and Its Application in Vehicle Diesel Engines.,” *Front. Bioeng. Biotechnol.*, vol. 3, p. 164, 2015.

[48] C. Gao, Y. Wang, Y. Shen, D. Yan, and X. He, “Oil accumulation mechanisms of the oleaginous microalga *Chlorella protothecoides* revealed through its genome, transcriptomes, and proteomes,” *BMC Genomics*, vol. 15, no. 1, Jul. 2014.

[49] C. Darpito, W. S. Shin, S. Jeon, H. Lee, and J. H. Kwon et al., “Cultivation of *Chlorella protothecoides* in anaerobically treated brewery wastewater for cost-effective biodiesel production,” *Bioprocess Biosyst. Eng.*, vol. 38, no. 3, pp. 523–530, Feb. 2015.

[50] W. Zhou, Y. Li, M. Min, B. Hu, and X. Ma et al., “Growing wastewater-born microalga *Auxenochlorella protothecoides* UMN280 on concentrated municipal wastewater for simultaneous nutrient removal and energy feedstock production,” *Appl. Energy*, vol. 98, pp. 433–440, 2012.

[51] Y. H. Lee and L. T. Fan, “Kinetic studies of enzymatic hydrolysis of insoluble cellulose: (II). Analysis of extended hydrolysis times,” *Biotechnol. Bioeng.*, vol. 25, no. 4, pp. 939–966, Apr. 1983.

[52] M. M. EL-Sheekh, M. Y. Bedaiwy, M. E. Osman, and M. M. Ismail, “Mixotrophic and heterotrophic growth of some microalgae using extract of fungal-treated wheat bran,” *Int. J. Recycl. Org. Waste Agric.*, vol. 1, no. 1, Dec. 2012.

[53] T. Heredia-Arroyo, W. Wei, and B. Hu, “Oil accumulation via heterotrophic/mixotrophic *Chlorella protothecoides*,” *Appl. Biochem. Biotechnol.*, vol. 162, no. 7, pp. 1978–1995, Nov. 2010.

[54] Q. Wen, Z. Chen, P. Li, R. Duan, and N. Ren, “Lipid production for biofuels from hydrolyzate of waste activated sludge by heterotrophic *Chlorella protothecoides*,”

Bioresour. Technol., vol. 143, pp. 695–698, 2013.

[55] Q. Fei, R. Fu, L. Shang, C. J. Brigham, and H. N. Chang, "Lipid production by microalgae *Chlorella protothecoides* with volatile fatty acids (VFAs) as carbon sources in heterotrophic cultivation and its economic assessment," *Bioprocess Biosyst. Eng.*, vol. 38, no. 4, pp. 691–700, Mar. 2015.

[56] A. Patel, L. Matsakas, U. Rova, and P. Christakopoulos, "Heterotrophic cultivation of *Auxenochlorella protothecoides* using forest biomass as a feedstock for sustainable biodiesel production.," *Biotechnol. Biofuels*, vol. 11, p. 169, 2018.

[57] X. Li, H. Xu, and Q. Wu, "Large-scale biodiesel production from microalga *Chlorella protothecoides* through heterotrophic cultivation in bioreactors," *Biotechnol. Bioeng.*, vol. 98, no. 4, pp. 764–771, Nov. 2007.

[58] M. P. Caporgno, I. Haberkorn, L. Böcker, and A. Mathys, "Cultivation of *Chlorella protothecoides* under different growth modes and its utilisation in oil/water emulsions," *Bioresour. Technol.*, vol. 288, Sep. 2019.

[59] M. B. Ariede, T. M. Candido, A. L. M. Jacome, M. V. R. Velasco, J. C. M. de Carvalho, and A. R. Baby, "Cosmetic attributes of algae - A review," *Algal Research*, vol. 25. Elsevier B.V., pp. 483–487, 01-Jul-2017.

[60] L. Grossmann, J. Hinrichs, and J. Weiss, "Solubility and aggregation behavior of protein fractions from the heterotrophically cultivated microalga *Chlorella protothecoides*," *Food Res. Int.*, vol. 116, pp. 283–290, Feb. 2019.

[61] S. Benelhadj, A. Gharsallaoui, P. Degraeve, H. Attia, and D. Ghorbel, "Effect of pH on the functional properties of *Arthrospira (Spirulina) platensis* protein isolate," *Food Chem.*, vol. 194, pp. 1056–1063, Mar. 2016.

[62] X. M. Shi and F. Chen, "Production and rapid extraction of lutein and the other lipid-soluble pigments from *Chlorella protothecoides* grown under heterotrophic and mixotrophic conditions," *Nahrung/Food*, vol. 43, no. 2, pp. 109–113, Mar. 1999.

[63] "*Chlorella protothecoides* is a New Generation Dietary Source of Omega-3 Fatty Acids and Carotenoids for Human Ocular Health | IOVS | ARVO Journals." [Online]. Available: https://iovs.arvojournals.org/article.aspx?articleid=2380351. [Accessed: 14-Jan-2020].

[64] A. Patel, L. Matsakas, U. Rova, and P. Christakopoulos, "Heterotrophic cultivation of *Auxenochlorella protothecoides* using forest biomass as a feedstock for sustainable biodiesel production," *Biotechnol. Biofuels*, vol. 11, p. 169, Jun. 2018.

[65] H. H. Chen and J. G. Jiang, "Lipid Accumulation Mechanisms in Auto and Heterotrophic Microalgae.," *J. Agric. Food Chem.*, vol. 65, no. 37, pp. 8099–8110, Sep. 2017.

[66] J. Hu, D. Nagarajan, Q. Zhang, J.-S. Chang, and D.-J. Lee, "Heterotrophic cultivation of microalgae for pigment production: A review," *Biotechnol. Adv.*, vol. 36, no. 1, pp. 54–67, 2018.

[67] T. Xiang, R. E. Jinkerson, S. Clowez, C. Tran, and M. Onishi et al., "Glucose-Induced Trophic Shift in an Endosymbiont Dinoflagellate with Physiological and Molecular

Consequences.," *Plant Physiol.*, vol. 176, no. 2, pp. 1793–1807, Feb. 2018.

[68] M. Kröger and F. Müller-Langer, "Impact of heterotrophic and mixotrophic growth of microalgae on the production of future biofuels," *Biofuels*, vol. 2, no. 2, pp. 145–151, Mar. 2011.

[69] R. Katiyar, B. R. Gurjar, R. K. Bharti, A. Kumar, and V. Pruthi et al., "Heterotrophic cultivation of microalgae in photobioreactor using low cost crude glycerol for enhanced biodiesel production," *Renew. Energy*, vol. 113, pp. 1359–1365, 2017.

[70] Y. X. Li, F. J. Zhao, and D. D. Yu, "Effect of nitrogen limitation on cell growth, lipid accumulation and gene expression in *Chlorella sorokiniana*," *Brazilian Archives of Biology and Technology* , vol. 58. scielo , pp. 462–467, 2015.

[71] J. R. Benavente-Valdés, C. Aguilar, J. C. Contreras-Esquivel, A. Méndez-Zavala, and J. Montañez, "Strategies to enhance the production of photosynthetic pigments and lipids in chlorophycae species," *Biotechnol. Reports*, vol. 10, pp. 117–125, 2016.

[72] B. D. Shoener, S. M. Schramm, F. Béline, O. Bernard, and B. G. Plósz et al., "Microalgae and cyanobacteria modeling in water resource recovery facilities: A critical review," *Water Res. X*, vol. 2, p. 100024, Feb. 2019.

[73] M. J. Griffiths, "Advantages and Challenges of Microalgae as a Source of Oil for Biodiesel," R. G. Dicks, Ed. Rijeka: IntechOpen, 2011, p. Ch. 9.

[74] R. Bosma, K. Miazek, S. M. Willemsen, M. H. Vermue, and R. H. Wijffels, "Growth inhibition of Monodus subterraneus by free fatty acids.," *Biotechnol. Bioeng.*, vol. 101, no. 5, pp. 1108–1114, Dec. 2008.

[75] W. Xiong, C. Gao, D. Yan, C. Wu, and Q. Wu, "Double CO_2 fixation in photosynthesis-fermentation model enhances algal lipid synthesis for biodiesel production.," *Bioresour. Technol.*, vol. 101, no. 7, pp. 2287–2293, Apr. 2010.

[76] H. De la Hoz Siegler, W. C. McCaffrey, R. E. Burrell, and A. Ben-Zvi, "Optimization of microalgal productivity using an adaptive, non-linear model based strategy," *Bioresour. Technol.*, vol. 104, pp. 537–546, Jan. 2012.

[77] J. C. Ogbonna, H. Yoshizawa, and H. Tanaka, "Treatment of high strength organic wastewater by a mixed culture of photosynthetic microorganisms," *J. Appl. Phycol.*, vol. 12, no. 3, pp. 277–284, 2000.

[78] M. L. Shuler, F. Kargi, and M. DeLisa, *Bioprocess Engineering: Basic Concepts*. Prentice Hall, 2017.

[79] C. González-Figueredo, R. Alejandro Flores-Estrella, and O. A. Rojas-Rejón, "Fermentation: Metabolism, Kinetic Models, and Bioprocessing," in *Current Topics in Biochemical Engineering*, IntechOpen, 2019.

[80] J. E. Ferrell and S. H. Ha, "Ultrasensitivity part I: Michaelian responses and zero-order ultrasensitivity," *Trends Biochem. Sci.*, vol. 39, no. 10, pp. 496–503, Oct. 2014.

[81] O. Perez-Garcia, G. Lear, and N. Singhal, "Metabolic Network Modeling of Microbial

Interactions in Natural and Engineered Environmental Systems.," *Front. Microbiol.*, vol. 7, p. 673, 2016.

[82] J. D. Tibocha-Bonilla, C. Zuñiga, R. D. Godoy-Silva, and K. Zengler, "Advances in metabolic modeling of oleaginous microalgae," *Biotechnol. Biofuels*, vol. 11, no. 1, p. 241, 2018.

[83] E. Stalidzans, A. Seiman, K. Peebo, V. Komasilovs, and A. Pentjuss, "Model-based metabolism design: constraints for kinetic and stoichiometric models," *Biochem. Soc. Trans.*, p. BST20170263, Feb. 2018.

[84] I. Thiele and B. Ø. Palsson, "A protocol for generating a high-quality genome-scale metabolic reconstruction," *Nat. Protoc.*, vol. 5, no. 1, pp. 93–121, Jan. 2010.

[85] Z. Ma, C. Ye, W. Deng, M. Xu, and G. Liu et al., "Reconstruction and Analysis of a Genome-Scale Metabolic Model of Ganoderma lucidum for Improved Extracellular Polysaccharide Production," *Front. Microbiol.*, vol. 9, p. 3076, Dec. 2018.

[86] C. Lieven, L. A. H. Petersen, S. B. Jørgensen, K. V. Gernaey, and N. Sonnenschein et al., "A Genome-Scale Metabolic Model for *Methylococcus capsulatus* (Bath) Suggests Reduced Efficiency Electron Transfer to the Particulate Methane Monooxygenase," *Front. Microbiol.*, vol. 9, p. 2947, Dec. 2018.

[87] S. Gama-Castro, V. Jimenez-Jacinto, M. Peralta-Gil, A. Santos-Zavaleta, and B. Contreras-Moreira et al., "RegulonDB (version 6.0): gene regulation model of *Escherichia coli* K-12 beyond transcription, active (experimental) annotated promoters and Textpresso navigation," *Nucleic Acids Res.*, vol. 36, no. Database, pp. D120–D124, Dec. 2007.

[88] C. Wu, W. Xiong, J. Dai, and Q. Wu, "Genome-based metabolic mapping and 13C flux analysis reveal systematic properties of an oleaginous microalga *Chlorella protothecoides.*," *Plant Physiol.*, vol. 167, no. 2, pp. 586–99, Feb. 2015.

[89] Q. Xiong, Wei Gao, Chunfang Yan, Dong Wu, Chao Wu, "Double CO_2 fixation in photosynthesis–fermentation model enhances algal lipid synthesis for biodiesel production," *Bioresour. Technol.*, vol. 101, no. 7, pp. 2287–2293, Apr. 2010.

[90] J. Almquist, M. Cvijovic, V. Hatzimanikatis, J. Nielsen, and M. Jirstrand, "Kinetic models in industrial biotechnology – Improving cell factory performance," *Metab. Eng.*, vol. 24, pp. 38–60, Jul. 2014.

[91] F. Hynne, S. Danø, and P. G. Sørensen, "Full-scale model of glycolysis in *Saccharomyces cerevisiae*," *Biophys. Chem.*, vol. 94, no. 1–2, pp. 121–163, Dec. 2001.

[92] R. Rutkis, U. Kalnenieks, E. Stalidzans, and D. A. Fell, "Kinetic modelling of the *Zymomonas mobilis* Entner-Doudoroff pathway: insights into control and functionality," *Microbiology*, vol. 159, no. Pt_12, pp. 2674–2689, Dec. 2013.

[93] C. Chassagnole, N. Noisommit-Rizzi, J. W. Schmid, K. Mauch, and M. Reuss, "Dynamic modeling of the central carbon metabolism of *Escherichia coli*," *Biotechnol. Bioeng.*, vol. 79, no. 1, pp. 53–73, Jul. 2002.

[94] P. Mendes and D. Kell, "Non-linear optimization of biochemical pathways: applications to

metabolic engineering and parameter estimation," *Bioinformatics*, vol. 14, no. 10, pp. 869–883, Nov. 1998.

[95] J. B. Magnus, M. Oldiges, and R. Takors, "The identification of enzyme targets for the optimization of a valine producing *Corynebacterium glutamicum* strain using a kinetic model," *Biotechnol. Prog.*, vol. 25, no. 3, pp. 754–762, May 2009.

[96] V. Komasilovs, A. Pentjuss, A. Elsts, and E. Stalidzans, "Total enzyme activity constraint and homeostatic constraint impact on the optimization potential of a kinetic model," *Biosystems*, vol. 162, pp. 128–134, Dec. 2017.

[97] K. Mauch, K. Mauch, S. Buziol, J. Schmid, and M. Reuss, "Computer-Aided Design of Metabolic Networks," 2002.

[98] J. W. Schmid, K. Mauch, M. Reuss, E. D. Gilles, and A. Kremling, "Metabolic design based on a coupled gene expression—metabolic network model of tryptophan production in *Escherichia coli*," *Metab. Eng.*, vol. 6, no. 4, pp. 364–377, Oct. 2004.

[99] D. Visser, J. W. Schmid, K. Mauch, M. Reuss, and J. J. Heijnen, "Optimal re-design of primary metabolism in *Escherichia coli* using linlog kinetics," *Metab. Eng.*, vol. 6, no. 4, pp. 378–390, Oct. 2004.

[100] B. Volkmer and M. Heinemann, "Condition-Dependent Cell Volume and Concentration of Escherichia coli to Facilitate Data Conversion for Systems Biology Modeling," *PLoS One*, vol. 6, no. 7, p. e23126, Jul. 2011.

[101] C. S. Henry, L. J. Broadbelt, and V. Hatzimanikatis, "Thermodynamics-based metabolic flux analysis.," *Biophys. J.*, vol. 92, no. 5, pp. 1792–805, Mar. 2007.

[102] D. H. de Groot, C. van Boxtel, R. Planqué, F. J. Bruggeman, and B. Teusink, "The number of active metabolic pathways is bounded by the number of cellular constraints at maximal metabolic rates," *PLOS Comput. Biol.*, vol. 15, no. 3, p. e1006858, Mar. 2019.

[103] O. D. Kim, M. Rocha, and P. Maia, "A Review of Dynamic Modeling Approaches and Their Application in Computational Strain Optimization for Metabolic Engineering," *Front. Microbiol.*, vol. 9, p. 1690, Jul. 2018.

[104] J. J. DiStefano, *Dynamic systems biology modeling and simulation*, 1st ed. Los Angeles CA: Elsevier, 2013.

[105] A. L. Knorr, R. Jain, and R. Srivastava, "Bayesian-based selection of metabolic objective functions," *Bioinformatics*, vol. 23, no. 3, pp. 351–357, Feb. 2007.

[106] E. Bertolazzi, "A combination formula of Michaelis-Menten-Monod type," *Comput. Math. with Appl.*, vol. 50, no. 1–2, pp. 201–215, Jul. 2005.

[107] J. R. Pérez-Correa, G. Lefranc, and M. Fernández-Fernández, "A New Application of the Hill Repressor Function: Automatic Control of a Conic Tank Level and Local Stability Analysis," *Math. Probl. Eng.*, vol. 2015, pp. 1–6, May 2015.

[108] Edda, B. Simon, L. Wolfram, U. Jannis, and Klipp, "Automatically generated model of a metabolic network," in *International Conference on Genome Informatics 18*, 2007, pp. 215–

224.

[109] R. C. H. del Rosario, E. Mendoza, and E. O. Voit, "Challenges in lin-log modelling of glycolysis in *Lactococcus lactis*," *IET Syst. Biol.*, vol. 2, no. 3, p. 136, 2008.

[110] W. Liebermeister, J. Uhlendorf, and E. Klipp, "Modular rate laws for enzymatic reactions: thermodynamics, elasticities and implementation," *Bioinformatics*, vol. 26, no. 12, pp. 1528–1534, Jun. 2010.

[111] R. Schuetz, L. Kuepfer, and U. Sauer, "Systematic evaluation of objective functions for predicting intracellular fluxes in *Escherichia coli*.," *Mol. Syst. Biol.*, vol. 3, p. 119, 2007.

[112] A. P. Burgard and C. D. Maranas, "Optimization-based framework for inferring and testing hypothesized metabolic objective functions," *Biotechnol. Bioeng.*, vol. 82, no. 6, pp. 670–677, Jun. 2003.

[113] S. Klamt, S. Müller, G. Regensburger, and J. Zanghellini, "A mathematical framework for yield (vs. rate) optimization in constraint-based modeling and applications in metabolic engineering," *Metab. Eng.*, vol. 47, pp. 153–169, May 2018.

[114] C. Angione, J. Costanza, G. Carapezza, P. Lió, and G. Nicosia, "Multi-Target Analysis and Design of Mitochondrial Metabolism," *PLoS One*, vol. 10, no. 9, p. e0133825, Sep. 2015.

[115] A. R. Brochado, S. Andrejev, C. D. Maranas, and K. R. Patil, "Impact of Stoichiometry Representation on Simulation of Genotype-Phenotype Relationships in Metabolic Networks," *PLoS Comput. Biol.*, vol. 8, no. 11, p. e1002758, Nov. 2012.

[116] A. Oliveira, J. Nielsen, and J. Förster, "Modeling *Lactococcus lactis* using a genome-scale flux model," *BMC Microbiol.*, vol. 5, no. 1, p. 39, Jun. 2005.

[117] G. J. E. Baart and D. E. Martens, "Genome-Scale Metabolic Models: Reconstruction and Analysis," Humana Press, 2012, pp. 107–126.

[118] C. Angione, "Human Systems Biology and Metabolic Modelling: A Review—From Disease Metabolism to Precision Medicine," *Biomed Res. Int.*, vol. 2019, pp. 1–16, Jun. 2019.

[119] A. von Kamp and S. Klamt, "Growth-coupled overproduction is feasible for almost all metabolites in five major production organisms," *Nat. Commun.*, vol. 8, no. 1, p. 15956, Dec. 2017.

[120] A. M. Feist and B. O. Palsson, "What do cells actually want?," *Genome Biol.*, vol. 17, no. 1, p. 110, Dec. 2016.

[121] N. R. Boyle, N. Sengupta, and J. A. Morgan, "Metabolic flux analysis of heterotrophic growth in *Chlamydomonas reinhardtii*," *PLoS One*, vol. 12, no. 5, p. e0177292, May 2017.

[122] C. Gomes de Oliveira Dal'Molin, L. E. Quek, R. W. Palfreyman, and L. K. Nielsen, "AlgaGEM – a genome-scale metabolic reconstruction of algae based on the *Chlamydomonas reinhardtii* genome," *BMC Genomics*, vol. 12, no. Suppl 4, p. S5, Dec. 2011.

[123] K. Yoshikawa, Y. Kojima, T. Nakajima, C. Furusawa, and H. Shimizu et al., "Reconstruction and verification of a genome-scale metabolic model for *Synechocystis sp.* PCC6803," *Appl.*

Microbiol. Biotechnol., vol. 92, no. 2, pp. 347–358, Oct. 2011.

[124] M. Muthuraj, B. Palabhanvi, S. Misra, V. Kumar, and D. Das et al., "Flux balance analysis of *Chlorella sp.* FC2 IITG under photoautotrophic and heterotrophic growth conditions," *Photosynth. Res.*, vol. 118, no. 1–2, pp. 167–179, Nov. 2013.

[125] X. Johnson and J. Alric, "Central carbon metabolism and electron transport in *Chlamydomonas reinhardtii*: metabolic constraints for carbon partitioning between oil and starch.," *Eukaryot. Cell*, vol. 12, no. 6, pp. 776–93, Jun. 2013.

[126] H. Sun, W. Zhao, X. Mao, Y. Li, and F. Chen et al., "High-value biomass from microalgae production platforms: strategies and progress based on carbon metabolism and energy conversion.," *Biotechnol. Biofuels*, vol. 11, p. 227, 2018.

[127] A. Pandey, D. J. Lee, Y. Chisti, and C. R. Soccol, *Biofuels from Algae*. Elsevier, 2013.

[128] O. Perez-Garcia, F. M. E. Escalante, L. E. de-Bashan, and Y. Bashan, "Heterotrophic cultures of microalgae: Metabolism and potential products," *Water Res.*, vol. 45, no. 1, pp. 11–36, Jan. 2011.

[129] C. Yang, B. Ko, C. Hensley, L. Jiang, and A. Wasti *et al.*, "Glutamine Oxidation Maintains the TCA Cycle and Cell Survival during Impaired Mitochondrial Pyruvate Transport," *Mol. Cell*, vol. 56, no. 3, pp. 414–424, Nov. 2014.

[130] J. Masojídek, G. Torzillo, and M. Koblížek, "Photosynthesis in Microalgae," in *Handbook of Microalgal Culture*, Oxford, UK: John Wiley & Sons, Ltd, 2013, pp. 21–36.

[131] W. Xiong, L. Liu, C. Wu, C. Yang, and Q. Wu, "13C-tracer and gas chromatography-mass spectrometry analyses reveal metabolic flux distribution in the oleaginous microalga *Chlorella protothecoides*.," *Plant Physiol.*, vol. 154, no. 2, pp. 1001–11, Oct. 2010.

[132] S. Gopalakrishnan, J. Baker, L. Kristoffersen, and M. J. Betenbaugh, "Redistribution of metabolic fluxes in *Chlorella protothecoides* by variation of media nitrogen concentration," *Metab. Eng. Commun.*, vol. 2, pp. 124–131, Dec. 2015.

[133] R. A. Cairns, I. Harris, S. McCracken, and T. W. Mak, "Cancer cell metabolism.," *Cold Spring Harb. Symp. Quant. Biol.*, vol. 76, pp. 299–311, Jan. 2011.

[134] V. Rai, M. Muthuraj, M. N. Gandhi, D. Das, and S. Srivastava, "Real-time iTRAQ-based proteome profiling revealed the central metabolism involved in nitrogen starvation induced lipid accumulation in microalgae," *Sci. Rep.*, vol. 7, no. 1, p. 45732, May 2017.

[135] P. S. Bilbao, G. A. Salvador, and P. I. Leonardi, "Fatty Acids from Microalgae: Targeting the Accumulation of Triacylglycerides," in *Progress in Carotenoid Research*, E. J.-L. and V. V. D. R. Leila Queiroz Zepka, Ed. InTech, 2017, pp. 119–141.

[136] C. Zuñiga, C.-T. Li, T. Huelsman, J. Levering, and B. O. McConnell et al., "Genome-Scale Metabolic Model for the Green Alga *Chlorella vulgaris* UTEX 395 Accurately Predicts Phenotypes under Autotrophic, Heterotrophic, and Mixotrophic Growth Conditions.," *Plant Physiol.*, vol. 172, no. 1, pp. 589–602, Sep. 2016.

[137] J. Levering, J. Broddrick, C. L. Dupont, G. Peers, and J. Mayers et al., "Genome-Scale Model

Reveals Metabolic Basis of Biomass Partitioning in a Model Diatom," *PLoS One*, vol. 11, no. 5, p. e0155038, May 2016.

[138] A. R. Shah, A. Ahmad, S. Srivastava, and B. M. Jaffar Ali, "Reconstruction and analysis of a genome-scale metabolic model of *Nannochloropsis gaditana*," *Algal Res.*, vol. 26, pp. 354–364, Sep. 2017.

[139] N. Loira, S. Mendoza, M. Paz Cortés, N. Rojas, and A. Di Genova et al., "Reconstruction of the microalga *Nannochloropsis salina* genome-scale metabolic model with applications to lipid production," *BMC Syst. Biol.*, vol. 11, no. 1, p. 66, Dec. 2017.

[140] C. Zuñiga, J. Levering, M. R. Antoniewicz, M. T. Guarnieri, and K. Zengler et al., "Predicting Dynamic Metabolic Demands in the Photosynthetic Eukaryote *Chlorella vulgaris.*," *Plant Physiol.*, vol. 176, no. 1, pp. 450–462, Jan. 2018.

[141] S. Imam, S. Schäuble, J. Valenzuela, A. López García de Lomana, and N. D. Price, "A refined genome-scale reconstruction of *Chlamydomonas* metabolism provides a platform for systems-level analyses," *Plant J.*, vol. 84, no. 6, pp. 1239–1256, Dec. 2015.

[142] Y. Li-Beisson, B. Shorrosh, F. Beisson, M. X. Andersson, and P. D. Bates et al., "Acyl-Lipid Metabolism," *Arab. B.*, vol. 8, p. e0133, Jan. 2010.

[143] O. Avidan, A. Brandis, I. Rogachev, and U. Pick, "Enhanced acetyl-CoA production is associated with increased triglyceride accumulation in the green alga *Chlorella desiccata*," *J. Exp. Bot.*, vol. 66, no. 13, pp. 3725–3735, Jul. 2015.

[144] J. Fan, Y. Cui, M. Wan, W. Wang, and Y. Li, "Lipid accumulation and biosynthesis genes response of the oleaginous *Chlorella pyrenoidosa* under three nutrition stressors," *Biotechnol. Biofuels*, vol. 7, no. 1, p. 17, Jan. 2014.

[145] A. P. Brown, A. R. Slabas, and J. B. Rafferty, "Fatty Acid Biosynthesis in Plants — Metabolic Pathways, Structure and Organization," Springer, Dordrecht, 2009, pp. 11–34.

[146] H. Rismani-Yazdi, B. Z. Haznedaroglu, C. Hsin, and J. Peccia, "Transcriptomic analysis of the oleaginous microalga *Neochloris oleoabundans* reveals metabolic insights into triacylglyceride accumulation," *Biotechnol. Biofuels*, vol. 5, no. 1, p. 74, Sep. 2012.

[147] B. K. S. Chung, M. Lakshmanan, M. Klement, B. Mohanty, and D. Y. Lee, "Genome-scale in silico modeling and analysis for designing synthetic terpenoid-producing microbial cell factories," *Chem. Eng. Sci.*, vol. 103, pp. 100–108, Nov. 2013.

[148] L. Zhao, W. Chang, Y. Xiao, H. Liu, and P. Liu, "Methylerythritol phosphate pathway of isoprenoid biosynthesis.," *Annu. Rev. Biochem.*, vol. 82, pp. 497–530, 2013.

[149] M. Lohr, J. Schwender, and J. E. W. Polle, "Isoprenoid biosynthesis in eukaryotic phototrophs: A spotlight on algae," *Plant Science*, vol. 185–186. pp. 9–22, Apr-2012.

[150] C. Zhang, "Biosynthesis of Carotenoids and Apocarotenoids by Microorganisms and Their Industrial Potential," in *Progress in Carotenoid Research*, InTech, 2018.

[151] Y. Xie, B. Sen, and G. Wang, "Mining terpenoids production and biosynthetic pathway in thraustochytrids," *Bioresour. Technol.*, vol. 244, pp. 1269–1280, Nov. 2017.

[152] P. Córdova, M. Baeza, V. Cifuentes, and J. Alcaíno, "Microbiological Synthesis of Carotenoids: Pathways and Regulation," in *Progress in Carotenoid Research*, InTech, 2018.

[153] S. Kato, S. Takaichi, T. Ishikawa, M. Asahina, and T. Shinomura et al., "Identification and functional analysis of the geranylgeranyl pyrophosphate synthase gene (crtE) and phytoene synthase gene (crtB) for carotenoid biosynthesis in *Euglena gracilis*," *BMC Plant Biol.*, vol. 16, no. 1, p. 4, Dec. 2016.

[154] L. Mata-Gómez, J. Montañez, A. Méndez-Zavala, and C. Aguilar, "Biotechnological production of carotenoids by yeasts: an overview," *Microb. Cell Fact.*, vol. 13, no. 1, p. 12, Jan. 2014.

[155] G. Chang, Z. Luo, S. Gu, Q. Wu, and X. Wang et al., "Fatty acid shifts and metabolic activity changes of *Schizochytrium* sp. S31 cultured on glycerol," *Bioresour. Technol.*, vol. 142, pp. 255–260, Aug. 2013.

[156] P. Martinez-Moya, K. Niehaus, J. Alcaíno, M. Baeza, and V. Cifuentes, "Proteomic and metabolomic analysis of the carotenogenic yeast *Xanthophyllomyces dendrorhous* using different carbon sources," *BMC Genomics*, vol. 16, no. 1, p. 289, Dec. 2015.

[157] S. H. J. Chan, J. Cai, L. Wang, M. N. Simons-Senftle, and C. D. Maranas, "Standardizing biomass reactions and ensuring complete mass balance in genome-scale metabolic models," *Bioinformatics*, vol. 33, no. 22, pp. 3603–3609, Nov. 2017.

[158] Y. K. Oh, B. O. Palsson, S. M. Park, C. H. Schilling, and R. Mahadevan, "Genome-scale reconstruction of metabolic network in *Bacillus subtilis* based on high-throughput phenotyping and gene essentiality data.," *J. Biol. Chem.*, vol. 282, no. 39, pp. 28791–9, Sep. 2007.

[159] A. M. Feist, C. S. Henry, J. L. Reed, M. Krummenacker, and P. D. Karp et al., "A genome-scale metabolic reconstruction for *Escherichia coli* K-12 MG1655 that accounts for 1260 ORFs and thermodynamic information," *Mol. Syst. Biol.*, vol. 3, no. 1, p. 121, Jan. 2007.

[160] Y.C. Liao, T.W. Huang, F.C. Chen, P. Charusanti, and H.Y. Chang et al., "An experimentally validated genome-scale metabolic reconstruction of *Klebsiella pneumoniae* MGH 78578, iYL1228.," *J. Bacteriol.*, vol. 193, no. 7, pp. 1710–7, Apr. 2011.

[161] I. Thiele, D. R. Hyduke, B. Steeb, G. Fankam, and S. Bazzani et al., "A community effort towards a knowledge-base and mathematical model of the human pathogen *Salmonella Typhimurium* LT2," *BMC Syst. Biol.*, vol. 5, no. 1, p. 8, Jan. 2011.

[162] N. Jamshidi and B. Ø. Palsson, "Investigating the metabolic capabilities of *Mycobacterium tuberculosis* H37Rv using the in silico strain iNJ 661 and proposing alternative drug targets," *BMC Syst. Biol.*, vol. 1, no. 1, p. 26, Dec. 2007.

[163] J. Nogales, S. Gudmundsson, E. M. Knight, B. O. Palsson, and I. Thiele, "Detailing the optimality of photosynthesis in cyanobacteria through systems biology analysis.," *Proc. Natl. Acad. Sci. U. S. A.*, vol. 109, no. 7, pp. 2678–83, Feb. 2012.

[164] Y. Zhang, I. Thiele, D. Weekes, Z. Li, and K. Ginalski et al., "Three-dimensional structural view of the central metabolic network of *Thermotoga maritima*.," *Science*, vol. 325, no. 5947, pp. 1544–9, Sep. 2009.

[165] J. C. Xavier, K. R. Patil, and I. Rocha, "Metabolic models and gene essentiality data reveal essential and conserved metabolism in prokaryotes," *PLOS Comput. Biol.*, vol. 14, no. 11, p. e1006556, Nov. 2018.

[166] Y. Zhong and F. Shahidi, "Methods for the assessment of antioxidant activity in foods," in *Handbook of Antioxidants for Food Preservation*, Elsevier Inc., 2015, pp. 287–333.

[167] Q. Liao, J. S. Chang, C. Herrmann, and A. Xia, *Bioreactors for microbial biomass and energy conversion*, 1st ed. Springer Singapore, 2018.

[168] M. S. Roth, S. D. Gallaher, D. J. Westcott, M. Iwai, and M. Mueller, "Regulation of oxygenic photosynthesis during trophic transitions in the green alga *Chromochloris zofingiensis*," *Plant Cell*, vol. 31, no. 3, pp. 579–601, Mar. 2019.

[169] Y. Oshio and E. Hase, "Studies on red pigments excreted by cells of *Chlorella protothecoides* during the process of bleaching induced by glucose or acetate II. Mode of formation of the red pigments," *Plant Cell Physiol.*, vol. 10, no. 1, pp. 41–49, Mar. 1969.

[170] S. Hörtensteiner, J. Chinner, P. Matile, H. Thomas, and I. S. Donnison, "Chlorophyll breakdown in *Chlorella protothecoides*: Characterization of degreening and cloning of degreening-related genes," *Plant Mol. Biol.*, vol. 42, no. 3, pp. 439–450, 2000.

[171] T. Osafune and E. Hase, "Some Structural Characteristics of the Chloroplasts in the 'Glucose-bleaching' and Re-greening Cells of *Chlorella protothecoides* 1)Dedicated to Prof. Kurt Mothes on the occasion of his 75th birthday.," *Biochem. und Physiol. der Pflanz.*, vol. 168, no. 5–6, pp. 533–542, 1975.

[172] S. Pierucci, J. J. Klemeš, L. Piazza, S. Bakalis, and F. Di Caprio et al., "Microalgae Cultivation for Lipids and Carbohydrates Production," in *Chemical Engineering Transactions*, 2017, vol. 57.

[173] A. S. Verkman, "Aquaporins," *Current Biology*, vol. 23, no. 2. Cell Press, 21-Jan-2013.

[174] A. Goyal, "Osmoregulation in *Dunaliella*, Part II: Photosynthesis and starch contribute carbon for glycerol synthesis during a salt stress in *Dunaliella tertiolecta*," *Plant Physiol. Biochem.*, vol. 45, no. 9, pp. 705–710, Sep. 2007.

[175] G. Kim, G. Mujtaba, and K. Lee, "Effects of nitrogen sources on cell growth and biochemical composition of marine *Chlorophyte tetraselmis* sp. For lipid production," *Algae*, vol. 31, no. 3, pp. 257–266, Sep. 2016.

[176] I. Flynn, Kevin J. Butler, "Nitrogen sources for the growth of marine microalgae: role of dissolved free amino acids," *Mar. Ecol. - Prog. Ser.*, vol. 34, pp. 281–304, 1986.

[177] Y. Panahi, A. Y. Khosroshahi, A. Sahebkar, and H. R. Heidari, "Impact of cultivation condition and media content on *Chlorella vulgaris* composition," *Advanced Pharmaceutical Bulletin*, vol. 9, no. 2. Tabriz University of Medical Sciences, pp. 182–194, 2019.

[178] K. Goiris, W. Van Colen, I. Wilches, F. León-Tamariz, and K. Muylaert et al., "Impact of nutrient stress on antioxidant production in three species of microalgae," *Algal Res.*, vol. 7, pp. 51–57, Jan. 2015.

[179] W. Huang, Y. Lin, M. He, Y. Gong, and J. Huang, "Induced High-Yield Production of Zeaxanthin, Lutein, and β-Carotene by a Mutant of *Chlorella zofingiensis*," *J. Agric. Food Chem.*, vol. 66, no. 4, pp. 891–897, Jan. 2018.

[180] A. C. Guedes, H. M. Amaro, and F. X. Malcata, "Microalgae as sources of carotenoids," *Marine Drugs*, vol. 9, no. 4. pp. 625–644, Apr-2011.

[181] N. J. Sallehudin, R. A. Raus, M. Mustapa, and R. Othman, "Screening of lutein content in several fresh-water microalgae," *Int. Food Res. J.*, vol. 25, no. 6, pp. 2307–2312, 2018.

[182] A. K. Minhas, P. Hodgson, C. J. Barrow, and A. Adholeya, "A review on the assessment of stress conditions for simultaneous production of microalgal lipids and carotenoids," *Frontiers in Microbiology*, vol. 7, no. MAY. Frontiers Research Foundation, 2016.

[183] E. Hiltunen, E. Antila, J. J. Zhong, Z. H. Yuan, and Z. M. Wang, "Microalgal biofuels: Flexible bioenergies for sustainable development," *Renew. Sustain. Energy Rev.*, vol. 150, pp. 69–79, 2015.

[184] T. Chen, J. Liu, B. Guo, X. Ma, and B. Liu et al., "Light attenuates lipid accumulation while enhancing cell proliferation and starch synthesis in the glucose-fed oleaginous microalga *Chlorella zofingiensis*," *Sci. Rep.*, vol. 5, Oct. 2015.

[185] E. E. Roden and Q. Jin, "Thermodynamics of microbial growth coupled to metabolism of glucose, ethanol, short-chain organic acids, and hydrogen," *Appl. Environ. Microbiol.*, vol. 77, no. 5, pp. 1907–1909, Mar. 2011.

[186] X. Ren, J. S. Deschênes, R. Tremblay, S. Peres, and M. Jolicoeur, "A kinetic metabolic study of lipid production in *Chlorella protothecoides* under heterotrophic condition," *Microb. Cell Fact.*, vol. 18, no. 1, p. 113, Dec. 2019.

[187] E. O. Voit, "The best models of metabolism.," *Wiley Interdiscip. Rev. Syst. Biol. Med.*, vol. 9, no. 6, 2017.

[188] The MathWorks Inc., "MATLAB version 9.3.0.713579 (R2017b)." Natick, Masachusettes, 2017.

[189] X.M. Shi, Y. Jiang, and F. Chen, "High-yield production of lutein by the green microalga *Chlorella protothecoides* in heterotrophic fed-batch culture.," *Biotechnol. Prog.*, vol. 18, no. 4, pp. 723–727, 2002.

[190] M. Kanehisa, M. Araki, S. Goto, M. Hattori, and M. Itoh et al., "KEGG for linking genomes to life and the environment.," *Nucleic Acids Res.*, vol. 36, no. Database issue, pp. D480-4, Jan. 2008.

[191] S. Placzek, I. Schomburg, A. Chang, L. Jeske, and J. Tillack et al., "BRENDA in 2017: New perspectives and new tools in BRENDA," *Nucleic Acids Res.*, vol. 45, no. D1, pp. D380–D388, Jan. 2017.

[192] J. O'Grady and J. A. Morgan, "Heterotrophic growth and lipid production of *Chlorella protothecoides* on glycerol.," *Bioprocess Biosyst. Eng.*, vol. 34, no. 1, pp. 121–125, Jan. 2011.

[193] H. Nishimura, F. V Pallardo, G. A. Seidner, S. Vannucci, and M. J. Birnbaum et al., “Kinetics of GLUT1 and GLUT4 glucose transporters expressed in *Xenopus oocytes*.,” *J. Biol. Chem.*, vol. 268, no. 12, pp. 8514–20, Apr. 1993.

[194] Y. Chen, B. O. McConnell, V. Gayatri Dhara, H. Mukesh Naik, and M. R. Antoniewicz et al., “An unconventional uptake rate objective function approach enhances applicability of genome-scale models for mammalian cells,” *npj Syst. Biol. Appl.*, vol. 5, no. 1, Dec. 2019.

[195] P. Cloutier, R. Al-Khoury, M. Lavallée-Adam, and C. Poitras et al., “High-resolution mapping of the protein interaction network for the human transcription machinery and affinity purification of RNA polymerase II-associated complexes,” *Methods*, vol. 48, no. 4, pp. 381–386, Aug. 2009.

[196] M. A. Savageau, “Chapter 5 Enzyme kinetics in vitro and in vivo: Michaelis-Menten revisited,” in *Principles of Medical Biology*, vol. 4, no. PART 1, Elsevier Inc., 1995, pp. 93–146.

[197] M. Goličnik, “Exact and approximate solutions for the decades-old Michaelis-Menten equation: Progress-curve analysis through integrated rate equations,” *Biochem. Mol. Biol. Educ.*, vol. 39, no. 2, pp. 117–125, Mar. 2011.

[198] P. D. Fraser, H. Shimada, and N. Misawa, “Enzymic confirmation of reactions involved in routes to astaxanthin formation, elucidated using a direct substrate in vitro assay,” *Eur. J. Biochem.*, vol. 252, no. 2, pp. 229–236, Mar. 1998.

[199] R. C. H., E. Mendoza, and E. O. Voit, *IET systems biology*, vol. 2, no. 3. Institution of Engineering and Technology, 2007.

[200] T. Zhang, A. Parker, R. P. Carlson, P. S. Stewart, and I. Klapper, “Flux-Balance Based Modeling of Biofilm Communities,” *bioRxiv*, p. 441311, 2018.

[201] K. W. M. Tan, H. Lin, H. Shen, and Y. K. Lee, “Nitrogen-induced metabolic changes and molecular determinants of carbon allocation in *Dunaliella tertiolecta*.,” *Sci. Rep.*, vol. 6, p. 37235, 2016.

Appendices

Appendix A

A.1 Optimization function

Enz_opt_mod.m

```
% Optimization model for Enzyme quantities
%
% This was created by Safina Ujan
%
% University of Calgary, 2019.
%
```

Initial values for enzymes and constraints

Loading initial values for Constraints

```
load 'C:\Users\safina.ujan1\Documents\MATLAB\Test_opt_met\opt_Ab_Vi_mod.mat' % Store
initial enzyme value
%
```

Algorithm settings

Applying Interior-point algorithm for solution

```
options = optimoptions(@fmincon,'Algorithm','Interior-point','Display','iter');
%
```

Optimization function

```
E_opt_mod=fmincon(@(E_opt)
Enz_dynmod(E_opt),E_init,A_mod,b_mod,[],[],lb_mod,ub_mod,[],options);
%
%
```

Published with MATLAB® R2018a

A.2 Dynamic ODE solver

Enz_dynmod.m

```
function met_err = Enz_dynmod(E_opt)

% Import global parameters
load 'myKs.mat'

% Import initial concentrations
load 'C:\Users\safina.ujan1\Documents\MATLAB\Test_opt_met\conc_met_init.mat'
load 'C:\Users\safina.ujan1\Documents\MATLAB\Test_opt_met\opt_Ab_Vi.mat'

% Store initial concentrations in Initial vector
y_init=[conc_ATP_init,conc_ADP_init,conc_NADx_init,conc_NADH_init,conc_NADPH_init,conc_
NADPx_init,conc_GLC_init,conc_GLY_init,conc_H2O_init,conc_GCN_init,conc_G6P_init,conc_F
6P_init,conc_F16BP_init,conc_GCNP_init,conc_G3P_init,conc_OP_init,conc_3BPG_init,conc_H
x_init,conc_SG3O_init,conc_OA_init,conc_PEP_init,conc_GL6P_init,conc_6PG_init,conc_R5P_
init,conc_X5P_init,conc_CT_init,conc_CoA_init,conc_IC_init,conc_AKG_init,conc_MCoA_init
,conc_SM_init,conc_R15B_init,conc_3PG_init,conc_PY_init,conc_SAMP_init,conc_METF_init,c
onc_NH3_init,conc_GTM_init,conc_LGM_init,conc_DX5P_init,conc_DPH_init,conc_PPDP_init,co
nc_15cP_init,conc_LYC_init,conc_LTN_init,conc_BCRT_init,conc_ZXN_init,conc_MADP_init,co
nc_IPP_init,conc_BCRT_init,conc_GDP_init,conc_FDP_init,conc_CO2_init,conc_ACoA_init,con
c_GGDP_init,conc_Xb_init];

% Time period
t_period=0.1;
t_end=5;

% ODE Solver
opts=odeset('RelTol',1.e+3,'NonNegative',1:56);
[t,M]=ode15s(@(t,M) Enz_ODE(t,M,E_opt),0:t_period:t_end,(y_init),opts);

% Storing concentration increments in matrix M
conc_ATP=M(:,  1 );
conc_ADP=M(:,  2 );
conc_NADx=M(:,  3 );
conc_NADH=M(:,  4 );
conc_NADPH=M(:,  5 );
conc_NADPx=M(:,  6 );
conc_GLC=M(:,  7 );
conc_GLY=M(:,  8 );
conc_H2O=M(:,  9 );
conc_GCN=M(:,  10 );
conc_G6P=M(:,  11 );
conc_F6P=M(:,  12 );
conc_F16BP=M(:,  13 );
conc_GCNP=M(:,  14 );
```

```
conc_G3P=M(:,  15 );
conc_OP=M(:,  16 );
conc_3BPG=M(:,  17 );
conc_Hx=M(:,  18 );
conc_SG3O=M(:,  19 );
conc_OA=M(:,  20 );
conc_PEP=M(:,  21 );
conc_GL6P=M(:,  22 );
conc_6PG=M(:,  23 );
conc_R5P=M(:,  24 );
conc_X5P=M(:,  25 );
conc_CT=M(:,  26 );
conc_CoA=M(:,  27 );
conc_IC=M(:,  28 );
conc_AKG=M(:,  29 );
conc_MCoA=M(:,  30 );
conc_SM=M(:,  31 );
conc_R15B=M(:,  32 );
conc_3PG=M(:,  33 );
conc_PY=M(:,  34 );
conc_SAMP=M(:,  35 );
conc_METF=M(:,  36 );
conc_NH3=M(:,  37 );
conc_GTM=M(:,  38 );
conc_LGM=M(:,  39 );
conc_DX5P=M(:,  40 );
conc_DPH=M(:,  41 );
conc_PPDP=M(:,  42 );
conc_15cP=M(:,  43 );
conc_LYC=M(:,  44 );
conc_LTN=M(:,  45 );
conc_BCRT=M(:,  46 );
conc_ZXN=M(:,  47 );
conc_MADP=M(:,  48 );
conc_IPP=M(:,  49 );
conc_BCRT=M(:,  50 );
conc_GDP=M(:,  51 );
conc_FDP=M(:,  52 );
conc_CO2=M(:,  53 );
conc_ACoA=M(:,  54 );
conc_GGDP=M(:,  55 );
conc_Xb=M(:,  56 );
```

```
% Objective function for Optimization
met_err = -(conc_Xb(end))/(conc_GLC(end)+conc_GLY(end));
disp(E_opt);

 save('E_opt_runv6.mat')
end
```

Published with MATLAB® R2018a

A.3 ODE matrix multiplication

Enz_ODEmod.m

```
function dExdt = Enz_ODEmod(t,M,E_opt)

% Calling rates function
r = Enz_Ratesmod(M,E_opt);

% Load the Stoichiometry matrix
load('C:\Users\safina.ujan1\Documents\MATLAB\Test_opt_met\myStoichiom.mat')
S_mod=S_43(1:56,1:43);
% Ordinary differential equations
dExdt(:,1)=(S_mod*r);

end
```

Published with MATLAB® R2018a

A.4 **Algorithm**

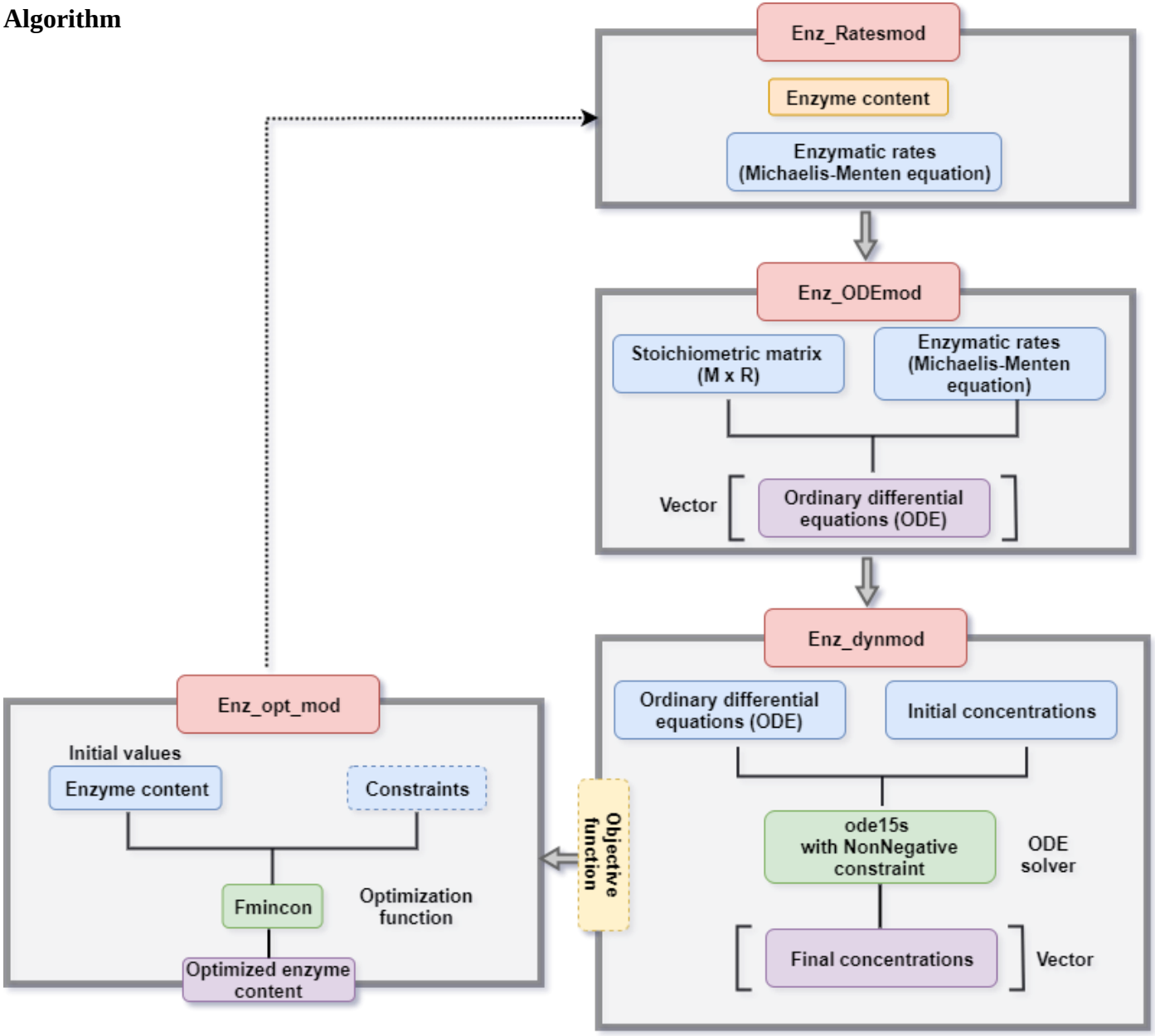

Appendix B

EC Abb.	EC No.	Enzyme	Vmax_EC (mmol.d^{-1}.mgE^{-1})	Km_EC_m1 (mmol.gDW^{-1})	Km_EC_m2 (mmol.gDW^{-1})
		Glucose assimilation [193] [191]			
GLUT1		Hexose carriers (glucose transporter protein)	0.0035	4.3	
GK	2.7.1.199	Glucokinase	3250	25	0.015
G6PI	5.3.1.9	Glucose-6-phosphate isomerase	21.2	0.28	
6PFK	2.7.1.11	6-Phosphofructokinase	18.9	0.005	0.006
FBPA	4.1.2.13	Fructose-biphosphate aldolase	20	0.45	
GY3PD	1.2.1.12	Glyceraldehyde-3-phosphate dehydrogenase-NAD	51.1	0.081	0.0066
		Glycerol assimilation [193] [191]			
GYK	2.7.1.30	Glycerol kinase	4500	0.006	2
SG3PO	1.1.1.8	sn-glycerol-3-phosphate NAD+ oxidoreductase	53.6	0.12	0.41
TPI	5.3.1.1	Triose-phosphate isomerase	7193	0.88	
		Glycolysis [193] [191]			
PPHD	4.2.1.11	Phosphopyruvate hydratase	675	0.27	0.035
PYK	2.7.1.40	Pyruvate kinase	8.16	99.98	
G3PDN	1.2.1.59	Glyceraldehyde-3-phosphate dehydrogenase-NADP dependent	0	0.27	0.035
F16BP	3.1.3.11	Fructose-1,6-bisphosphatase	8.16	99.98	
PEPCK	4.1.1.49	Phosphoenolpyruvate carboxykinase (ATP)	40.5	0.0011	0.0156
		Pentose phosphate pathway [193] [191]			
G6PD	1.1.1.49	Glucose-6-phosphate dehydrogenase	100	0.0075	0.07
6PGA	3.1.1.3	6-phosphogluconolactonase	68	0.038	
6PGD	1.1.1.44	6-phosphogluconate dehydrogenase	21	0.0102	0.0041
RP3E	5.1.3.1	Ribulose-phosphate 3-epimerase	11610	0.00033	3.3e-4
		Calvin-Benson cycle [193] [191]			
RBPC	4.1.1.39	Ribulose-bisphosphate carboxylase	1.21	0.0015	0.015
G3PD	1.2.1.59	Glyceraldehyde-3-phosphate dehydrogenase	18.6	0.0625	0.22
PPKT	4.1.2.9	Phosphoketolase	0.083	0.19	0.19
R5PK	2.7.1.19	Phosphoribulokinase	16	0.0053	0.0053
PEC	4.1.1.31	Phosphoenolpyruvate carboxylase	30	0.19	0.19
		TCA cycle [193] [191]			
PYAT	1.2.4.1	Pyruvate dehydrogenase	40.5	0.0221	0.00077
ATCS	2.3.3.8	ATP citrate synthase	108	0.00225	0.0021
CS	2.3.3.1	Citrate synthase	108	0.018	0.018
AH	4.2.1.3	Aconitate Hydratase	1.9	0.12	

EC Abb.	EC No.	Enzyme	Vmax_EC ($mmol.d^{-1}.mgE^{-1}$)	Km_EC_m1 ($mmol.gDW^{-1}$)	Km_EC_m2 ($mmol.gDW^{-1}$)
ICDN1	1.1.1.41	Isocitrate dehydrogenase-NADH dependent	0.084	0.2	0.12
ICDN2	1.1.1.42	Isocitrate dehydrogenase-NADPH dependent	18.6	0.007	0.007
KGD	1.2.4.2	Ketoglutarate dehydrogenase	0.2	0.1	0.041
SCL	6.2.1.5	Succinate-CoA Ligase (ADP forming)	0.083	0.0221	0.0077
SD	1.3.5.1	Succinate dehydrogenase	16	0.0025	0.002
FH	4.2.1.2	Fumarate hydratase	1047	0.031	
MDN	1.1.1.37	Malate Dehydrogenase-NADP dependent	1920	0.178	0.00012
ICL	4.1.3.1	Isocitrate lyase	0.636	7.6	
		Glycine assimilation [193] [191]			
GYND	1.4.4.2	Glycine dehydrogenase	0.25	2.84	0.47
AMT	2.1.2.10	Aminomethyltransferase	1.08	0.0037	0.17
GS	6.3.1.2	Glutamine synthetaste (GS)	33.9	0.79	5.71
		Fatty acid synthesis [193] [191]			
ACAC	6.4.1.2	Acetyl-CoA carboxylase	1047	0.9640	0.0068
MDOD	1.1.1.40	Malate dehydrogenase	0.571	0.0053	0.00014
PFL	2.3.1.54	NADP dependent pyruvate formate-lyase	60	0.0068	0.964
		Terpenoid backbone synthesis [193] [191]			
1XPS	2.2.1.7	1-deoxy-D-xylulose-5-phosphate synthase	1.6	0.53	0.64
1XPR	1.1.1.267	1-deoxy-D-xylulose-5-Phosphate reductoisomerase	2.1	0.47	0.972
2E4PC	2.7.7.60	2-C-methyl-D-erythritol 4-phosphate cytidylyltransferase	23	0.061	2.8
MDEK	2.7.1.148	4-(cytidine 5'-diphospho)-2-C-methyl-D-erythritol kinase	1.5	0.02	0.2
MDECL	4.6.1.12	2-Phospho-4-(cytidine 5'-diphospho)-2-C-methyl-D-erythritol CMP-lyase (cyclizing)	0.75	0.483	
FLAV	1.17.7.1	(E)-4-hydroxy-3-methylbut-2-enyl-diphosphate synthase (flavodoxin)	25	0.483	
MDFO	1.17.7.4	dimethylallyl diphosphate:ferredoxin oxidoreductase	2.1	0.039	
IDI	5.3.3.2	Isopentenyl-diphosphate delta3-delta2-isomerase	0.046	0.001	
DMAT	2.5.1.1	Dimethylallyltranstransferase	0.636	0.125	0.001
FDS	2.5.1.10	Farnesyl-diphosphate synthase	0.04	0.036	0.048
FT	2.5.1.29	Farnesyltranstransferase	0.0087	0.0028	0.0003
		Carotenoid biosynthesis [198]			
PDS	2.5.1.32	Prephytoene-diphosphate synthase	0.067	0.003	68
CPS	2.5.1.32	15-cis-phytoene synthase	0.067	0.0027	2.8
PD	1.3.99.28	Phytoene desaturase	0.00029	0.0048	0.0331
CPD	1.3.5.5	15-cis-phytoene desaturase	0.09	0.039	
ZCD	1.3.5.6	zeta-carotene desaturase		0.0084	

EC Abb.	EC No.	Enzyme	Vmax_EC ($mmol.d^{-1}.mgE^{-1}$)	Km_EC_m1 ($mmol.gDW^{-1}$)	Km_EC_m2 ($mmol.gDW^{-1}$)
LEC	5.5.1.18	Lycopene epsilon-cyclase	60	0.4830	
LBC	5.5.1.19	Lycopene beta-cyclase	0.356	0.035	
BCH	1.14.15.24	Beta-carotene 3-hydroxylase	0.001	0.0025	
		Biomass synthesis [198]			
XB1	N/A	Biomass formation reaction 1	150	4	
XB2	N/A	Biomass formation reaction 2	203	0.05	
XB3	N/A	Biomass formation reaction 3	22	0.05	
XB4	N/A	Biomass formation reaction 4	108	3	

Appendix C

C.1 Biomass dry weight

This method utilizes freeze drying for obtaining dry biomass pellets.

Chemicals:

1. Mono-potassium phosphate (KH_2PO_4).
2. Dipotassium phosphate (K_2HPO_4).
3. Hydrochloric acid (HCl).

Materials:

1. Micro-centrifuge tubes.

Phosphate buffered saline (1 L) preparation procedure:

1. Measure and fill a container with 800 ml of distilled water.
2. Weigh and add 17.5 g of KH_2PO_4 to the water.
3. Weigh and add 7.5 g of K_2HPO_4 to the water.
4. Adjust the pH to 7.4 with HCl.
5. Add distilled water to make up a total volume of 1 litre.

Procedure for collection, treatment and measurement of biomass pellets:

Follow the steps below to collect and measure the mass of the biomass pellet:

1. Weigh the mass of the micro-centrifuge tubes with and without biomass pellets, m_t and m_{t+p} respectively, using an analytical balance (Kern ABT 120-5DM).
2. Collect 2 ml samples of the microalgal culture in pre-weighted micro-centrifuge tubes (PP Natural, 2 ml).
3. Separate the supernatant from the microalgal biomass using a centrifuge (Beckman Coulter Allegra X-22R) for 12 minutes at 3901 rcf.

4. Store the supernatant in HPLC vials after filtration with hydrophilic filters for further analysis through high pressure liquid chromatography as seen in Section C.2.
5. Wash the residual biomass pellets with Phosphate buffered saline (PBS), containing 17.5 $g.L^{-1}$ KH_2PO_4 and 7.5 $g.L^{-1}$ K_2HPO_4, to remove the residual salts from the culture.
6. Separate the PBS buffer from the pellets through the centrifuge for 12 minutes at 3901 rcf.
7. Repeat steps 4-5 twice.
8. After separation using the centrifuge, place the tubes in vacuum conditions at -50°C in freeze dryer (TOPT-10C Toption group Co. Ltd.) for 24 hours.
9. Substitute in the following equation to determine the biomass growth in $g.L^{-1}$.

$$\frac{(m_{t+p} - m_t)\ g}{1\ ml} \cdot \frac{1000\ ml}{1}$$

C.2 **Substrate consumption**

This method utilizes the high pressure liquid chromatography method to analyze the glucose and glycerol content in the supernatant using the Hi-Plex H column.

Chemicals:

1. Sulfuric acid (H_2SO_4).

Materials:

1. Hi-plex H column.
2. Hydrophilic (0.2 µm) filters.

Pretreatment of HPLC vials to prevent bacterial contamination:

1. Place HPLC vials inside beaker and cover in aluminium.
2. Place beaker in solid 30 setting in the autoclave.

Sample filtration procedure:

1. Filter samples into autoclaved HPLC vials using hydrophilic filters.

Protocol for HPLC analysis method:

1. Follow the method settings in the table below to run the method in Agilent HPLC system.

Method settings	**Description**
HPLC column	Agilent Hi-Plex H
Column dimensions	7.7 x 300 mm
Particle diameter	8 µm
Eluent	0.005 M H_2SO_4
Eluent flowrate	0.5 $ml.min^{-1}$
Injection volume	20 µL
Column temperature	65°C
Column pressure	60 bar
Detection method	RI (35°C)

C.3 **Glycine assimilation**

This method utilizes the ortho-phthalaldehyde (OPA) chemistry protocol, which derivatizes amino acids for high-performance liquid chromatographic (HPLC) analysis with the Agilent 1260 system. This method is used on the supernatant samples collected from the microalgal cultivation.

Chemicals:

1. Sodium hydrogen phosphate (NaH_2PO_4).
2. Acetonitrile
3. Methanol
4. Borate buffer
5. Ortho-phthalaldehyde (Sterile ampoules by Agilent 10 mg/ml)

Materials:

1. Zorbax Eclipse AAA column
2. Hydrophilic (0.2 µm) filters.
3. Conical insert for vial

Pretreatment of HPLC vials to prevent bacterial contamination:

1. Place HPLC vials inside beaker and cover in aluminium.
2. Place beaker in solid 30 setting in the autoclave.

Sample filtration procedure:

1. Filter samples into autoclaved HPLC vials using hydrophilic filters.

Protocol for the tray in the HPLC agilent system:

1. Crack the ampoule and use within 7-10 days.
2. Transfer acetonitrile, borate buffer, OPA, milliQ water and distilled water in separate HPLC vials.

3. Follow the configuration shown in the image below for the derivatization chemicals. (Skip FMOC as glycine is a primary amino acid and only requires OPA.)

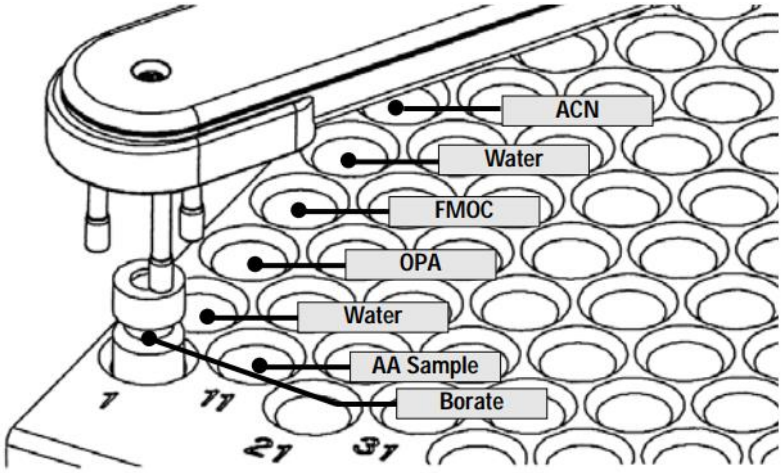

Protocol for the injector program in the HPLC system:

According to the method for Eclipse Zorbax AAA column, the injector program for the derivatization of amino acids is entered into the HPLC autosampler G1313A.

1. Draw 2.5 µL from the borate buffer vial.
2. Draw 0.5 µL from sample
3. Mix 3 µL "in air" at maximum speed and repeat twice.
4. Wait 0.5 min.
5. Draw 0 µL from uncapped vial of water for needle wash.
6. Draw 0.5 µL from the vial containing OPA reagent.
7. Mix 3.5 µL "in air" at maximum speed and repeat six times.
8. Draw 32 µL from the capped vial containing water.
9. Mix 18 µL "in air" at maximum speed and repeat twice.

Protocol for the method in the HPLC system:

Follow the steps in the table below to setup the method for the glycine analysis in the Agilent system.

Method settings	Description
HPLC column	ZORBAX Eclipse AAA
Column dimensions	4.6 x 150 mm
Particle diameter	3.5 µm
Eluent	Solvent A: 40 mM NaH_2PO_4 pH 7.8 Solvent B: Acetonitrile: Methanol: water (45:45:10, v/v)
Eluent flowrate	2 ml/min
Injection volume	Refer to injection program
Column temperature	35°C
Column pressure	220 bar
Detection method	UV/Vis detection 338 nm, 10 nm bandwidth Reference: 390 nm, 20 nm bandwidth

The variation in gradient elution for the analytical method is listed below.

Time (min)	Eluent A	Eluent B
0	100	0
1.9	100	0
18.1	43	57
18.6	0	100
22.3	0	100

Time (min)	Eluent A	Eluent B
23.2	100	0
26	100	0

C.4 **Solvent extraction for lipid, total antioxidant and specific antioxidant analysis**

The method below is used to recover lipids and antioxidants from the microalgal biomass.

Chemicals:

1. Hexane
2. Ethyl acetate
3. Milli-Q water (place at 80ºC)
4. Mono-potassium phosphate (KH_2PO_4).
5. Dipotassium phosphate (K_2HPO_4).

Materials:

1. Homogenizer
2. Glass centrifuge tubes
3. Disposable glass Pasteur pipette

Phosphate buffered saline (1 L) preparation procedure:

1. Measure and fill a container with 800 ml of distilled water.
2. Weigh and add 17.5 g of KH_2PO_4 to the water.
3. Weigh and add 7.5 g of K_2HPO_4 to the water.
4. Adjust the pH to 7.4 with HCl.
5. Add distilled water to make up a total volume of 1 litre.

Protocol for product recovery from the biomass:

1. Collect the total biomass from the experiment and wash twice with phosphate buffer solution.
2. Separate the supernatant from the microalgal biomass using a centrifuge (Beckman Coulter Allegra X-22R) for 12 minutes at 3901 rcf.

3. Place the total biomass from the experiment for 48 hours at -50°C vacuum conditions using the freeze dryer (TOPT-10C Toption Group Ltd.).
4. Weigh about 200 mg of the dried biomass and record the specific mass for each sample.
5. Carry out cell disruption using a homogenizer (PT 2500 E system) with a 7 mm probe at 25000 rpm in a glass vial in the presence of a small portion of hexane for about 10 minutes. (Ensure the sample is stored in glass for hexane extraction to prevent contamination of the recovered products).
6. Dissolve the sample in 2 ml of hexane, mixed by shaking and allowed to rest for 30 minutes before separation.
7. Then separate the samples using the centrifuge (Beckman Coulter Allegra X-22R) for 12 minutes at 3901 rcf.
8. Repeat hexane extraction by adding 2 ml of hexane and allow the sample to rest for 2 minutes after shaking. Repeat separation of the extract with the centrifuge.
9. Transfer hexane extract to a glass tube with a glass Pasteur pipette to prevent contamination of hexane.
10. For the second solvent recovery, using the residue left in the tubes after centrifuge, repeat steps 7-8 twice with 2 ml of ethyl acetate. Transfer ethyl acetate extract to separate tubes.
11. For the recovery of polar antioxidants, repeat steps 7-8 twice with water. Water must be at 80ºC.
12. Dry the hexane and ethyl acetate extracts in nitrogen gas while the water assay should be immediately used towards Trolox antioxidant equivalency assay.

Refer to C.5-7 for further analysis of recovered extracts to evaluate total antioxidant analysis, specific antioxidants and lipid content.

C.5 **Total antioxidant analysis**

This method is used to analyze the total antioxidants from the solvent extraction method in C.4 using trolox equivalent antioxidant capacity.

Chemicals:

1. Sodium chloride (NaCl)
2. Potassium chloride (KCl)
3. Hydrochloric acid (HCl)
4. Dipotassium phosphate (K_2HPO_4).
5. Trolox
6. 2,2'-azino-bis(3-ethylbenzothiazoline-6-sulfonic acid) (ABTS)
7. Methanol

Materials:

1. Homogenizer
2. Glass centrifuge tubes
3. Disposable cuvettes
4. Pipette controller

Protocol for preparation of PBS buffer:

1. Add 8 g of NaCl to 800 mL of distilled water.
2. Add 0.2 g of KCl.
3. Add 1.76 g of K_2HPO_4.
4. Adjust the pH to 7.4 with HCl.
5. Add distilled water to a total volume of 1 L. (Always check the pH of PBS before any experiments: pH = 4.0)

Protocol for preparation of Trolox standard:

1. Dissolve 7.5 mg of Trolox in 20 mL of PBS at pH = 7.4.
2. Use gentle sonication to ensure complete dissolution of Trolox. Trolox stock can be stored at -80°C for up to 6 months.

Protocol for preparation of ABTS standard:

1. Prepare an $ABTS^{+}$ stock solution by mixing equal proportions of solution A containing 7mM ABTS (7.18 mg in 1 ml of distilled water) and solution B containing 2.45 mM potassium persulfate (13.2 mg in 10 ml of water).
2. Leave the stock solution for 12-16 hours in the dark and use within two days.

   Prepare a working solution by adding ethanol and adjusting absorbance to 0.700 ± 0.05 at 734 nm in the UV spectrophotometer (VWR UV-3100 PC).
3. Prepare a calibration curve using a 1.5 mM stock solution of Trolox and the final concentrations are listed below: (Either use PBS or ethanol as a solvent in this method)

Sample	**Trolox stock solution (µL)**	**PBS (µL)**	**Final concentration (µM)**
A	0	1000	0
B	50	950	75
C	100	900	150
D	150	850	225
E	200	800	300

4. For calibration, dissolve 40 µL of Trolox solution to the disposable cuvettes in addition to 800 µL of ABTS radical cation working solution.
   a) Allow the solution to react with the ABTS cation for 15 minutes at room temperature.

b) After the designated time, measure the absorbance for each cuvette at 734 nm and obtain a calibration curve.

c) For sample assessment, dissolve 2 ml of ethanol in the dried hexane and ethyl acetate extracts. Immediately test the water sample with the ABTS working solution without further dilution after recovery.

d) Mix about 40 µL of the sample with 800 µL of the ABTS working solution and allow to react for 15 minutes at room temperature.

e) Test the absorbance of the reaction mixture at 734 nm to investigate the scavenging effect of the antioxidant assay. Hence, test the hexane, ethyl acetate and water assay and report as µmol Trolox.gDW^{-1} of microalgae.

C.6 **Specific antioxidant analysis**

This method is used to analyze the specific antioxidants recovered from the solvent extraction method in C.4.

Chemicals:

1. Acetone
2. Methanol

Materials:

1. Hydrophobic filter (0.2 µm)
2. HPLC vials
3. Syringe

Protocol for high pressure liquid chromatography (HPLC) method:

1. Dry the hexane extract from the solvent extraction method in nitrogen gas.
2. Dissolve the residual extract in 2 ml of a solution of acetone and methanol (50:50 v/v).
3. Use a syringe to transfer the sample to a HPLC vial after filtering with a hydrophobic filter.
4. This sample is analysed using the specific antioxidant analysis method as seen below:

Method settings	**Description**
HPLC column	Poroshell 120 EC-C18
Column dimensions	4.6 x 50 mm
Particle diameter	2.7 µm
Eluent	Solvent A: Water:Methanol 1:4 v/v Solvent B: Acetone:Methanol 1:1 v/v
Eluent flowrate	2 $ml.min^{-1}$
Injection volume	5 µL
Column temperature	35°C

Method settings	Description
Column pressure	260 bar
Detection method	UV/Vis detection 425 ± 3 nm, 446 ± 3 nm, 474 ± 3 nm

5. The gradient elution levels are listed in detail below as the solvents switch between aqueous and organic elements for enhanced separation of the lipophilic antioxidants.

Time (min)	Eluent A	Eluent B
2	75	25
5	25	75
6	10	90
8	0	100
9	75	25

C.7 **Lipid content**

This method further analyzes the lipid content recovered from the solvent extraction method in C.4.

Materials:

1. Top pan mass balance
2. Glass tube

Protocol for lipid measurement:

1. From the solvent extraction method, dry the hexane extract in a nitrogen gas environment.
2. Weigh the residual extract and glass tube on an analytical balance (Kern ABT 120-5DM) and substitute in the following equation.

$$\text{Lipid content (g.gDW}^{-1}) = \frac{(m_f - m_i)}{m_b}$$